FINITE ELEMENT MODELING OF SKEWED REINFORCED CONCRETE

BRIDGES AND THE BOND-SLIP RELATIONSHIP BETWEEN

CONCRETE AND REINFORCEMENT

Except where reference is made to the work of others, the work described in this thesis is my own or was done in collaboration with my advisory committee. This thesis does not include proprietary or classified information.

_____

Xin Li

Certificate of Approval:

_____	_____
Anton K. Schindler Gottlieb Associate Professor Civil Engineering	Mary L. Hughes, Chair Assistant Professor Civil Engineering
_____	_____
Robert W. Barnes James J. Mallett Associate Professor Civil Engineering	George T. Flowers Interim Dean Graduate School

FINITE ELEMENT MODELING OF SKEWED REINFORCED CONCRETE BRIDGES AND THE BOND-SLIP RELATIONSHIP BETWEEN CONCRETE AND REINFORCEMENT

Xin Li

A Thesis

Submitted to

the Graduate Faculty of

Auburn University

in Partial Fulfillment of the

Requirements for the

Degree of

Master of Science

Auburn, Alabama
December 17, 2007

FINITE ELEMENT MODELING OF SKEWED REINFORCED CONCRETE

BRIDGES AND THE BOND-SLIP RELATIONSHIP BETWEEN

CONCRETE AND REINFORCEMENT

Xin Li

_____

Signature of the Author

_____

Date of Graduation

THESIS ABSTRACT

FINITE ELEMENT MODELING OF SKEWED REINFORCED CONCRETE BRIDGES AND THE BOND-SLIP RELATIONSHIP BETWEEN CONCRETE AND REINFORCEMENT

Xin Li

Master of Science, December 17, 2007
(B.E., Southeast University, China, 2001)

162 Typed Pages

Directed by Mary L. Hughes

A bridge deck on US 331 near Montgomery, AL developed transverse and longitudinal cracking a few months after construction was completed. A refined finite element model of this continuous, skewed, composite bridge was developed in detail to predict the stress distribution and cracking behavior of the deck. This was accomplished using the commercial finite element package ABAQUS to efficiently capture the stress contours and cracking distribution of the bridge model. A parametric study using this model was also conducted to investigate the effects of various factors that could possibly have influenced the cracking behavior, such as skew angle and differential support settlement. The results of the model predict the development of cracking at the deck and emphasized the influence of those factors.

In the second part of the thesis, a finite element model was developed to simulate the bond behavior that exists between concrete and steel in reinforced concrete material using ABAQUS software. The spring-like translator, a connector element available in ABAQUS, was used to simulate the bond phenomena between concrete and steel in a pull-out test specimen model. The analysis results show that the translators did a very good job in simulating both the elastic range of response, and the behavior in the damaged range of the bond-slip relationship.

ACKNOWLEDGEMENTS

This thesis would not have been possible without the support of Dr. Mary L. Hughes, who not only served as my supervisor, but also encouraged and helped me throughout my graduate student career. Appreciation is also extended to my committee members, Dr. Anton K. Schindler and Dr. Robert W. Barnes, who offered guidance and support. Finally, thanks to my wife, Liping Chen, who endured this process with me, always offering support and love.

.

Style manual or journal used: Guide to Preparation and Submission of Theses and Dissertations, 2005

Computer software used: Microsoft Word, Microsoft Excel, ABAQUS 6.5-1, ABAQUS 6.6-1, AutoCAD 2004

TABLE OF CONTENTS

LIST OF FIGURES

LIST OF TABLES

PART I: MODELING OF SKEWED REINFORCED CONCRETE BRIDGES

CHAPTER 1 INTRODUCTION

1.1 Background

Extensive transverse and longitudinal cracking was discovered on a recently constructed bridge deck installed on a portion of US 331 near Montgomery, Alabama (see Figure 1.1). It was also noticed that this bridge deck had sustained somewhat extensive horizontal cracking. These cracks, which developed shortly after construction, even before regular traffic was permitted on the roadway, would likely have increased the maintenance cost of the bridge over its lifetime. A research project was conducted by the Auburn University Highway Research Center to study the cracking behavior of this reinforced concrete (RC) deck to minimize the risk of cracking in future bridge decks installed under similar conditions.

Figure 1.1 Transverse and Longitudinal Cracks in Deck of US 331

The bridge of interest in this study is a typical composite structure with a reinforced concrete deck supported by longitudinal steel girders. The shear studs, welded to the top of the steel girders and protruding into the deck slab, were installed to prevent slipping at the interface. In such a composite bridge, most of the tensile bending stresses in the middle of each span are carried by the steel girders and most of RC deck is under compression there (however, since the deck is continuous over the interior supports, it experiences tension in these locations). This composite behavior can not only increase the load capacity of the structure, but can also provide a cost savings for the structural steel over a system that doesn't take advantage of composite behavior.

For this study, a finite element (FE) model was developed to simulate the behavior of this concrete-steel composite bridge, and to evaluate the stress distribution and cracking in the deck. Since the cracked bridge has been demolished and reconstructed, a field study is no longer possible. When the simplified procedures presented in the design codes can not realistically describe this complex bridge behavior, to include the potential complexities in the deck stress distribution associated with the fact that the deck is continuous, and as full-scale laboratory testing is also very time-consuming and expensive, there is a need to develop a numerical model to simulate the behavior of the bridge, and to predict the response of the composite deck. Today, the rapid development of computer technology and FE software facilitate the development of advanced three-dimensional (3D) finite element models.

ABAQUS, a commercial finite element analysis code developed by HKS, was used as the basic platform for this numerical study. ABAQUS is a suite of powerful engineering simulation programs, based on the finite element method, which can solve

problems ranging from relatively simple linear analyses to the more complex nonlinear simulations (ABAQUS 2006).

1.2 Objective

The primary purpose of this investigation was to develop a series of finite element models to analyze the effects of factors that were believed to contribute to cracking on RC bridge decks. Thus, the secondary objectives to achieve this purpose are as follows:

1. Conduct a literature review to evaluate the results of previous FE models of this type.
2. Develop a three-dimensional finite element model of the composite bridge, representing real system characteristics and behaviors as closely as possible.
3. Use the model to predict the response of the bridge deck under different conditions, and make some judgments regarding the possible causes for the cracking that was observed.

1.3 Organization

This thesis consists of two parts: I. Modeling of Skewed Reinforced Concrete Bridges, and II. Modeling of the Bond-Slip Relationship between Concrete and Reinforcement. Part I will be described in its entirety in the first part of the thesis; Part II will follow, in its entirety.

Part I of the thesis consists of six chapters. Following this introductory chapter describing the background for the investigation and its objectives, the literature review involving previous FE models of composite bridges is presented in Chapter 2. In Chapter 3 the development of the FE model for the actual bridge of interest is described, and the modeling results are presented. A parametric study of the possible factors contributing to the observed cracking is presented in Chapter 4. An alternative model used to predict the

cracking behavior of the bridge deck is offered in Chapter 5. Finally, in Chapter 6, a summary of the study is provided, pertinent conclusions are drawn, and recommendations for future study are discussed.

CHAPTER 2 LITERATURE REVIEW

2.1 Possible Causes of Cracking

Hadidi and Ala Saadeghvaziri (2005) summarized several possible causes of transverse cracking in a paper describing an investigation of RC bridge deck behavior. They classified the possible causes into three categories: (1) effects of materials and mix design factors, such as aggregate type, cement type, water/cement ratio and concrete compressive strength; (2) effects of construction practices and ambient conditions such as weather conditions, curing characteristics, casting sequence and construction loads; (3) effects of structural design factors such as girder type, shear stud configuration, deck thickness and reinforcement characteristics.

Dr. Schindler, of the Auburn University Department of Civil Engineering, also presented a number of ideas regarding the possible causes of the cracking observed on the US 331 bridge deck to personnel at the Alabama Department of Transportation (ALDOT). Schindler suggested that sensitive material characteristics, differential settlement of supports, inadequate curing conditions for the deck material, casting sequence effects, and the effects of a severe skew angle were the most likely causes of the observed cracking (Schindler 2005). A parametric study of the skew effects, casting sequence effects, and the effects of differential settlement of the supports were incorporated in the present study using the FE model described in this thesis.

2.2 General Composite Bridge Models

Researchers have employed finite element methods to analyze the behavior of composite structures using various software packages, element types, and material models. Many of the past efforts that were focused on developing an accurate FE model to simulate the composite bridge behavior are presented in this chapter.

Barth and Wu (2006) developed a series of FE models to study the ultimate load behavior of composite bridge decks using ABAQUS. Two simple-span bridge models and one continuous bridge model were included in the study. All models were three-dimensional and included nonlinear material properties. Shell elements were used to model the steel girders and the concrete slab. The concrete material of the model was simulated by two alternative representations available in ABAQUS; one was the smeared crack concrete model, and one involved a concrete formulation incorporating damaged plasticity characteristics. The load and deflection curves resulting from the models were compared with experimental data. The comparison showed that the results from the smeared crack concrete deck model agreed better with the experimental data, but the authors encountered numerical convergence difficulties with this type of model when simulating the continuous, multispan bridge. The model including concrete with damaged plasticity characteristics was therefore suggested by the authors as the best technique for modeling the behavior of a continuous bridge.

Basker et al. (2002) described their FE modeling and nonlinear analysis in a study of composite plate girders. Although the research was focused primarily on the steel girder behavior of the composite bridge, the RC deck and the shear studs were simulated in detail as well, due to their importance in affecting girder behavior. The selected

elements are shown in Figure 2.1. The RC material was modeled using three different methods, including a concrete model, a cast iron model (i.e., a metal stress-strain formulation following the behavior for cast iron, but possessing concrete material values), and an elastic-plastic model. Results of the study showed that the cast iron model and the elastic-plastic model were able to predict the behavior of the composite system more accurately than the concrete model; however, the metal-like material properties for these models was not realistic for concrete. The concrete model failed to converge due to the complexity of its concrete material formulation.

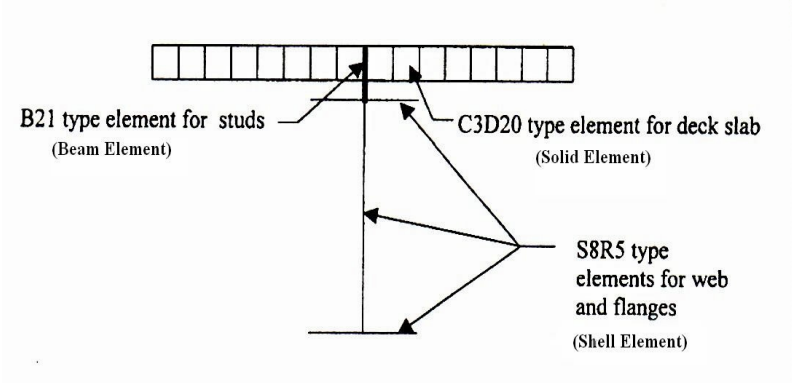

Figure 2.1 Finite Element Model of Composite Plate Girder (Basker et al. 2002)

Consideration of Basker et al.'s results, along with those mentioned above obtained by Barth and Wu, show that the particular technique used for simulating concrete material behavior plays a critical role in composite bridge modeling. Advanced simulations incorporating nonlinear, plastic and cracking properties are worthy attempts at being very realistic, but often, attempts to incorporate these capabilities are also the main reason for the failure of the model.

A three-dimensional FE model was proposed by Thevendran et al. (1999) to study curved steel concrete composite beams using ABAQUS software. In his model, the

concrete slab was modeled by four-node, thick-shell elements, and the steel flange and web were modeled using four-nod, thin-shell elements. A typical element grid is shown in Figure 2.2. Rigid beam elements were used to simulate the full composite behavior between the girders and deck. Nonlinear material properties were included in the model. This model was used to study the load-deflection relationship of the curved beam, and the results were compared with laboratory data. However, there was a large deviation between the numerical and experimental results in the nonlinear stage. The authors reasoned that the large discrepancy was due to the inadequacy in concrete modeling.

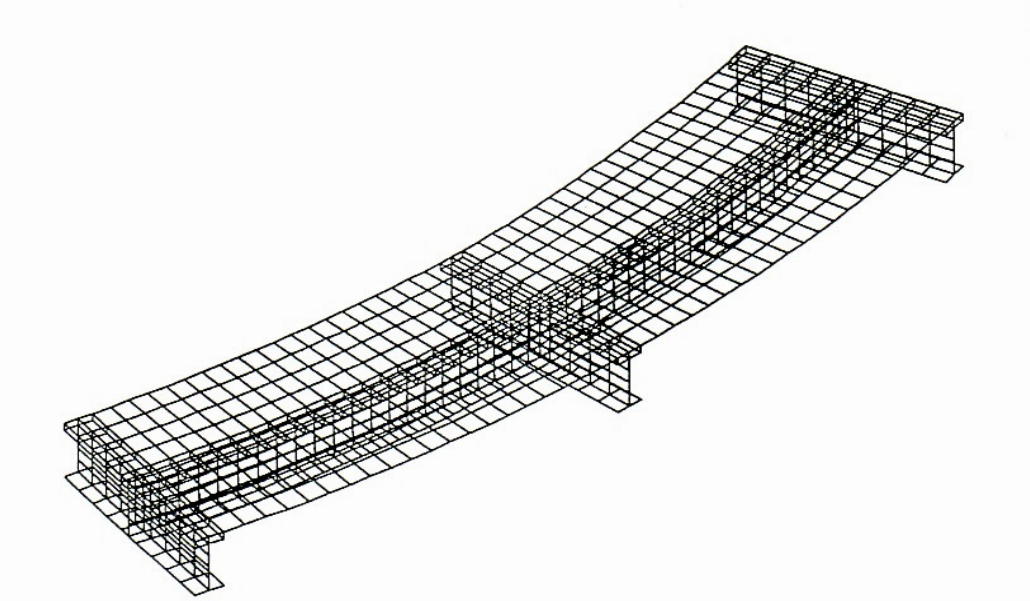

Figure 2.2 Finite Element Model of Composite Beams Curved in Plan (Thevendran et al. 1999)

Biggs et al. (2000) developed a three-dimensional composite bridge model, shown in Figure 2.3, to predict the behavior of a RC deck under vehicle loading. In his model, the RC deck was modeled with shell elements and the steel girders were simulated using beam elements. Multiple point constraints (MPC), available in ABAQUS, were used to simulate the interaction between the slab and the girders so that these members were

forced to undergo the same deformations for the degrees of freedom present at the interface. ABAQUS's smeared concrete model with tension stiffening was used to simulate the pre- and post-cracking behavior of the reinforced concrete. To verify the model, the authors tested a simply supported beam model, a RC slab model, and a single composite beam model with these model characteristics before running the final composite bridge model. The results of these four models all fundamentally agreed with theoretical values, proving the validity of this bridge modeling technique. The limitation of this study, though, was the lack of cracking information in the results, since the post-cracking behavior had been defined in the model.

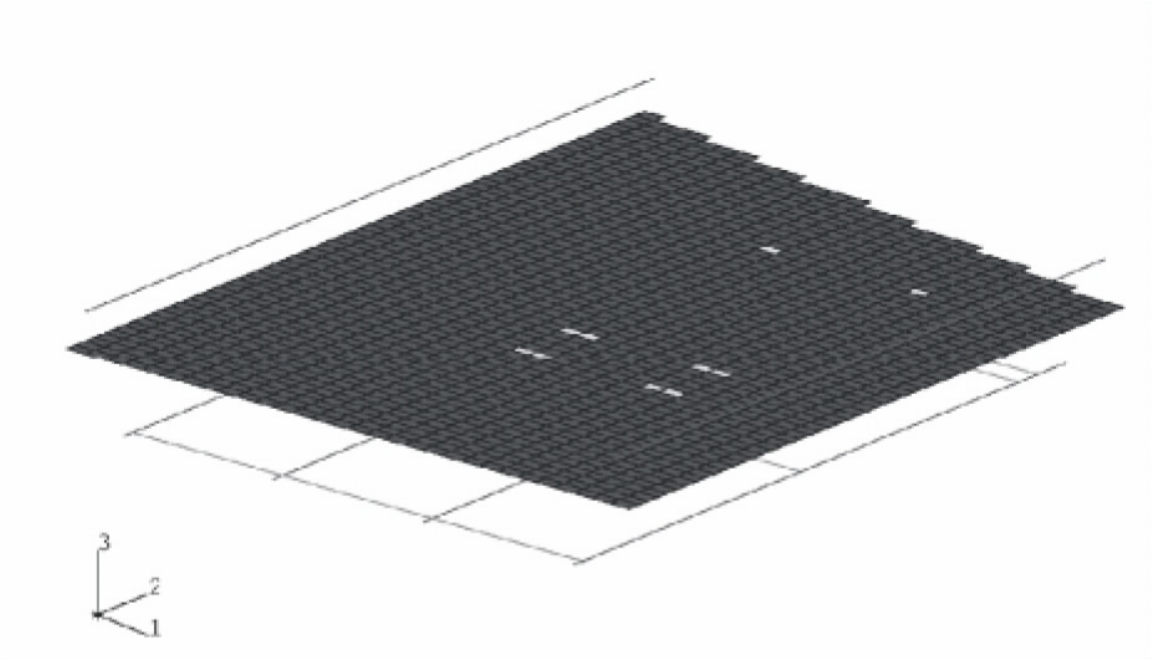

Figure 2.3 Finite Element Model of Composite Bridge (Biggs et al. 2000)

Lin et al. (1991) presented a nonlinear finite element model for the analysis of a composite bridge. In this study, triangular shell elements were used to simulate both the concrete deck and the steel girders. The shear studs were represented by bar elements, and contact elements were applied to simulate composite action. A nonlinear constitutive

relationship and yield criteria were defined for the concrete material. Three types of numerical examples were included in this report to verify the applicability of this FE method. They included a simply supported single-span beam model, a two-span continuous beam model, and a continuous composite bridge model. Post-cracking behavior of the concrete was considered in the material properties but there was no information provided about cracking in the results section of the paper (Lin et al. 1991).

Dicleli (2000) proposed a simplified structural model for computer-aided design of an integral composite bridge under construction. Compared with the conventional structural design model, shown schematically in Figure 2.4, in which the deck was simplified as a continuous beam, the new model presented in this study, which is depicted in Figure 2.5, considered the continuity of the deck at the deck-abutment and deck-pier joints, and reflected the effect of this continuity on the response of bridge deck. The comparison of these two models showed that the design using this new computer model might be more economical. The boundary condition assumption suggested by the author was employed in the present study, as will be described in a later chapter.

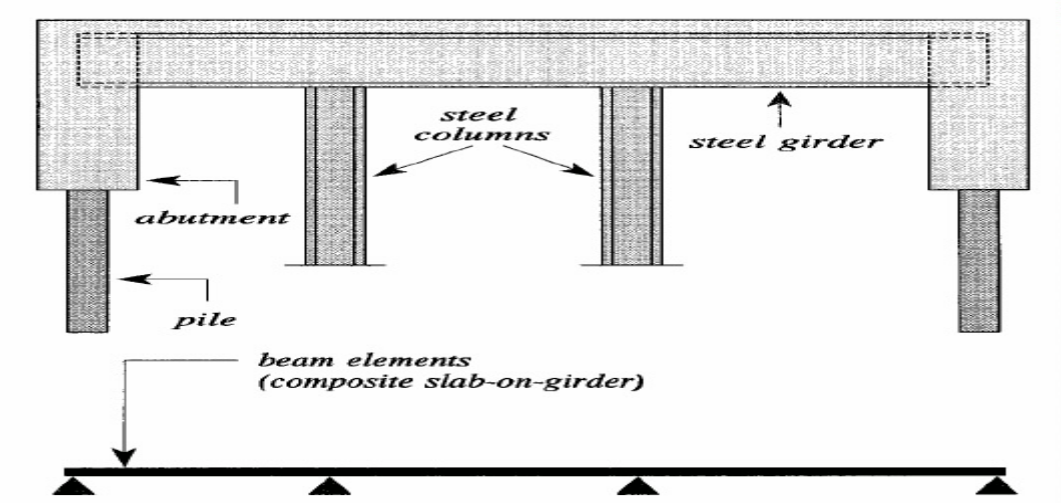

Figure 2.4 Conventional Model for Deck Design (Dicleli 2000)

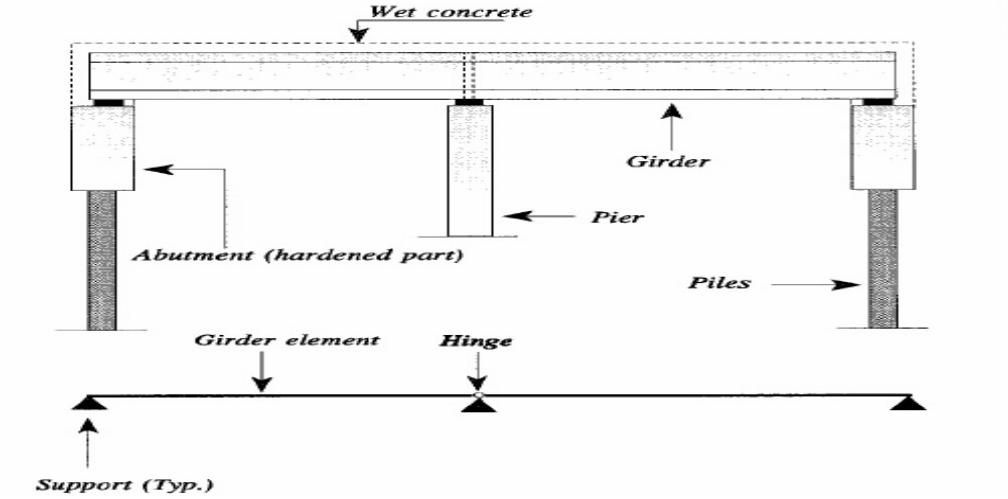

Figure 2.5 Proposed Model for Deck Design under Construction (Dicleli 2000)

2.3 Skewed Composite Bridge Models

An investigation was conducted by Choo et al. (2005) to study environmental, material and casting sequence effects on the behavior of a continuous, skewed composite bridge under construction. A three-dimensional FE bridge model, as illustrated in Figure 2.6, was developed using the SAP2000 software package, in which the deck and girders were all modeled using shell elements. Rigid links were used to model the connection between the deck and girders. All material behavior was assumed to be elastic, so cracking behavior was not included in the model. Temperature and concrete stiffness effects were incorporated in this study by varying the temperature of the surrounding environment and the concrete modulus of elasticity of the model. Casting direction effects (perpendicular to the bridge centerline, or parallel to the skew) were also subject to investigation using this model. Stress in the bottom flange of the steel girders was monitored during the parametric study, and the results showed that temperature had the largest effect on the

stress state. Effects of variation in the concrete modulus of elasticity, and the casting direction effects were less obvious (Choo et al. 2005).

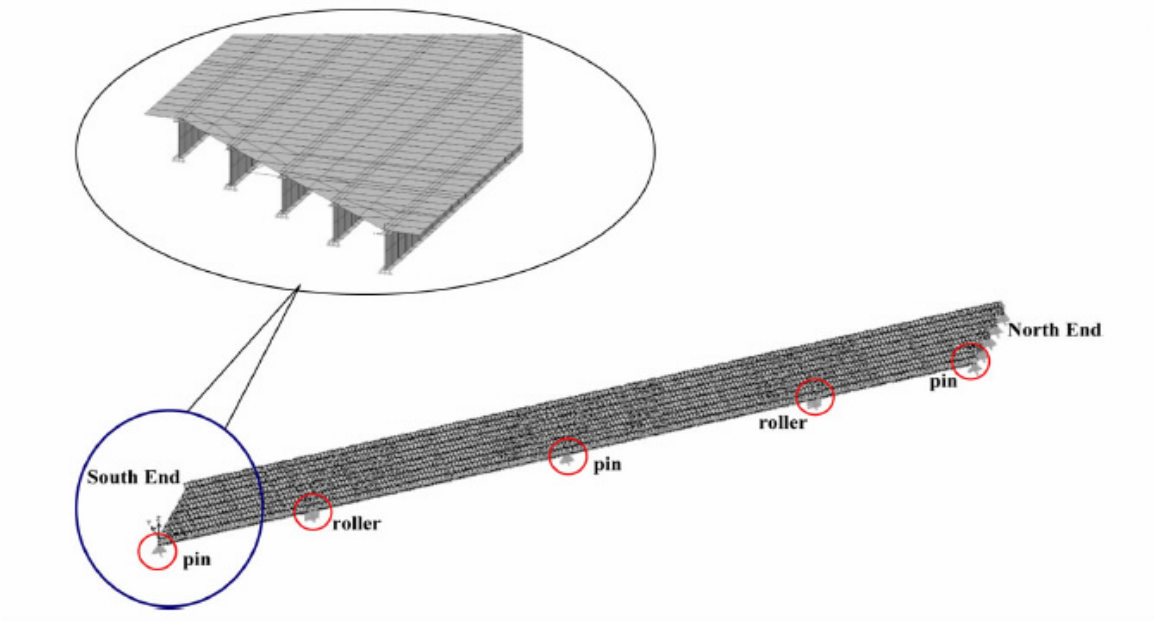

Figure 2.6 FE Model with Boundary Conditions (Choo et al. 2005)

To analyze the seismic response of a skewed slab-girder bridge under lateral seismic loading, Maleki (2002) developed a three-dimensional finite element model of a single span skewed RC deck using SAP2000; an illustration of the model is shown in Figure 2.7. For the model, the author assumed the RC deck to be rigid in its own plane in order to simplify the analysis. Girders were modeled by frame elements, and were connected with the shell elements of the deck at each node. Spring elements were attached at the ends of the girders to simulate the elastomeric bearing pad lateral stiffness. A parametric study was conducted using this model, subjected to seismic loading; the skew angle ranged from 0 degrees to 60 degrees in 15 degrees increments. The results proved that the critical assumption of a rigid concrete deck in the model was safe and

valid for modeling skewed bridges subjected to lateral loads with spans up to 20 m and skews up to 30 degrees (Maleki 2002).

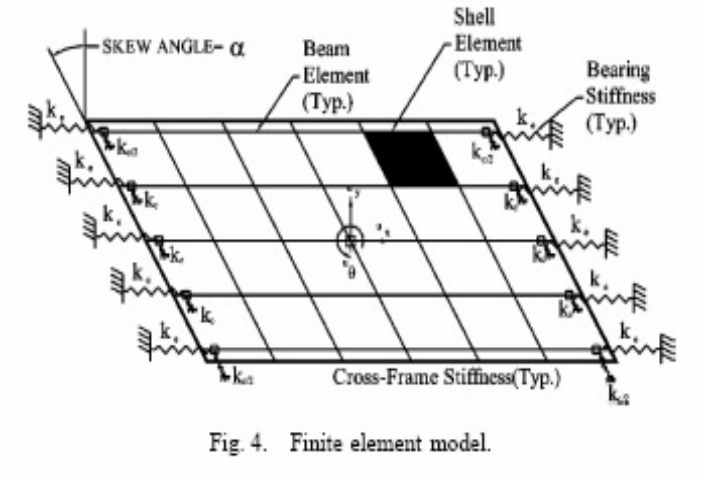

Fig. 4. Finite element model.

Figure 2.7 Finite Element Model (Maleki 2002)

2.4 Studies of Composite Bridge Models with Cracking

Ala Saadeghvaziri and Hadidi (2005) investigated the early transverse cracking of an RC deck by developing 3D finite element models of a subassembly of the composite structure (a single girder along with its tributary deck width) using the ANSYS software package. In this model, the concrete deck was modeled using solid elements, while the girders were modeled using shell elements. The ANSYS rebar element was used to simulate the reinforcement, and the bond between concrete and rebar was also considered through a series of spring connections; a linear elastic concrete material model was employed. Shear studs were modeled with nonlinear spring elements which connected the deck with the steel girders.

Deflection and stress at midspan were studied as they varied with varying temperature-induced shrinkage loads. A sudden jump in the deflection or stress curves was considered as an indication of transverse cracking. The boundary conditions of this

3D model were changed to study their effect on stresses and cracking of the RC deck. Other design factors such as span length, girder spacing and deck thickness were also analyzed in this study using a simplified 2D finite element model. Based on the results of the parametric study, recommendations were made regarding the composite bridge deck design. The primary recommendations were 1) construction practice should not introduce inconsistent boundary conditions on the girders, 2) the ratio of the girder and deck stiffness should be minimized to provide for the preference that the moment of inertia have a greater contribution from the deck, and 3) flexible superstructures should be employed because they have a lower tendency for deck cracking (Ala Saadeghvaziri and Hadidi 2005).

Shapiro (2006) created an ABAQUS model to study the post-cracking behavior of a damaged concrete bridge. The profile of the bridge was carefully modeled, including diaphragms, barriers rails and bearing pads. The whole bridge was modeled using 3D solid elements. Elastic material properties were selected for the bridge, with the inclusion of an equivalent modulus of elasticity applied to the concrete of the deck to approximately reflect the rebar's effect on the cracking behavior. The seam function of ABAQUS was used in the model to simulate cracks that were known to have formed in the concrete girders of the particular bridge under investigation. Several seams were assigned at the location of cracks, and during the computer analysis these seams separated and behaved like opening cracks (Shapiro 2006). The seam function is very powerful for simulating crack propagation, but the limitation is also obvious – a pre-definition of the cracked areas and crack properties is required prior to beginning the analysis.

2.5 Summary

From the literature review, it is obvious that finite element models have been widely applied to study the behavior of steel-concrete composite bridges, and have been greatly facilitated by the high-speed development of advanced computer technologies. Different methods of modeling were proposed by researchers using various commercial FE software packages. A summary of the modeling techniques reviewed herein is presented in Table 2.1.

As can be seen from the scope of literature reviewed, shell elements have been most popular for modeling the RC bridge deck. Shell elements were also the most widely used to simulate the steel girders, especially when the girder response was the core of the study. Biggs et al. proved that beam elements are suitable and economical for modeling the steel girders as well, if the research was focused primarily on investigating the deck's behavior (Biggs et al. 2000). As for the interaction between the deck and girder, eighty percent of the models summarized in Table 2.1 employed rigid beam elements. (The "Tie" connection of ABAQUS is an upgrade of a rigid beam element that demonstrates the same basic behavior as rigid beam; this connection element will be discussed in greater detail in a subsequent chapter.)

A relatively small amount of literature was found that described work focusing on numerical modeling of continuous, skewed bridge decks. There is also lack of available research focused on investigating the cracking behavior of a RC bridge deck using the FE method. Choo et al. developed a continuous, skewed bridge model, but this model was not able to explicitly predict the cracking behavior of the deck due to the use of elastic material properties only. Although Ala Saadeghvaziri and Hadidi and Shapiro considered

the cracking behavior in their FE models, their research was limited to study of the cracking behavior at a certain location of the bridge where cracking had been known to occur before running the model. It was decided, then, that it would be valuable to develop a finite element model of a continuous, skewed composite bridge as the focus of the investigation described herein. This model was then used to conduct a parametric study of bridge behavior and to predict the crack distribution on the RC deck as skew angle and differential support settlements varied.

Table 2.1 Summary of FE Models Reviewed in Chapter 2

Literature	Software	RC Deck Modeled By:	Steel Girders Modeled By:	Shear Connectors Modeled By:	Deck Material Behavior Employed	Skew Considered?	Continuous Deck Considered?	Primary Object of Analysis	Cracking Study Considered?
Lin et al. 1991	N/A	Shell element	Shell element	Bar element	Nonlinear	No	Yes	Deck	No
Thevendran et al. 1999	ABAQUS	Shell element	Shell element	Rigid beam element	Nonlinear	No	No	Girder	No
Biggs et al.2000	ABAQUS	Shell element	Beam element	MPC * -Beam	Linear	No	Yes	Deck	No
Dicleli 2000	SAP	User defined	User defined	User defined	Linear	No	Yes	Deck	No
Basker and Shanmugam 2002	ABAQUS	Solid element	Shell element	Rigid beam element	Nonlinear	No	No	Girder	No
Maleki 2002	SAP	Shell element	Beam element	N/A	Linear	Yes	No	Deck	No
Choo et al. 2005	SAP	Shell element	Shell element	Rigid link	Linear	Yes	Yes	Deck	No
Ala Saadeghvaziri and Hadidi 2005	ANSYS	Solid element	Shell element	Spring element	Linear	No	No	Deck	Yes
Barth and Wu 2006	ABAQUS	Shell element	Shell element	MPC* -Beam	Nonlinear	No	Yes	Deck	No
Shapiro 2006	ABAQUS	Solid element	Solid element	Tie	Linear	No	No	Girder	Yes

MPC: multiple point constraints

CHAPTER 3 MODEL OF US 331 BRIDGE

3.1 Description of the Bridge

The focus of this investigation was a three-span, continuous, skewed bridge that was recently constructed on US 331 near Montgomery, Alabama. The plan view and section view of the bridge are shown in Figure 3.1, along with the framing plan. The reinforced concrete deck has a length of 350.92 ft, a width of 40 ft and a design thickness of 7 inches. The three span lengths, ranging from the south end to the north end, measure 108.24', 134.43' and 108.24', and the skew angle for the bridge measured 61° (all the skew angles in this thesis are defined as shown for the angle α in Figure 3.1). There are "expansion" support conditions (i.e., roller supports) imposed at the abutments and at the left interior bent, and a pinned boundary condition is imposed at the right interior bent.

The RC deck (prior to its deconstruction) was supported by six AASTHO M270-Grade 36 steel girders with a transverse spacing of 7 ft. The web plate dimensions for each girder are ½" x 48". The flange for each girder measures 1¼" x 16" in the positive moment regions, and 1¾" x 16" in the negative moment regions (surrounding the interior bents). The top of the steel flanges are connected with the bottom of the RC deck using 96 rows of ¾" Ø x 5" equally spaced shear studs over the end span positive moment regions, and 94 rows of ¾" Ø x 5" equally spaced shear studs over the middle span positive moment region. Each of the rows contains three shear studs; one stud is placed

directly above the web centerline, and each of the other studs is placed 6" on either side of the web centerline.

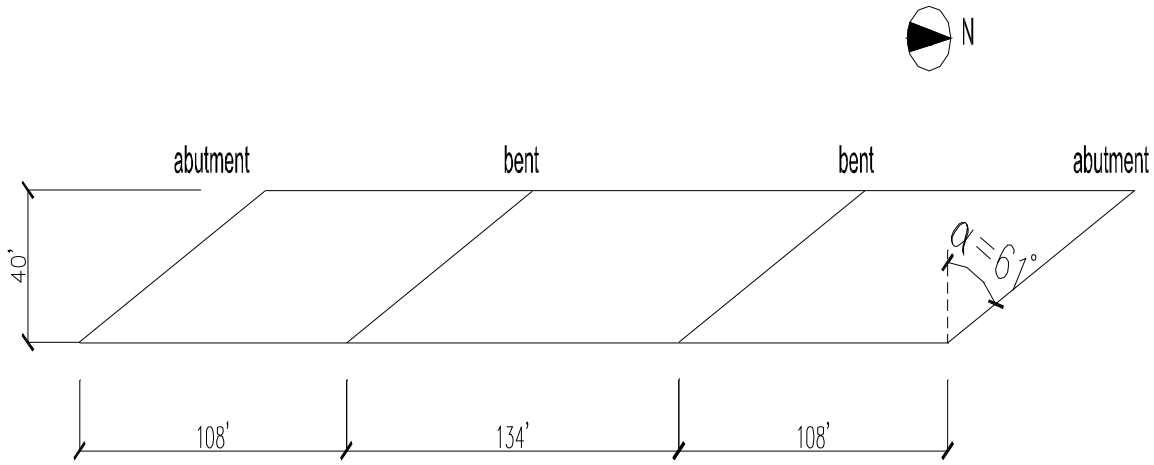

Plan View of the Bridge

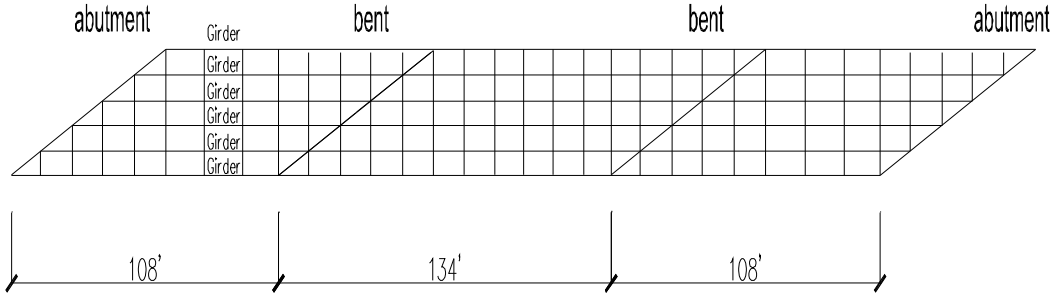

Framing Plan

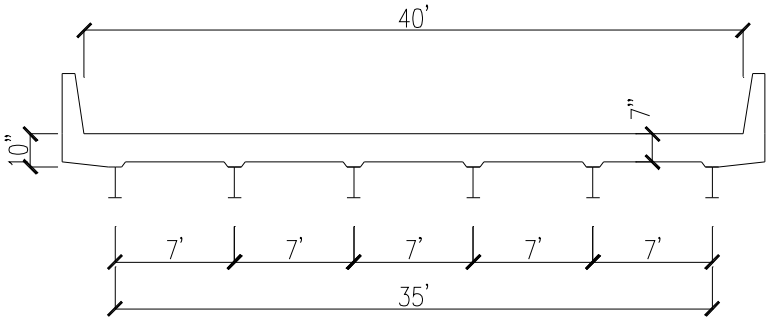

Typical Cross Section

Figure 3.1 Plan View and Section View of Bridge

Intermediate crossframe diaphragms constructed of L $4" \times 4" \times \frac{5}{16}"$ angles, as detailed in Figure 3.2, run between the girders in each span; these diaphragms are represented by the straight vertical lines in the framing plan shown in Figure 3.1. As can be seen in the framing plan, the crossframe diaphragms are perpendicular to the longitudinal direction of the bridge (i.e., they do not follow the 61° skew angle). Additionally, as indicated in Figure 3.1 by the slanted lines, W27 x 84 bearing diaphragms are located between the girders at the abutments and at the interior bents, placed parallel to the skew angle.

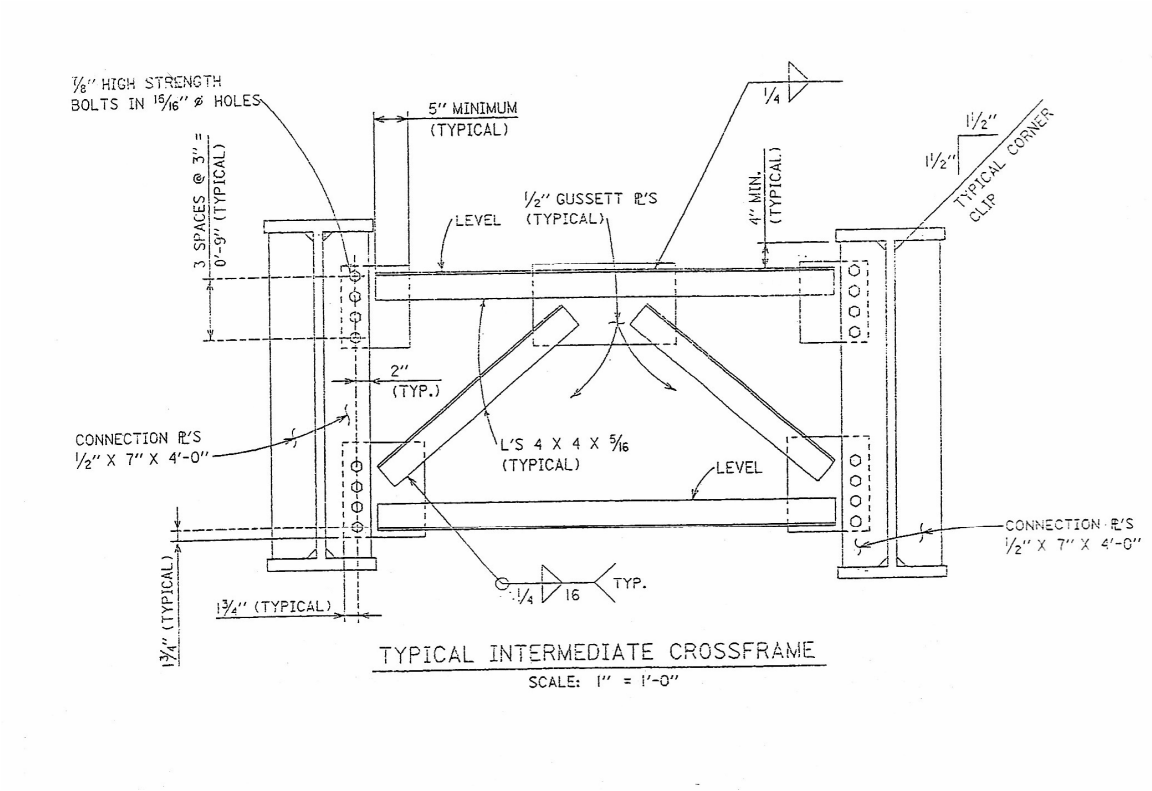

Figure 3.2 Typical Intermediate Crossframe Diaphragm Details

The RC deck slab, as mentioned, had an average depth of 7", deepening to 10" in a haunch shape above each of the girders. Test data collected from core samples taken from the deck exhibited an average concrete compressive strength of approximately 5300 psi. At the top of the slab, #4 longitudinal rebar was evenly spaced between the girders at 16.8" on center, and was also placed directly above the girder centerlines. #4 longitudinal rebar was also placed in the top of the deck on 12" centers between the location above the outermost edge of the top girder flange and the inner edge of the barrier on either side of the bridge. Additionally, extra #4 longitudinal bars spanning 30 ft were placed between the existing #4 bars at the top of the slab above each of the interior bents.

At the bottom of the slab, #5 longitudinal rebar was evenly spaced at 7.4" between each girder, was placed directly above the outer edge of each girder flange, and was placed 9" from the outside edge of the outermost girder flanges. Also, #5 transverse rebar was placed at the top and bottom of the slab, (above and below the upper and lower longitudinal reinforcement, respectively), spaced at 5½"on center.

The bridge deck was cast in three stages. First, 80 ft of the end spans were cast on the south side and the north side of the bridge. Next, an 80 ft portion was cast in the middle of the bridge. Finally, the two remaining 54'-10¾" sections above the interior bents were cast. As a result, after the final deck concrete was poured over the intermediate supports (but while the concrete was still fresh), since the construction was unshored, the girders were required to support the weight of the wet concrete, and were assumed to have undergone all deflection before the concrete in these closure pours was set. Due to this sequencing, the belief is that the stresses produced in the deck closure

castings were not affected by dead loads, since this gravity load was supported solely by the steel girders, but were affected only by any additional live load to which they were subjected.

3.2 Model Characteristics

3.2.1 Assumptions

To study the behavior of the bridge deck, a refined 3D finite element model of the bridge was developed using the commercial finite element software package ABAQUS. Several general assumptions were made to simplify the development of the model without loss of accuracy in the representation. First, material properties were held constant for all concrete components and for all steel components of the bridge. Secondly, it was decided that the deck haunches located directly above the girders would not be explicitly modeled, so that the deck was modeled using a constant thickness. Thirdly, the crossframe diaphragms placed between the girders were simplified as equivalent steel beams in the model. Details of the equivalency calculation will be provided in the following section.

3.2.2 Deck and Girder

Based on the bridge information and modeling assumptions stated above, the main components of the bridge were modeled using the ABAQUS elements shown in Table 3.1 below. The overall model and a close-up view are presented in Figures 3.3 and 3.4.

Table 3.1 Elements Selected for the Main Components of the Bridge

RC deck	Shell elements
Steel Girders	Beam elements
Diaphragms	Beam elements
Reinforcement	Rebar elements
Interaction between deck and girder	TIE function
Parapet	Ignored

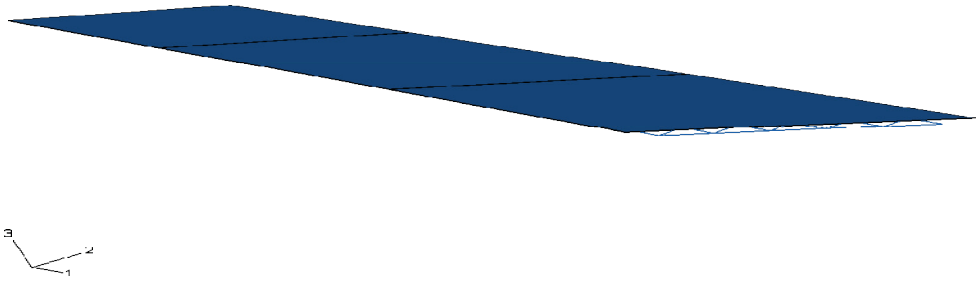

Figure 3.3 Three-dimensional FE Model of US 331 Bridge

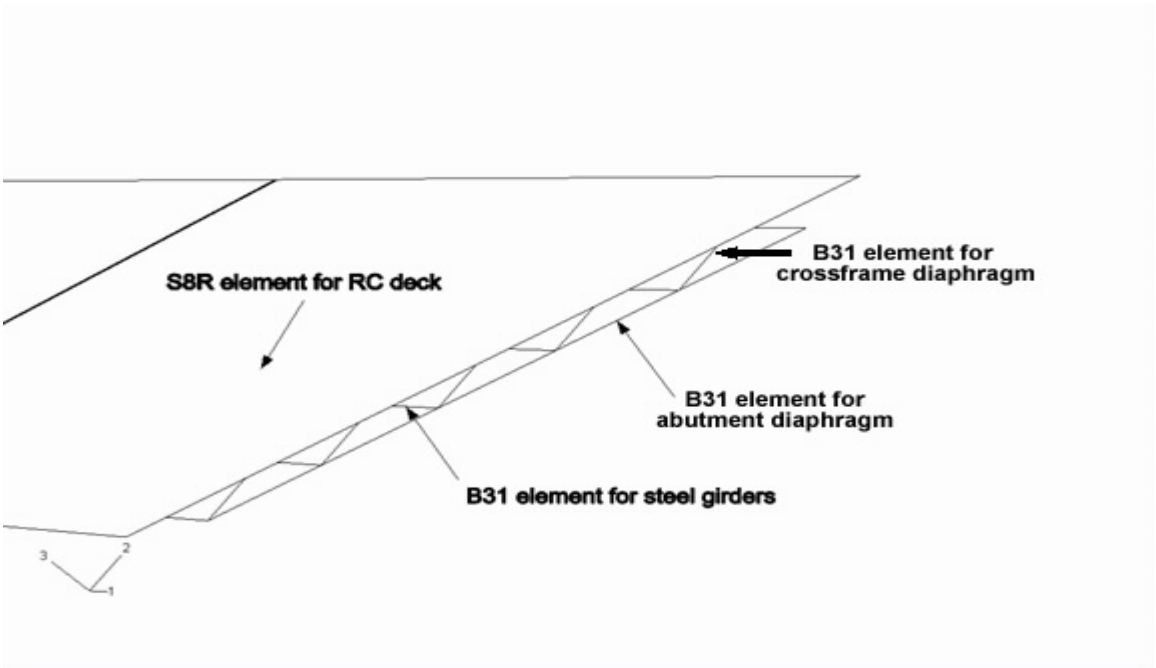

Figure 3.4 Close-up View of Bridge Model

The concrete deck was modeled using ABAQUS's S8R elements, which are eight-node, second-order, general-purpose thick-shell elements with reduced integration. The S8R elements can reflect the influence of shear flexibility in laminated composite shell models (ABAQUS 2006). In the skew sensitivity study presented in the ABAQUS Benchmark manual (ABAQUS Benchmark 2006), plates with varying skew angles were modeled using different shell elements of ABAQUS. The results proved that, with the finest mesh (14 x 14 for a 1.0 m x 1.0 m plate), S8R elements showed the smallest error (0.5%, 0.2%, and 0.8% for center-slab deflection and maximum and minimum moment, respectively), when the skew was as severe as 60°. This result indicates that S8R elements with a sufficiently refined mesh are the most likely ABAQUS elements to provide results that are quite accurate for simulating deck behavior for decks with large skew angles.

The top and bottom reinforcement in the concrete deck was represented using the "Rebar layer" option of ABAQUS. With this function, layers of reinforcement can be defined as a part of the reinforced concrete section properties. These layers are superimposed on the shell elements of the concrete deck and are treated as a smeared layer with a constant thickness equal to the area of each reinforcing bar divided by the reinforcing bar spacing (ABAQUS 2006). Bar diameters and spacings corresponding to the #4 and #5 longitudinal rebar, and #5 transverse rebar described above were provided as input for ABAQUS to define the rebar layers.

The steel girders and diaphragms were modeled with B31 elements, which are three-dimensional, two-node Timoshenko linear beam elements. B31 elements allow transverse shear strain to be represented, and can be subjected to large axial strains. The

ABAQUS Analysis manual stated that these shear-deformable beam elements (B31) should be used in any simulation that includes contact (ABAQUS 2006). That was one of the primary reasons that this type of element was selected, since deck and girder contact was considered to be important in this model. These elements are displayed as a line in ABAQUS, though the cross-sectional dimensions for each beam element are directly defined by the user, so that the effects of the cross-sectional properties can be represented. Nominal dimensions for the steel plate girders, and for the W27 x 84 shapes used for the abutment and bent diaphragms, were specified directly to ABAQUS.

As mentioned previously, dimensions for an equivalent wide-flange shape were used to represent the crossframe diaphragms. This technique was used because, to span between the plate girders, in the finite element model, a specific node had to be identified for attachment of the diaphragms to the beams. Since the girders were being represented by linear beam elements, there was only one node available for attachment to the girders (located at the centroid of the beam's profile). Therefore, attachment nodes could not be identified near the top and bottom of the girder, where the actual location of the attachment of the L4 x 4 x 5/16 crossframe diaphragm members occurs (via a gusset plate connection).

The method of virtual work was used to establish equivalent shear and bending stiffnesses for the bridge's actual crossframe dimensions. From the bending stiffness analysis, it was determined that only the top and bottom chords of the crossframes carry "bending" stresses, so it was deemed that the equivalent beam used to represent the crossframe diaphragm should have top and bottom flanges with cross-sectional areas equal to the cross-sectional area for the L4 x 4 x 5/16 angle (2.40 in^2) used for the top and

bottom chords of the actual diaphragm. It was decided that the equivalent beam should have a web height of 36" (the approximate distance between the centroids of the top and bottom L4 x 4 x 5/16 crossframe shapes). An appropriate web thickness was then determined based on the shear stiffness associated with the shearing deformation of a beam of rectangular cross section. The final cross-sectional dimensions chosen for the equivalent beam, then, were 0.24" x 10" for the top and bottom flanges, and 0.0583" x 36" for the web. The equivalent beams were rigidly attached in the model to the girder node on either end.

The selection of the element size and mesh density was also very critical for obtaining accurate results, because most FE results are sensitive to these parameters. A previous researcher found that selection of relatively small elements will eliminate unrealistically low predicted strengths due to the effects of stress concentrations (Barth and Wu 2006). It is also warned in the ABAQUS manual that a coarse mesh will cause S8R elements to have a great loss of accuracy if they are used to model a skewed plate. Therefore, a reasonably fine mesh was selected in this model. The length of the deck was divided into 400 transverse strips, giving a length of approximately 10.5 inches for each element in the longitudinal direction. Each transverse strip of the deck, then, was divided into 64 elements, giving a width of approximately 8.6 inches in the transverse direction for each element. The deck has only one shell element through the thickness, but information regarding stresses, strains, etc. are available from ABAQUS at any point in the thickness of that element using the section point definition feature of ABAQUS. The steel girders had the same number of elements in the longitudinal direction as the deck. This relatively fine mesh spacing was shown to provide accurate results when compared

to theoretical values (as will be described later), while allowing the cost (in terms of model run time) of the computer simulation to remain affordable.

3.2.3 Material

Both the concrete and steel were defined as linear elastic materials in this model. (A simulation incorporating nonlinear material properties for the concrete deck will be described in a subsequent chapter.) Table 3.2 lists the specific material properties that were input to ABAQUS for both materials. The average splitting tensile strength was defined as 600 psi, according to data obtained from field testing.

Table 3.2 Material Properties of the US 331 Bridge Model

	Modulus of Elasticity, E (psi)	Poisson's Ratio, ν	Density, ρ (lb/in^3)
Concrete	4.42×10^6	0.15	0.086
Steel	29×10^6	0.32	0.286

3.2.4 Load and Boundary Conditions

The applied load for this FE model consisted of a light traffic load equal to approximately 87 psf. A "normal", AASHTO-specified service live load was not applied in the model because the deck studied here was newly constructed, and regular vehicular traffic had not yet been allowed on the bridge.

Gravity effects for the bridge were not included, per se, since they will not affect the cracking behavior of the deck, due to the sequential casting sequence described earlier. In addition, temperature effects were not incorporated. Pin and roller boundary conditions were considered to reflect the abutment and bent restraints; these conditions were used in the model for both the RC deck and girders, as shown in Figure 3.5.

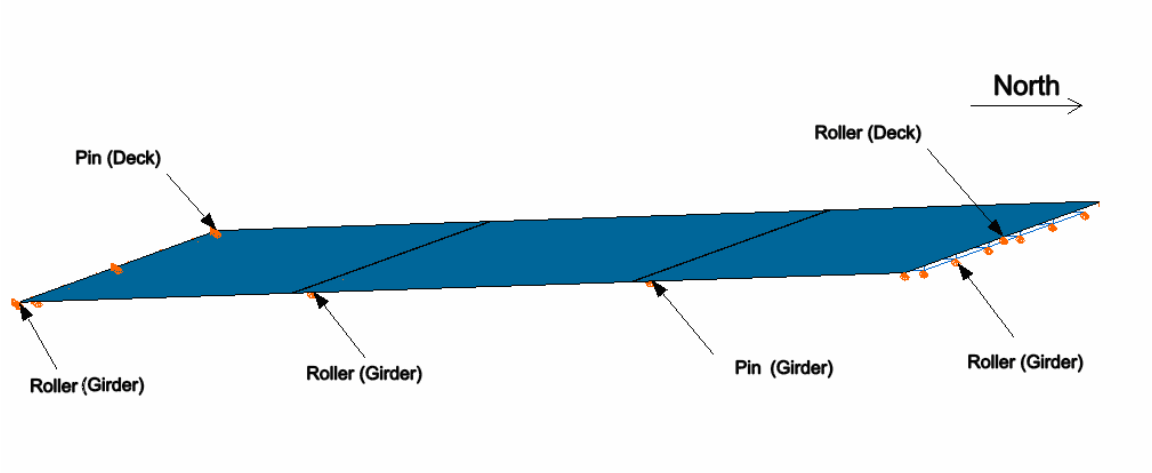

Figure 3.5 Boundary Conditions for the US 331 Bridge Model

3.2.5 Interaction between the Deck and Girders

The "Tie" function of ABAQUS was used to simulate the interaction between the concrete deck and the steel girders. Full composite action was assumed between these two totally different materials and no slip was allowed at the interface. Tie is a new surface-based connection which can be used to tie two surfaces together (the connection is a surface-to-surface connection, rather than a node-to-node connection). The essence of the Tie function is similar to that for a node-to-node connection, in which a rigid beam element is used to connect two nodes, but its surface-based property makes it more efficient to implement than traditional node-to-node rigid beam connections.

When connected with a surface-to-surface Tie constraint, the translational degrees of freedom of the slave surface are eliminated (elimination of the rotational degrees of freedom is optional) and each node of the slave surface will have the same motion as the point on the master surface to which it is closest (ABAQUS 2006). For the present model, a Tie connection was created between two surfaces: the bottom surface of the deck and the top surface of girder top flange. The deck bottom surface was defined as the

master surface, and the top flange surface was designated as the slave surface so that a load applied to the deck could be transferred from the deck to the girders. However, in reality, at the location of the piers, the girders are not able to deflect with their corresponding deck master, due to the boundary condition supports that are applied to the piers. Therefore, the master-slave relationship must be reversed at the pier locations to allow for a realistic deflected shape for the continuous bridge. Figure 3.6 gives the modeling details of the tie connections and boundary conditions surrounding the pier locations.

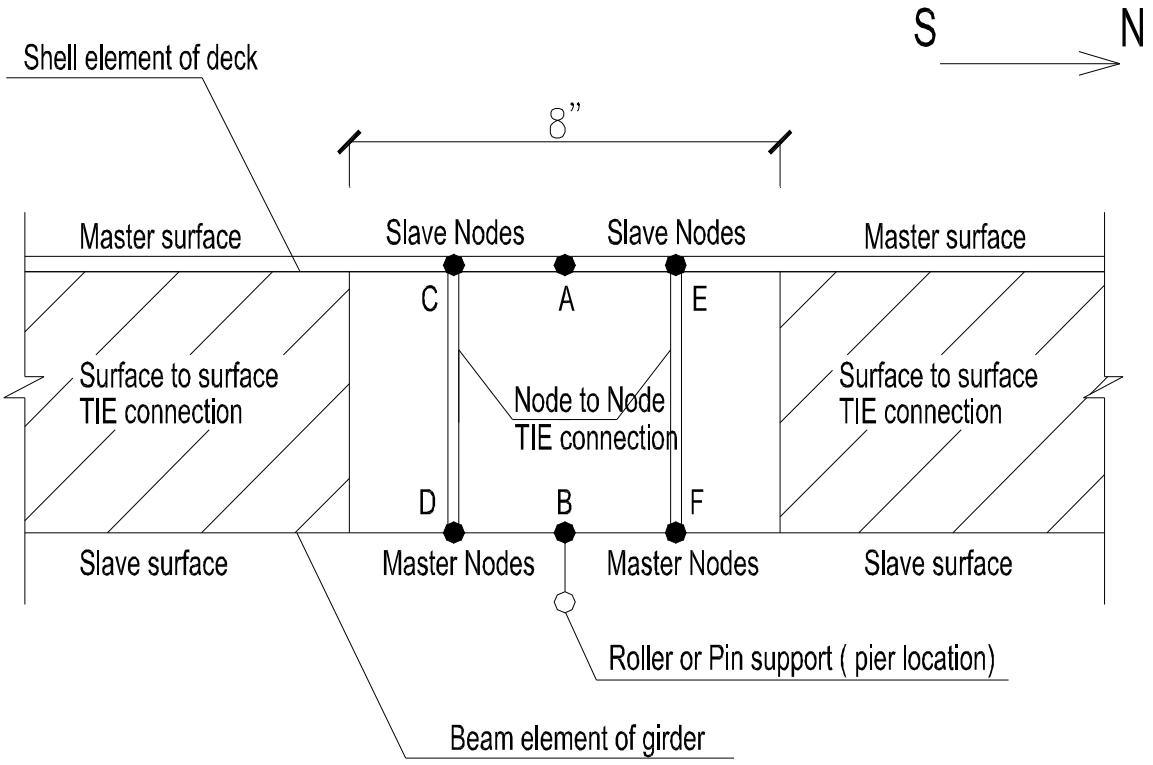

Figure 3.6 Interaction Modeling at Piers (Elevation View)

As can be seen from the figure, a somewhat complex model was created at the pier locations. In these areas, the master-slave relationship was reversed from the relationship that was used for every other location along the length of the bridge, and the

nodes of the girder centerline (node D and node F) became the master of the Tie connection. Without this complex modeling, node B of the girder (which would have been modeled as part of the slave surface without the master-slave reversal) was controlled by two contrary boundary conditions: (1) its master element was located in the deck, which forced the node B to deflect downward under the effect of gravity; (2) the roller support underneath node B, which resisted the downward deflection of node B. This phenomenon is called "overclosure" in ABAQUS and will cause failure of the model. The model in Figure 3.6 (wherein node-to-node contact having a girder master and deck slave was established for nodes D-C and F-E, but not for nodes B-A, and having a pin or roller boundary condition applied to node B) not only eliminated the "overclosure" problem, but also released the vertical degree of freedom of node A, which was a much more realistic condition for the continuous deck.

The shortcoming of this support model is that the response in these locations was distorted, due to such a complex simulation. However, since the area involved with this advanced interaction scheme was very small (8" in length) compared with the width of the whole deck (350 ft), it was deemed acceptable.

3.3 Validation

To validate the modeling techniques used in this study, a single girder and its tributary deck width were isolated from the bridge model, without changing any model characteristics (e.g., the TIE contacts representing the interaction between the deck and girder surfaces were preserved), as illustrated in Figure 3.7. This abbreviated model was analyzed with ABAQUS and by hand calculations. In this model, the load is the self-weight of the bridge. The skew effect was ignored in this simple validation model.

Figure 3.8 shows the longitudinal stresses produced for both the top and bottom surfaces from ABAQUS.

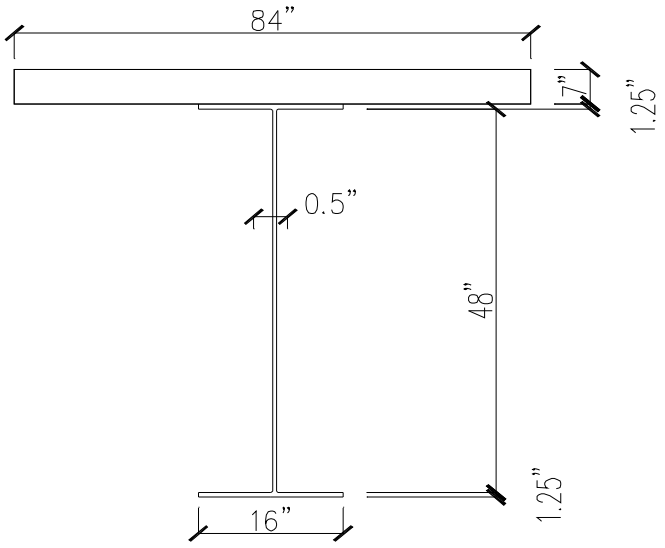

Figure 3.7 Cross Section of Composite Beam Model (Not to Scale)

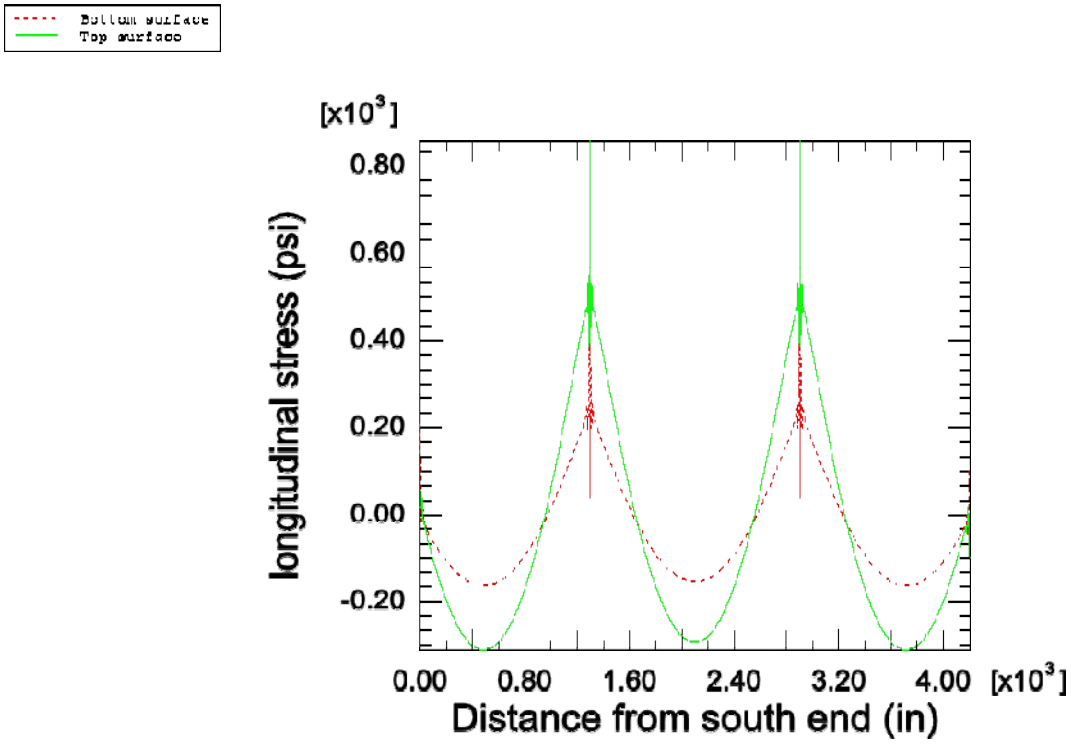

Figure 3.8 Longitudinal Stress of the Model

The effects of composite behavior are quite obvious in this figure. The neutral axis of the composite section is located in the girder (and thus completely underneath the concrete deck). Thus, at the middle of each span, both the top and the bottom surfaces of the deck are experiencing compressive stress, as expected. At the areas surrounding the interior supports, the entire deck was shown to be in a state of tension. The stress values at the locations just above the supports were abnormal due to the complex modeling of the support locations, described in Section 3.2.5 above. Thus, in the present study, these values were ignored.

The results of a hand calculation of the predicted stresses were compared with the FE results; the values are shown for comparison in Table 3.3. The stress was calculated at six locations, considering the symmetry. The maximum compressive stress at the middle of each span was computed for both the top and bottom surfaces, as well as the maximum tensile stress at location of the interior support for both surfaces.

Table 3.3 Validation Concrete Deck Stress Results

	Surface	Location	Hand Calculation	FE Model	Percent Difference
Stress (psi)	Top	Interior Span (Midspan)	-291.6	-293.2	0.55%
		End Span (Midspan)	-310.5	-311.7	0.38%
		Support	567.8	564.2	0.63%
	Bottom	Interior Span (Midspan)	-163.2	-153.8	5.76%
		End Span (Midspan)	-173.8	-163.0	6.21%
		Support	317.8	253.8	20.1%

The results show that the FE prediction of longitudinal stresses agree very well with the results calculated by hand, especially at the top surface where the effect of the

interaction with the girder stresses is not as prominent. This comparison served to confirm that the modeling techniques employed for the study were valid, since no field stresses were available for comparison. (The somewhat larger percent difference noted for the bottom surface at the support location is attributed to the artificial complexity of the stress pattern created there by the complex interaction modeling scheme.)

3.4 Results and Analysis of Results

3.4.1 Deformation and Stress Distribution

Since the main objective of the investigation was to study the behavior of the bridge deck, the results of the model were focused on the response of the deck, despite that the girders and diaphragms were also accurately represented. The deformed shape of the RC deck under external loading is shown in Figure 3.9.

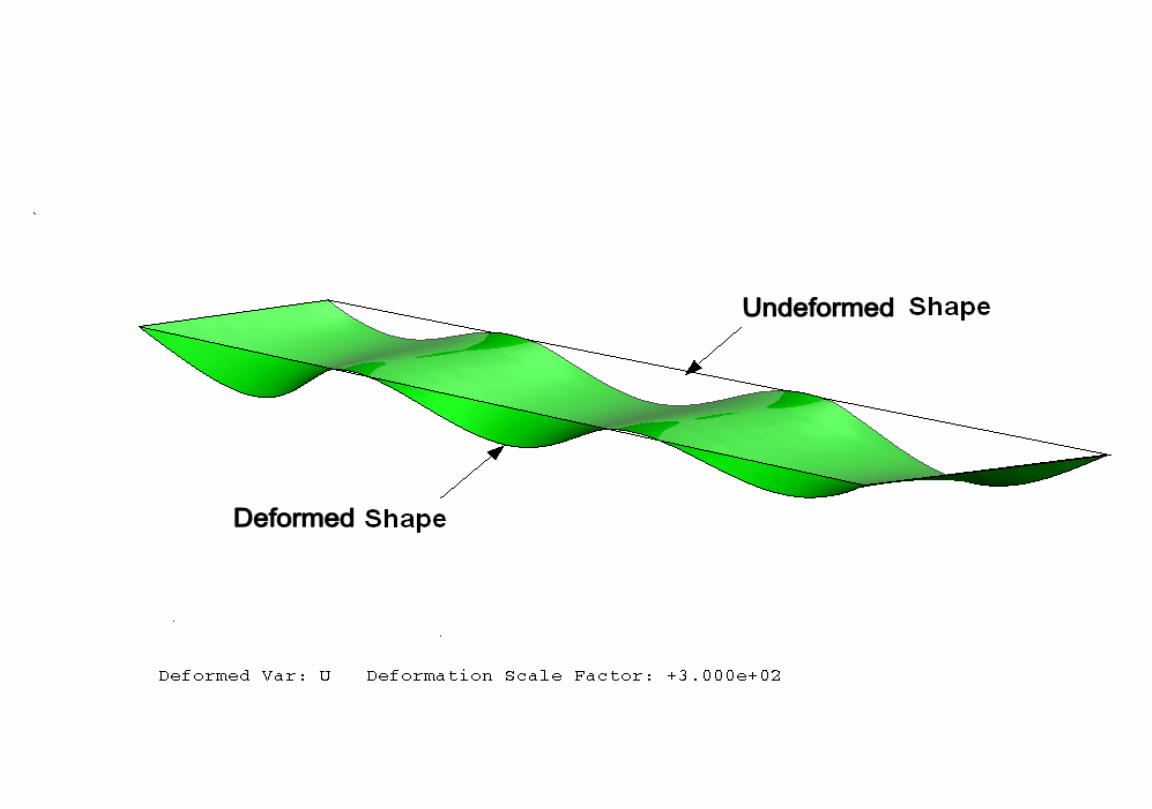

Figure 3.9 Deformed Shape of the US 331 Bridge Deck under External Loading

For the deck only, without the steel girders, the bottom deck surface at the midspan locations and the top deck surface at the supports would be in tension, based on the deformed shape shown. However, because of the contribution of composite bridge behavior, both the top and bottom surfaces of the deck were in compression at the midspan locations. For the same reason, the deck at the intermediate supports became the most likely areas to experience the maximum tensile stress and the most extensive cracking. Thus, the simulation results for the deck at the locations of the intermediate supports were carefully analyzed, including both the top and bottom surfaces. Figures 3.10 to 3.13 show the distribution of maximum principal stress for the RC deck at the supports.

Because the complex interaction model at the intermediate supports, shown previously in Figure 3.6, caused some unrealistic stresses, these unusually high stresses were ignored during the analysis of the results, and they are not displayed in Figures 3.10 to 3.13 (for the two narrow-width strips just above the interior supports).

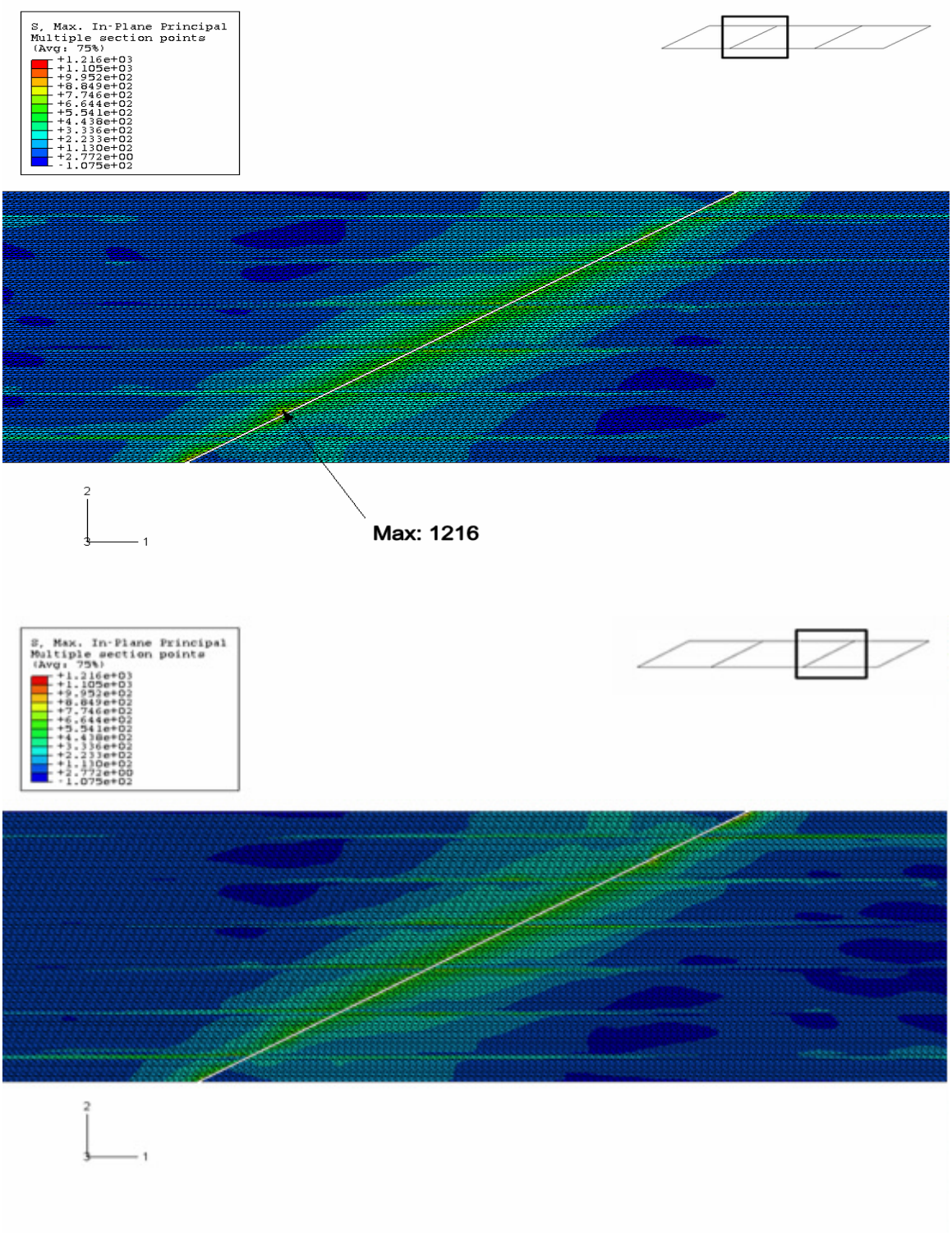

Figure 3.10 Maximum Principal Stress Distribution at the Top of the Deck for US 331 Bridge, α = 61° (psi)

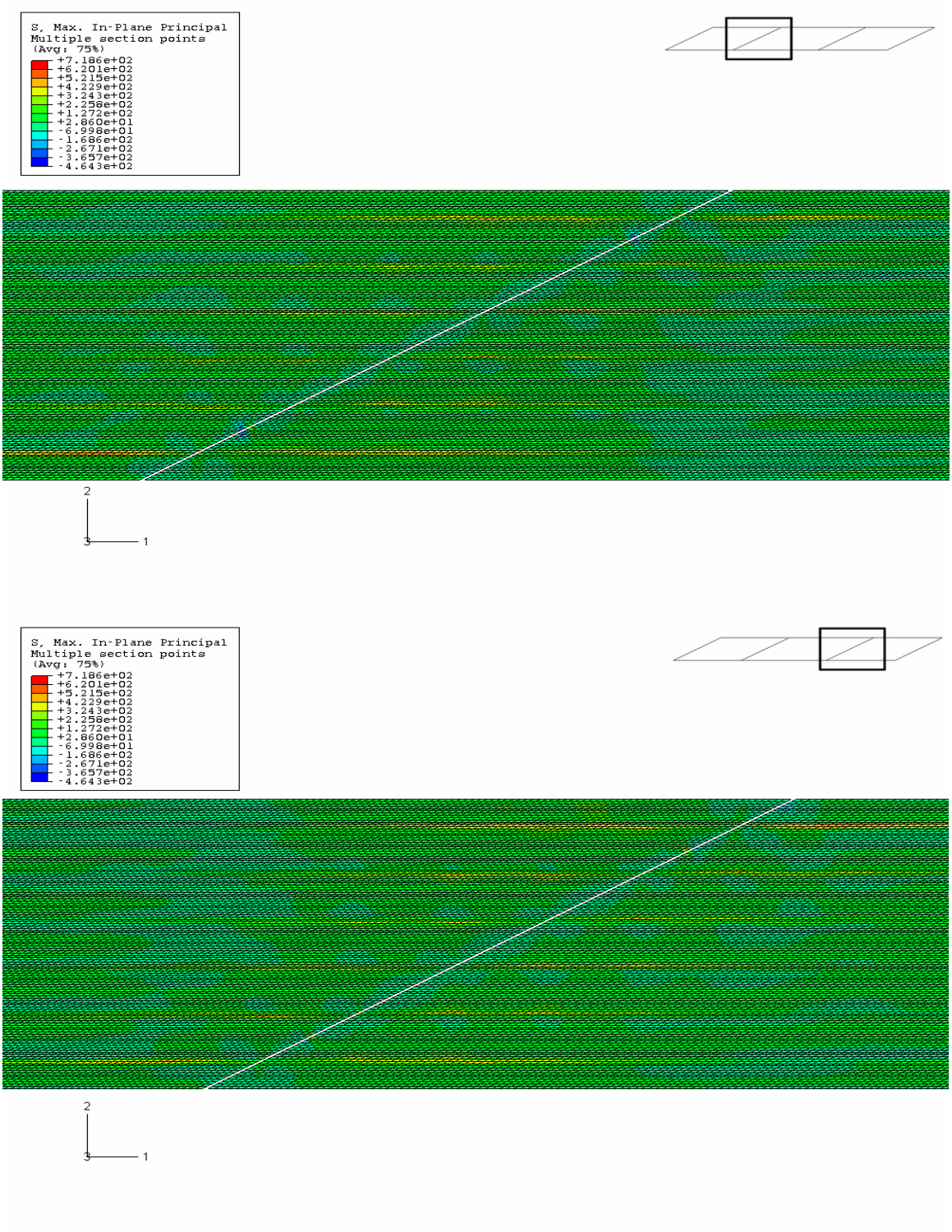

Figure 3.11 Maximum Principal Stress Distribution at the Bottom of the Deck for US 331 Bridge, α = 61° (psi)

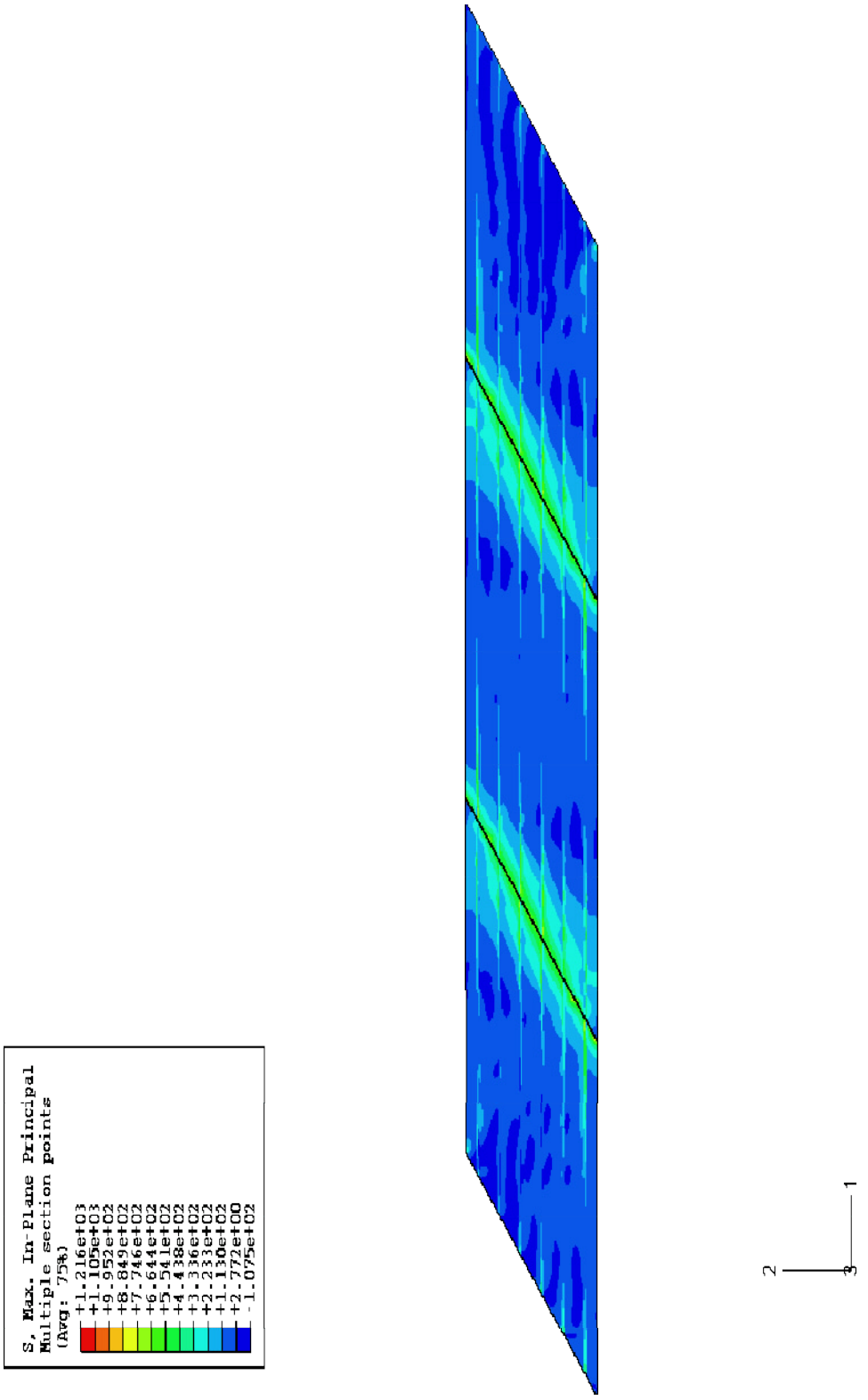

Figure 3.12 Full View of Maximum Principal Stress Distribution at the Top of the Deck for US 331 Bridge, α = 61° (psi)

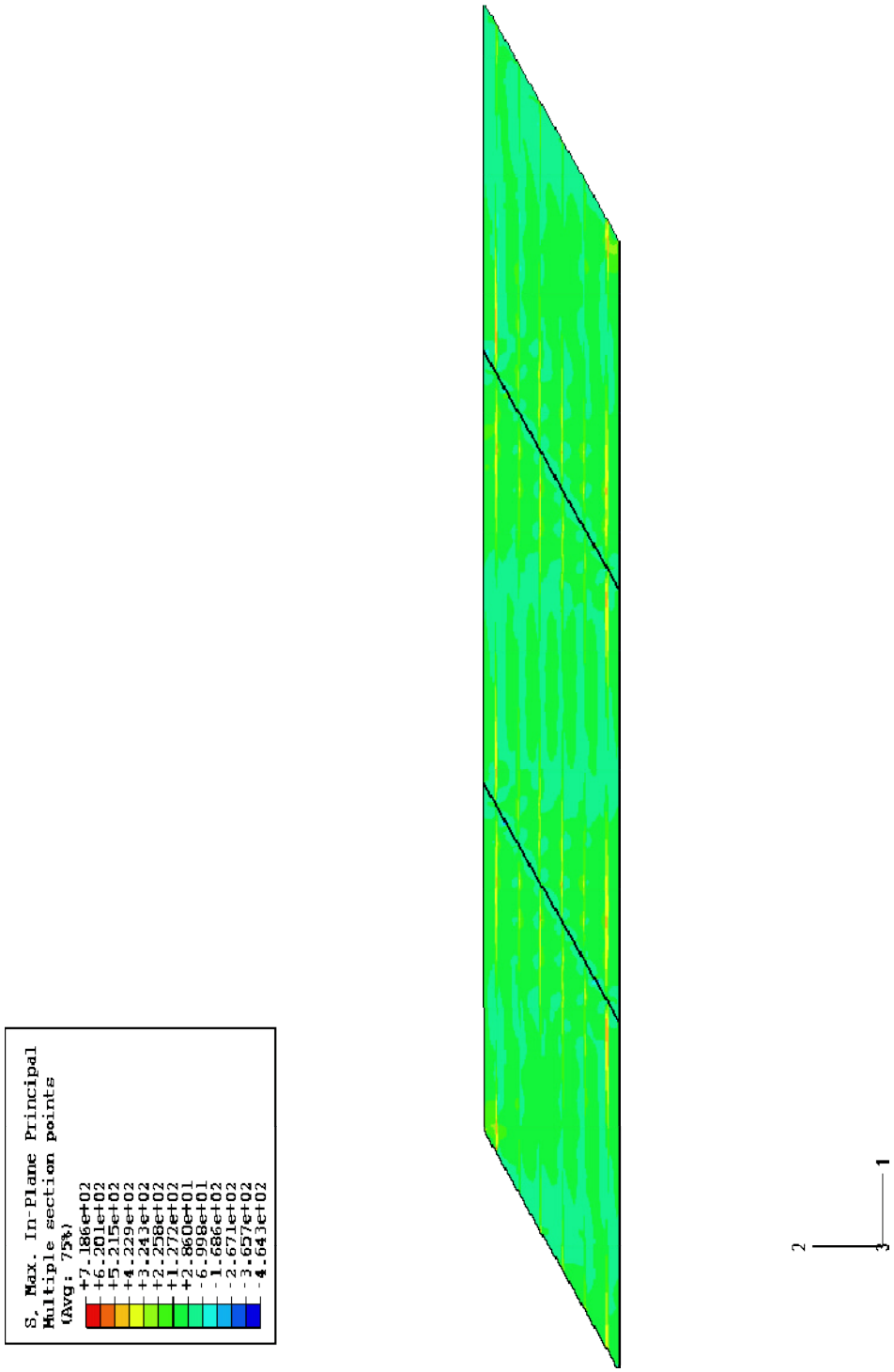

Figure 3.13 Full View of Maximum Principal Stress Distribution at the Bottom of the Deck for US 331 Bridge, α = 61° (psi)

As expected, both the top and the bottom of the deck at the intermediate supports are shown to be in tension, and the top surface experiences the largest tensile stress. From the figures, one can see that the tensile stress decreases from the support area towards the midspan area, finally becoming compressive in the midspan area. This behavior fundamentally matches the theoretical moment diagram for a continuous, one-way slab, as expected. As can be seen, this phenomenon was more obvious at the top surface of the deck than at the bottom surface. That is because the bottom of the deck is closer to the neutral axis of bending. The skew effect was also very obvious; in Figure 3.10, one can observe that the edge of the contour has a skew angle similar to that for the bridge deck.

3.4.2 Cracking Detection

For this study, in which a linear elastic material model was used to characterize the concrete deck, cracking was assumed to occur when the maximum principal tensile stress of the concrete reached its tensile strength. The tensile strength was defined as 600 psi, based on field testing results. By studying the contours of the maximum principal stress (Figures 3.10 and Figure 3.11), one can identify the cracked area of the model according to the stress level of the elements. Figures 3.14 and 3.15 highlight the cracking zone of the bridge deck. For these figures, and for similar figures in the remaining chapters of this thesis, the red-colored elements are those identified by ABAQUS as possessing maximum principal stresses greater than the cracking stress.

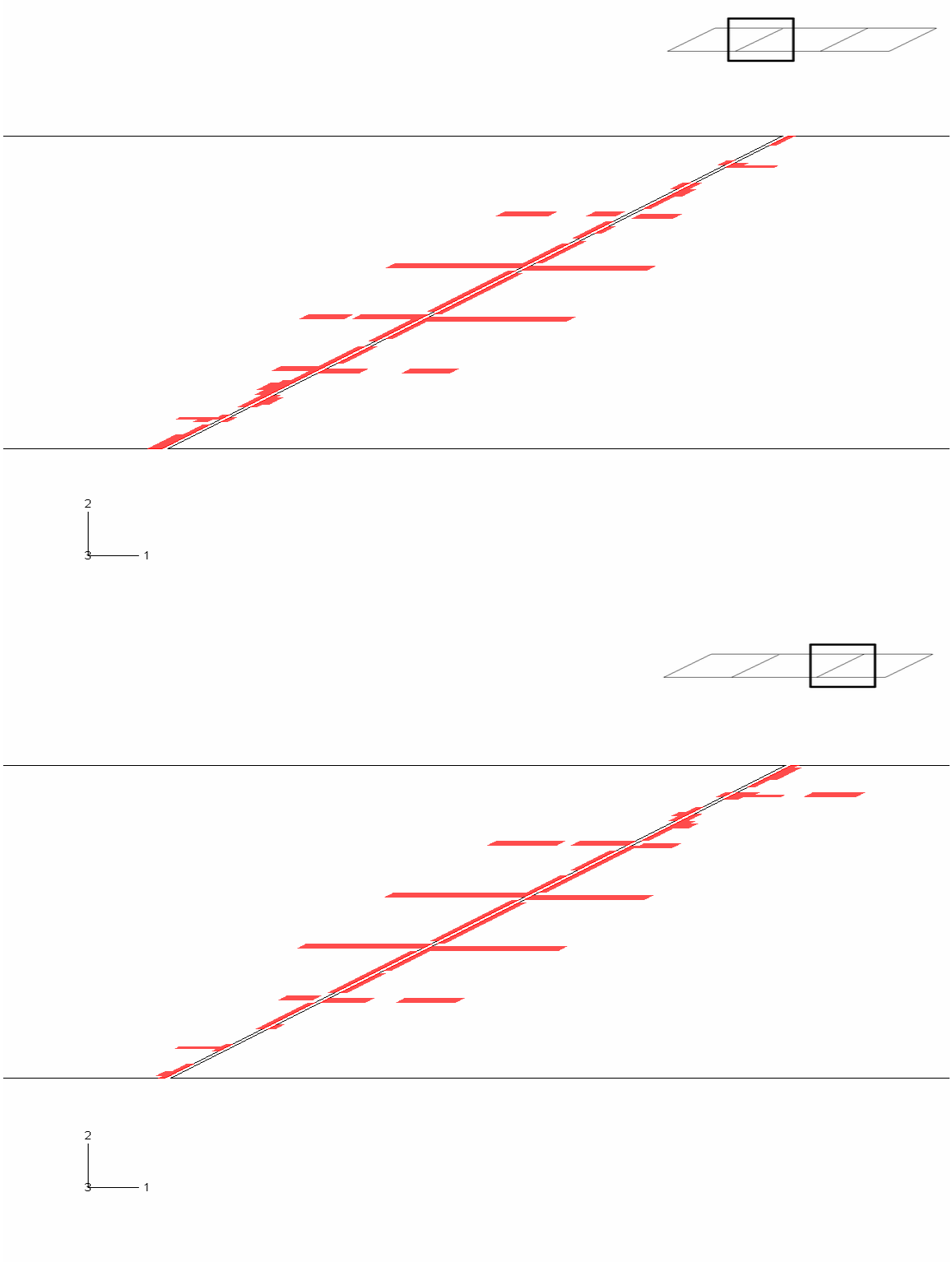

Figure 3.14 Cracked Zone at the Top of the Deck for US 331 Bridge, α = 61°

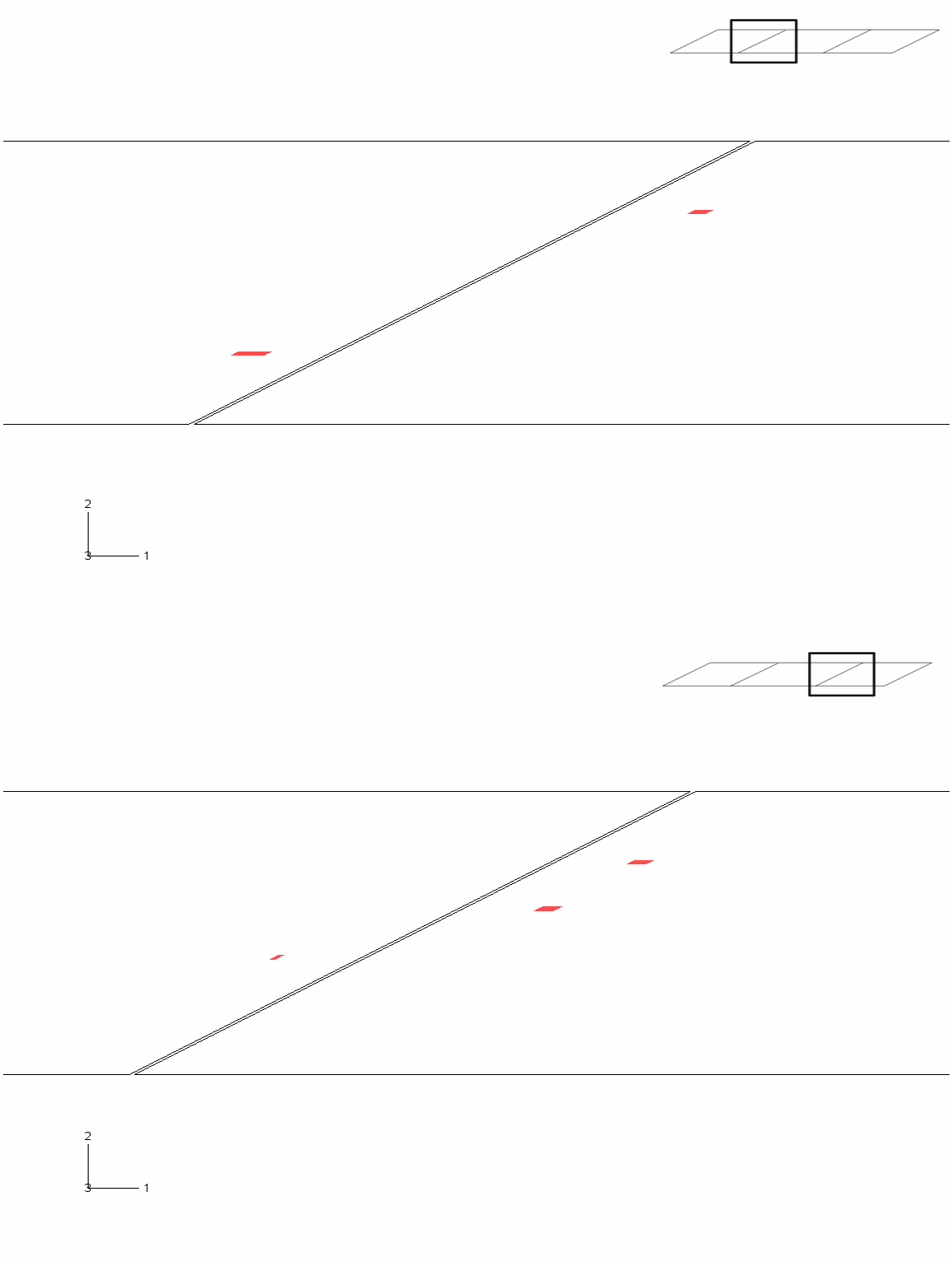

Figure 3.15 Cracked Zone at the Bottom of the Deck for US 331 Bridge, α = 61°

As can be seen, at the top surface, cracking primarily occurs at the areas surrounding the intermediate supports. Additionally, the crack distribution exhibits the same degree of skew as the deck. Several strip areas in the longitudinal direction are also seen to be cracked at the top surface. It is believed that this cracking is due to the contribution of the girder stiffness, which increases the bending stress relative to areas that are further removed from the girders.

At the bottom of the deck, the tensile stress produced was not very large, because this surface is much nearer to the neutral axis of the composite section than is the top surface. The remaining deck area that is not shown in these figures (surrounding the midpoint of each span) only exhibited a few minor cracks in the model results, and was therefore not presented in figures here. These areas experienced either compressive stress, or very small amounts of tensile stress.

The direction of the maximum principal tensile stress can indicate the orientation of the crack for each cracked element. Using the SYMBOLS function of ABAQUS, symbols (headless arrows here) can be plotted that display the relative magnitude of the stress through varying symbol lengths (the greater the length of the headless arrow, the greater the magnitude of stress), while the orientation of the symbol corresponds to the axis normal to the crack. In Figure 3.16, these symbols are shown as the black lines for the top deck surface.

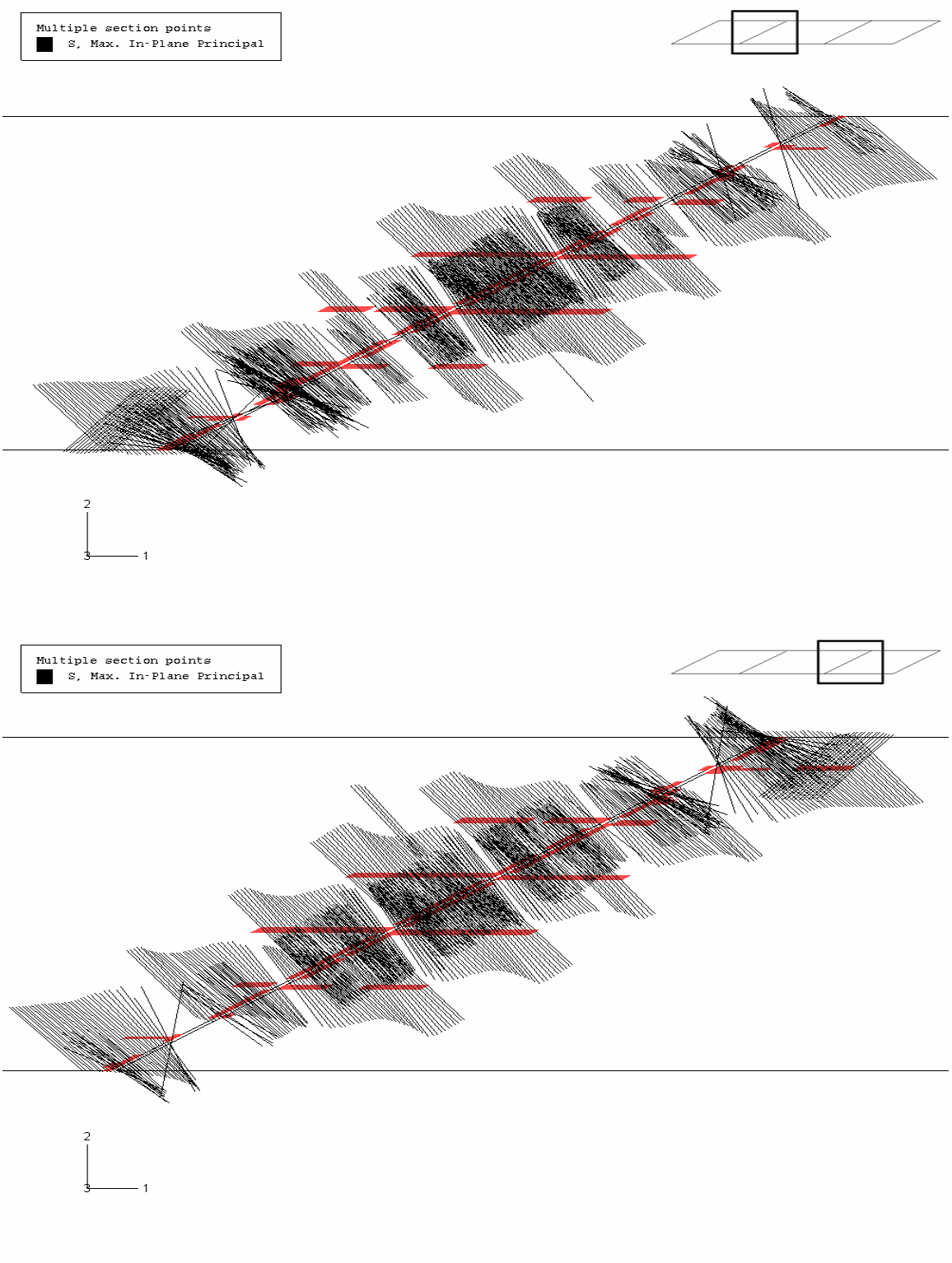

Figure 3.16 Normal Direction of Cracks (Black Lines) at Top of Deck, US 331 Bridge, $\alpha = 61°$

From these results, it can be observed that cracking is somewhat extensive on the top surface of the deck near the intermediate supports. Additionally, almost all of the cracks are oriented parallel to the bent, which possessed the same degree of skew as the bridge deck. The remaining few cracks are located near the edge of deck at the support.

At the bottom surface of the deck, despite that a very small number of cracked elements were observed, as shown in Figure 3.15, no black lines were indicated by ABAQUS. This is because the black lines represent the stress level at the finite element integration points, while the highlighted cracked zone is decided by the element nodal values of stress. There is a difference between these two values because ABAQUS employs an algorithm to interpolate nodal values from calculated values at the integration points. Due to this difference, at the bottom surface of the deck, the stress at the integration points has not reached the cracking stress, so there are no black lines, but one or more interpolated nodal values have reached the cracking stress, so elements with those nodes have been highlighted as cracked elements.

The crack illustration sequence employed above (plot of maximum principal stress, followed by a plot of cracked elements, followed by a display of the normals to the crack direction) will be utilized again in the next chapter, in which a parametric study of bridge deck behavior is described.

CHAPTER 4 PARAMETRIC STUDY

Two physical characteristics of the US 331 bridge, specifically the skew angle and the locations of possible support settlement, were varied parametrically to study their effects on the cracking behavior of the RC deck. The results of this parametric study will be presented and discussed in this chapter.

4.1 Effect of Skew

Skewed bridges like the bridge on US 331 are very useful at complex intersections where roadway alignment changes are not feasible or economical. However, when the skew angle is larger than 30 degrees, it is quite possible that the effect of the skew becomes significant to the behavior of the bridge. Previous researchers have found that skewed bridges are at risk of experiencing greater vertical defections and bending moments than similar, non skewed bridges (Choo et al. 2005).

Figures 4.1 to 4.8 show the results obtained from the FE model of the US331 bridge, modified to include 0°, 30°, and 45° skew angles, instead of the actual skew angle of 61°. Each of these FE models possessed the same characteristics, and the same load, as the base model discussed in Chapter 3; only the skew angle was changed. From the results presented in the last chapter, it was evident that most cracking occurred at the top surface of the deck near the intermediate supports, where large tensile stresses were experienced. Therefore, for the parametric study, only the results for the top surface of

the deck were monitored. The deck areas which are not shown in the following figures (far removed from the interior bents) only exhibited a very few cracked elements.

Again, because of the nature of the complex modeling utilized for the very narrow areas just over the intermediate supports (detailed in Figure 3.6), some unrealistic stresses were produced at these locations. As was the case for the model with the actual bridge skew angle, these abnormal stress results were ignored during the analysis of the results of the parametric study, and they are not displayed in the two narrow strip areas above the interior supports in the following figures.

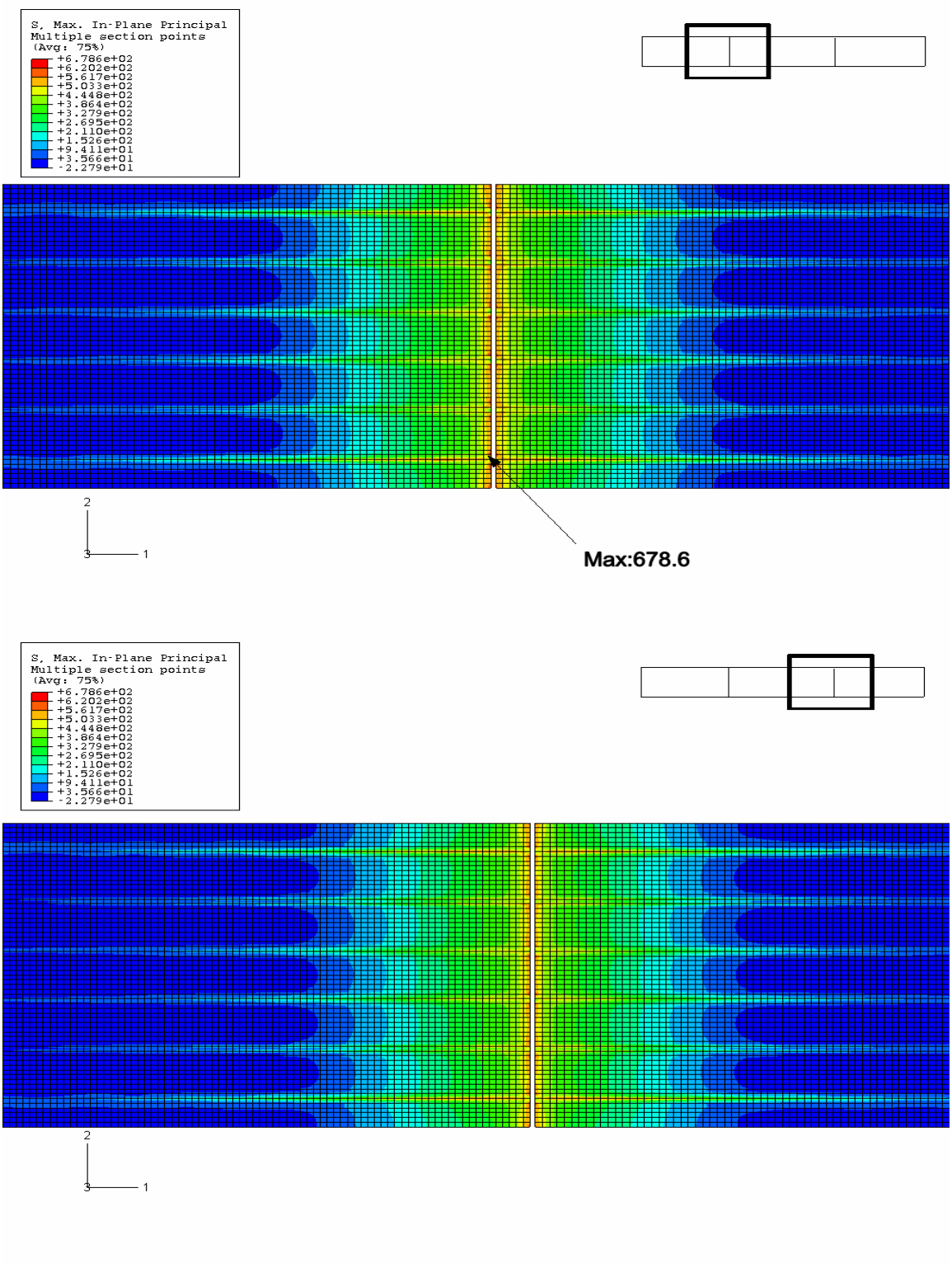

Figure 4.1 Maximum Principal Stress Distribution at Top of 0° Skewed Deck (psi)

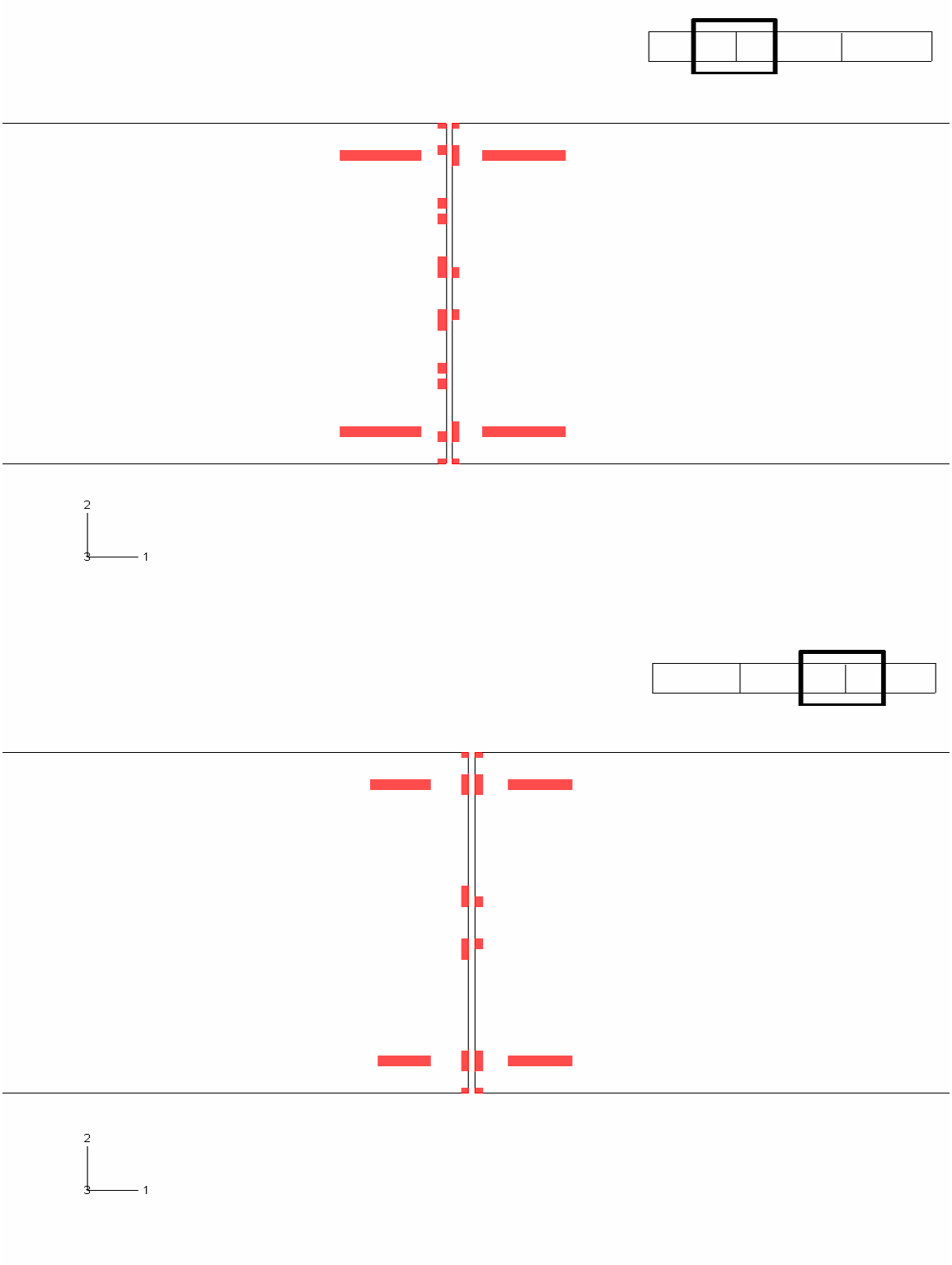

Figure 4.2 Cracking Zone at Top of 0° Skewed Deck

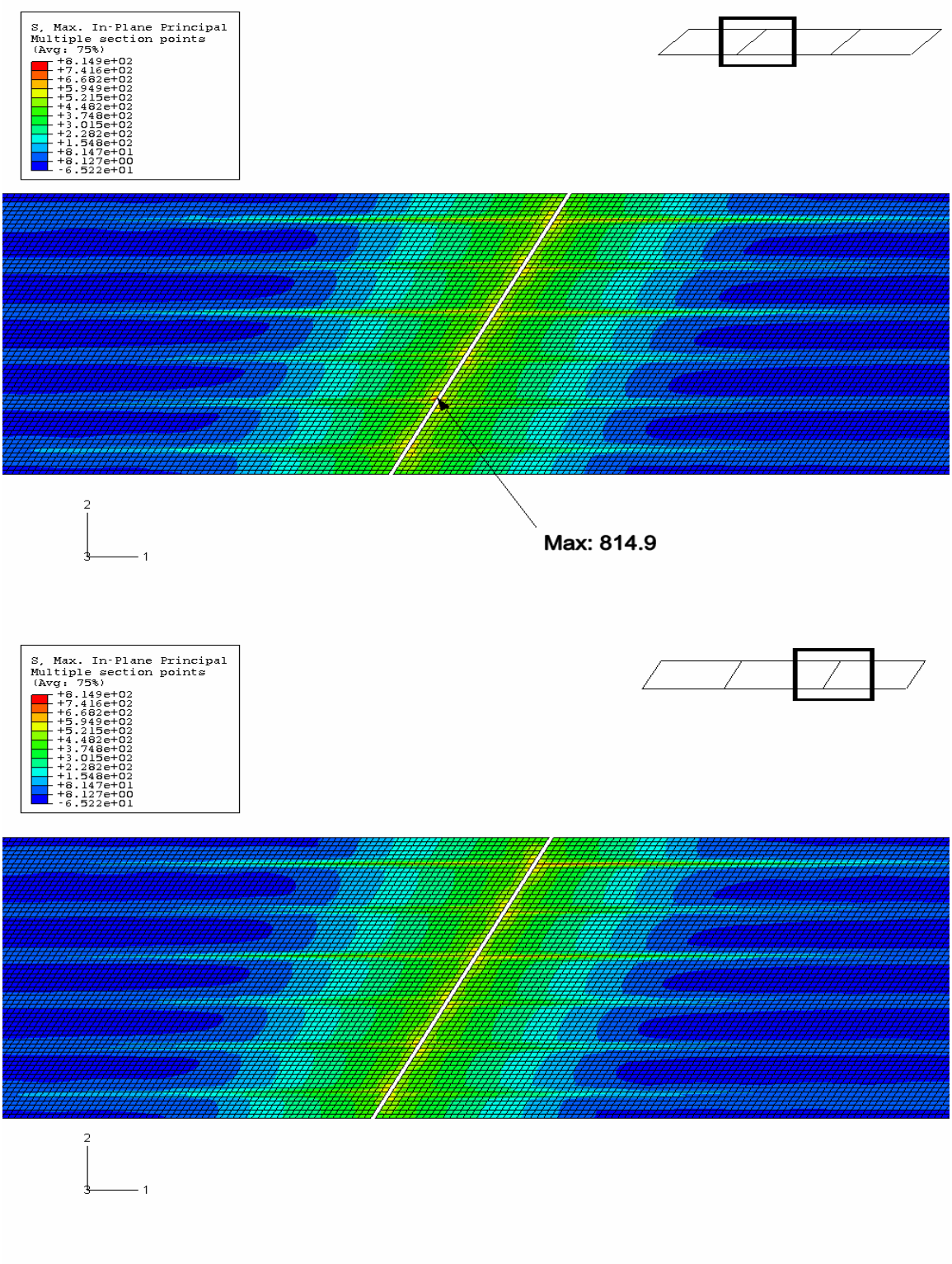

Figure 4.3 Maximum Principal Stress Distribution at Top of 30˚ Skewed Deck (psi)

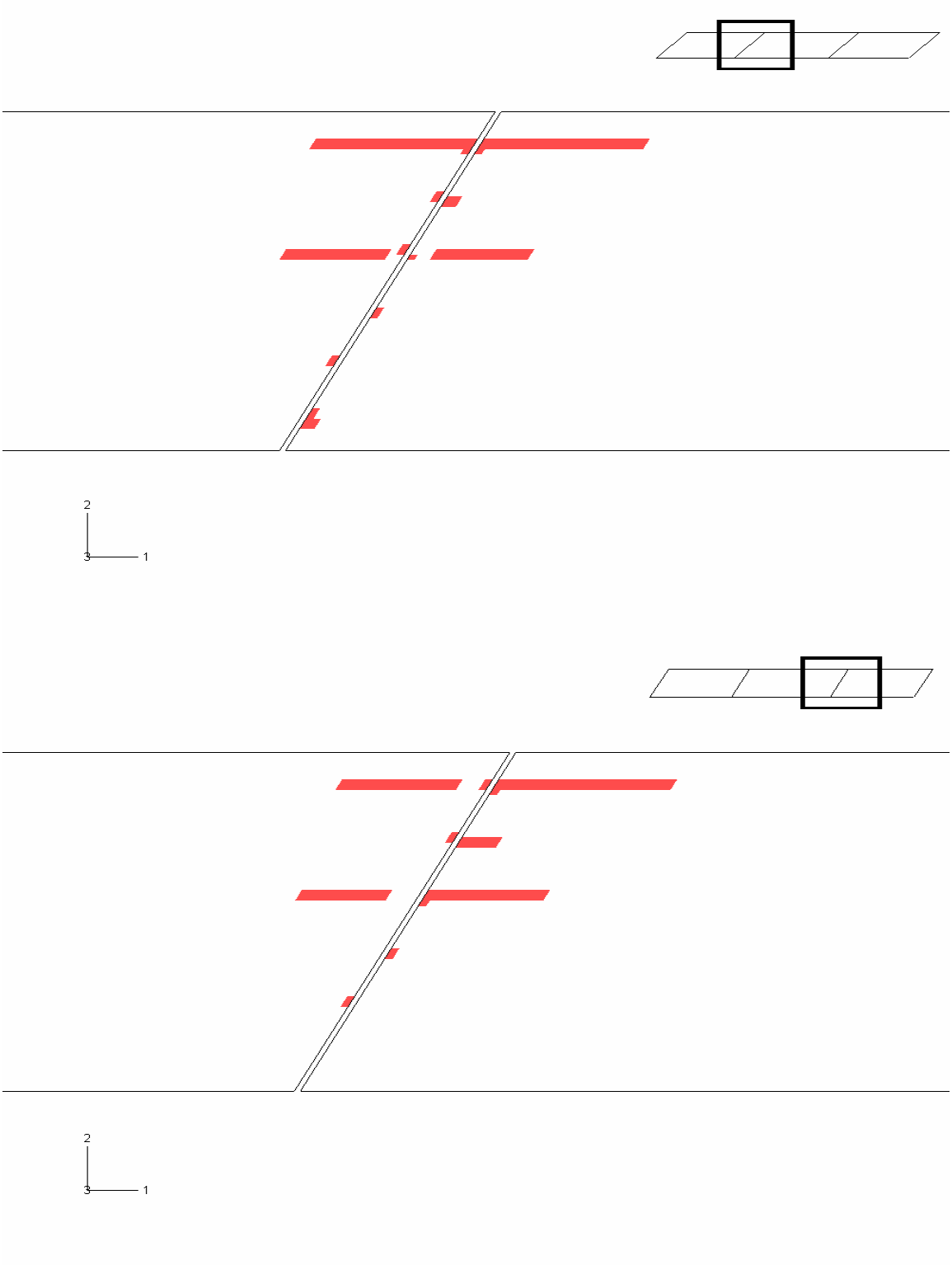

Figure 4.4 Cracking Zone at Top of 30° Skewed Deck

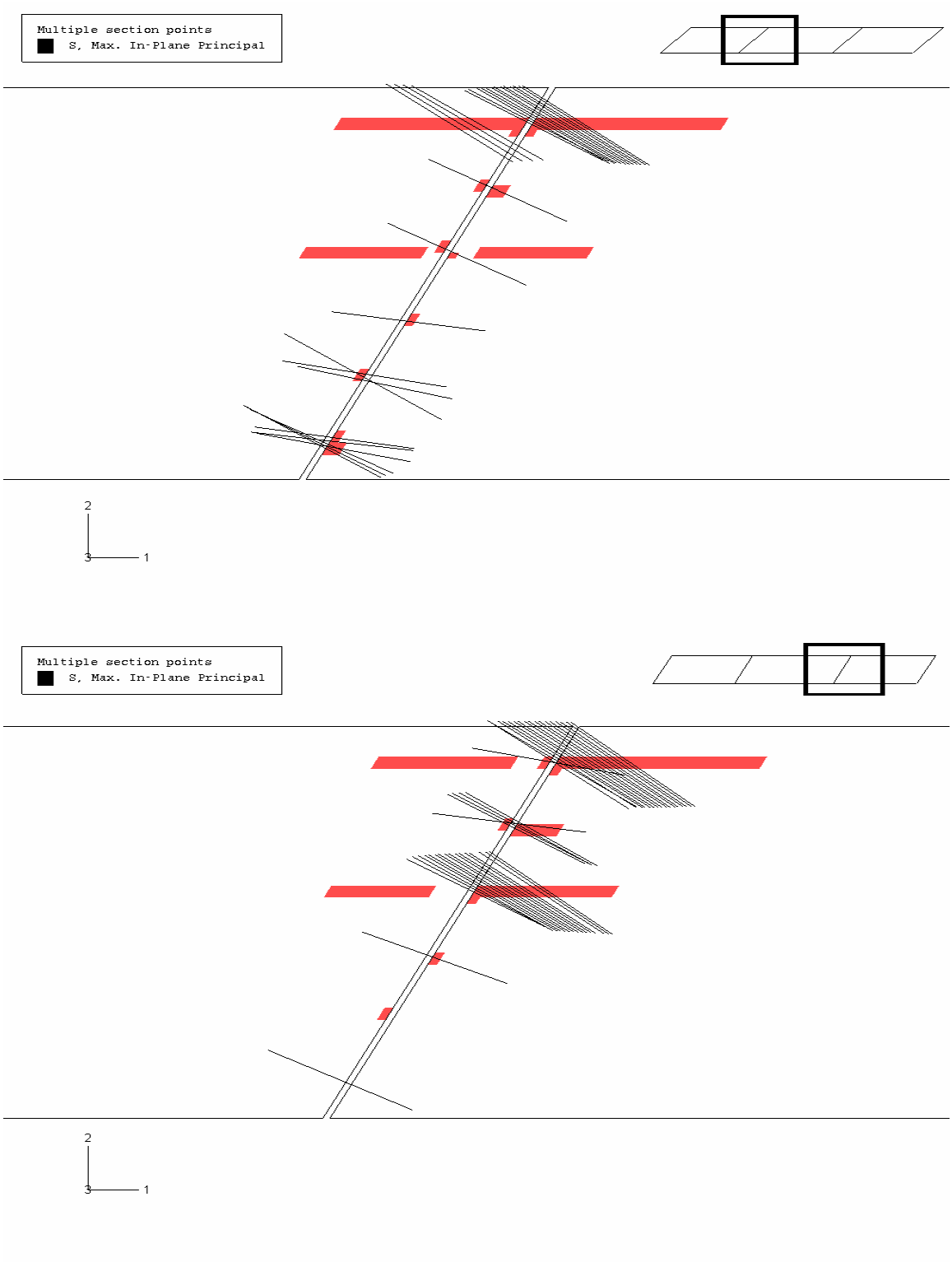

Figure 4.5 Normal Direction of Cracking (Black Lines) at Top of 30˚ Skewed Deck

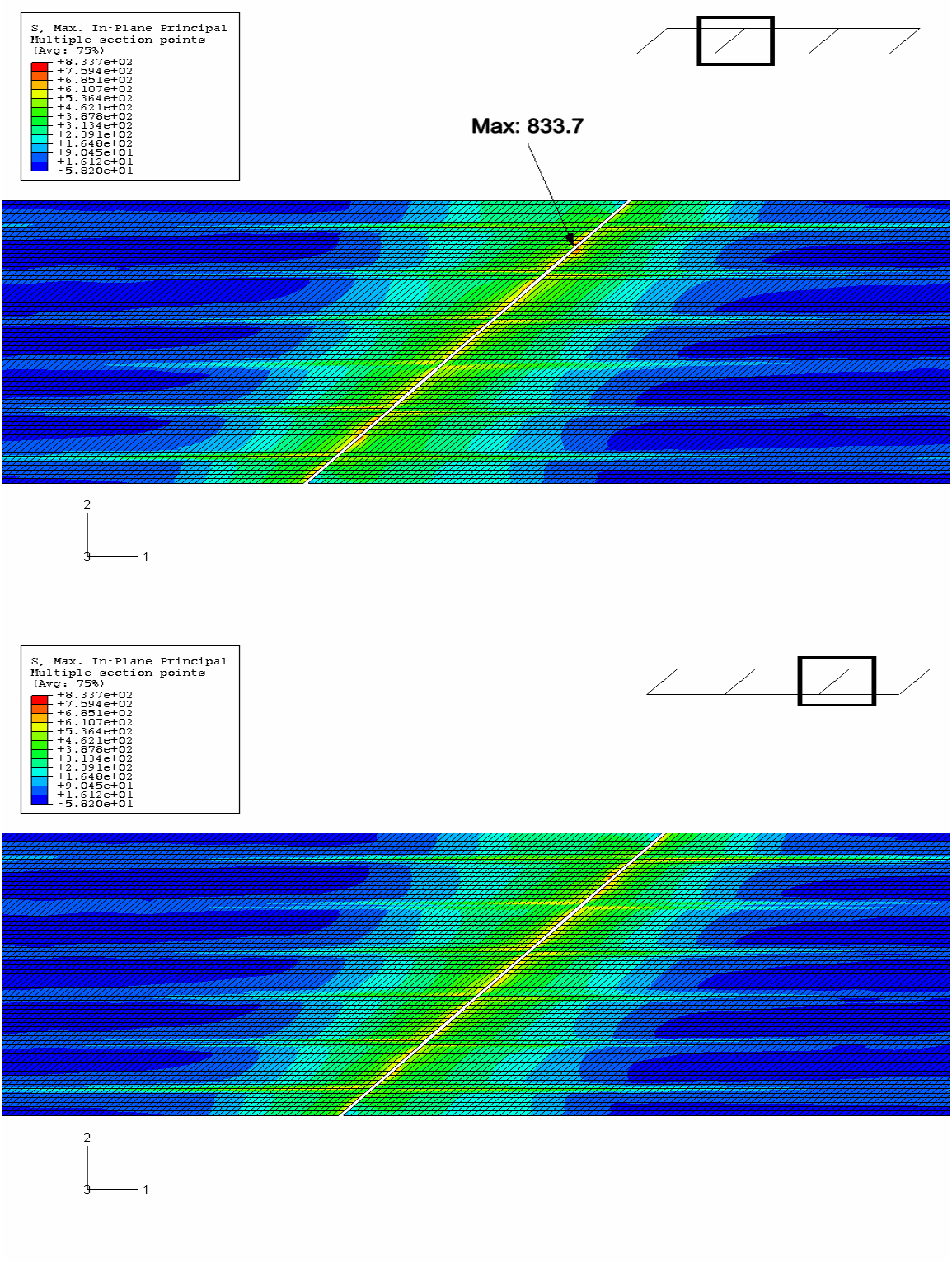

Figure 4.6 Maximum Principal Stress Distribution at Top of 45˚ Skewed Deck (psi)

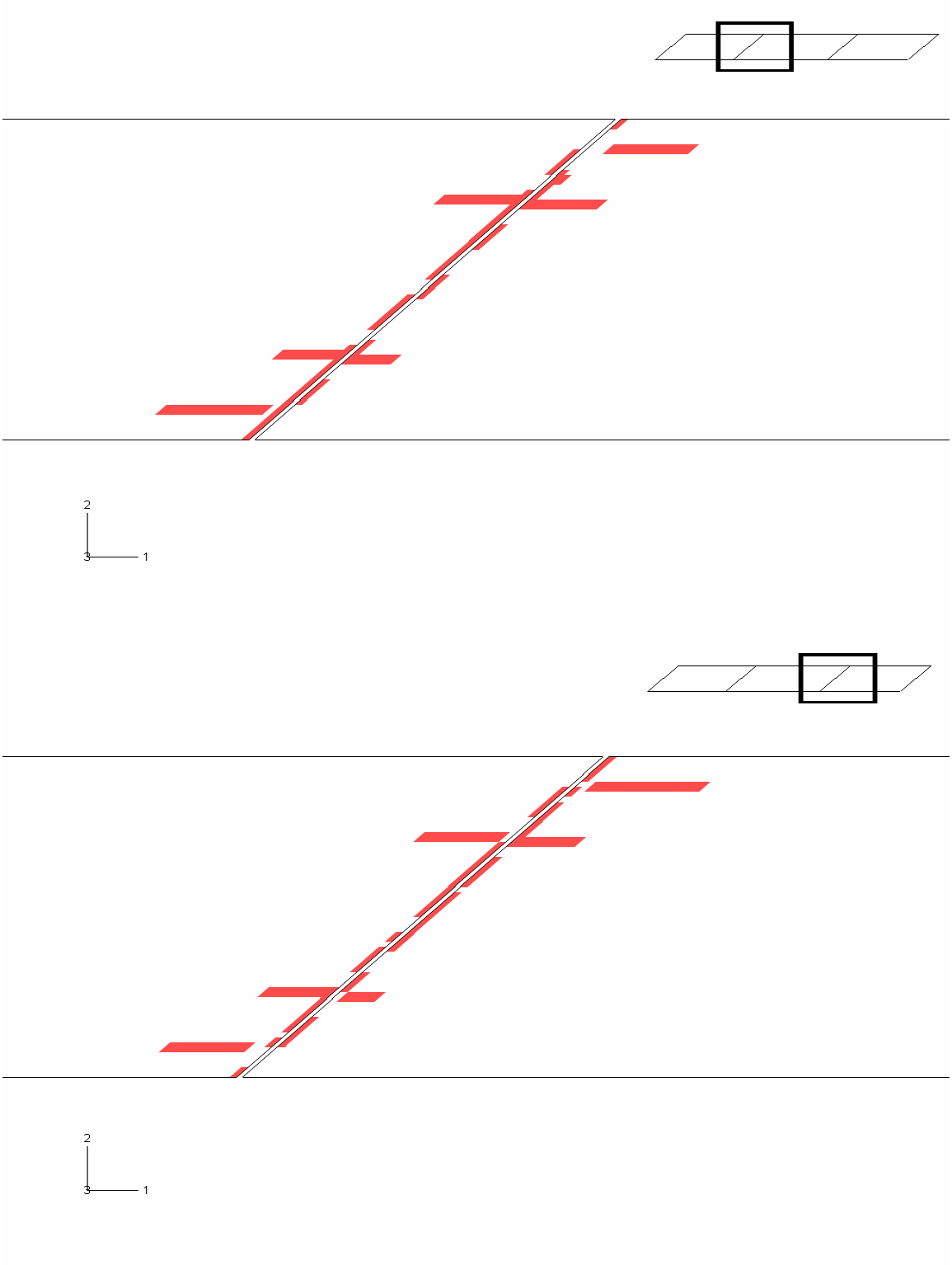

Figure 4.7 Cracking Zone at Top of 45° Skewed Deck

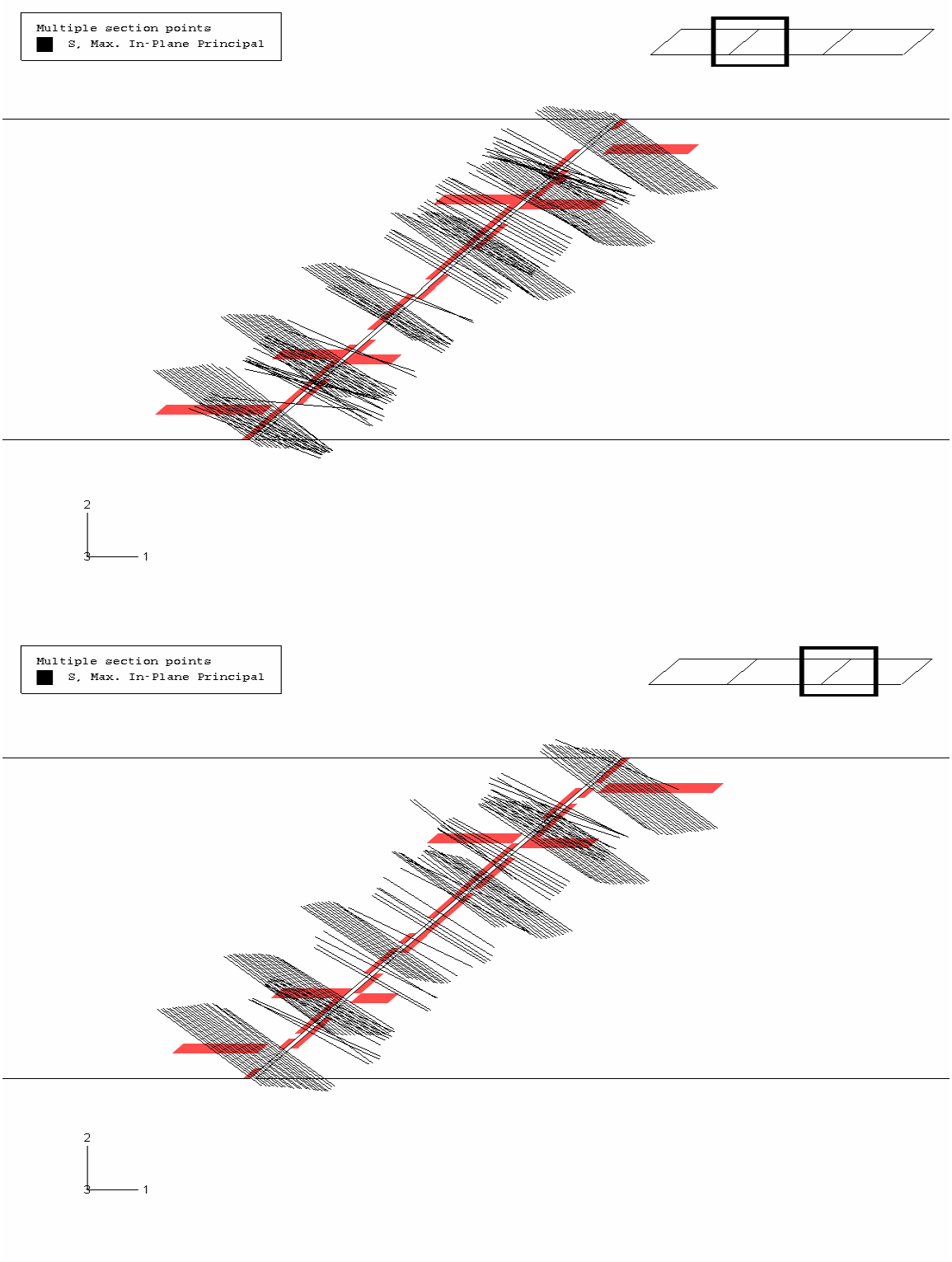

Figure 4.8 Normal Direction of Cracking (Black Lines) at Top of 45° Skewed Deck

Comparing these figures with the results obtained for the 61° skewed deck model of Chapter 3, one can clearly see that the skew angle does indeed have an effect on the cracking behavior of the deck. Figure 4.9 shows a summary of the cracking information for the deck at the southern-most intermediate support of the bridge, as the skew angle is varied.

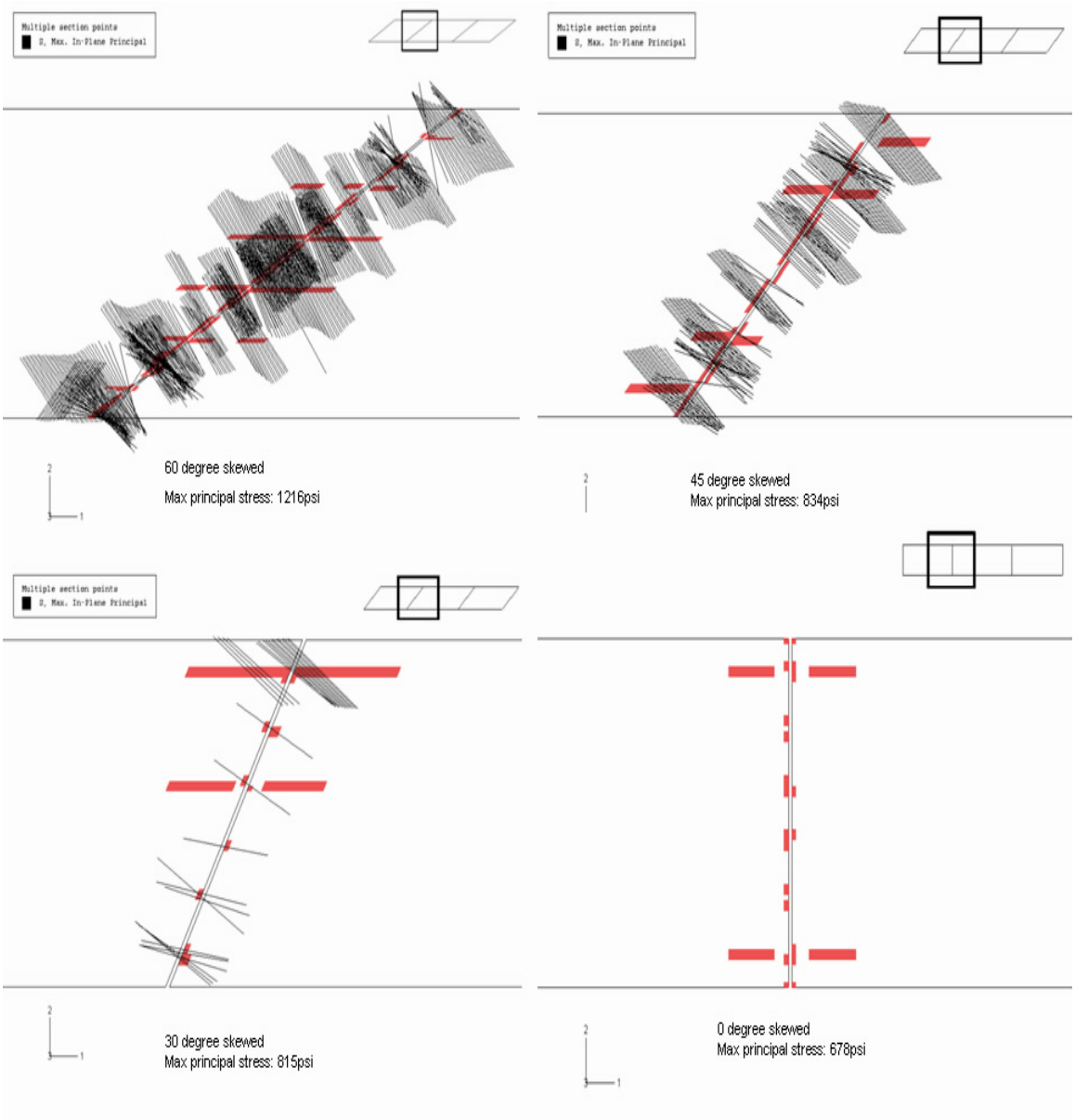

Figure 4.9 Cracking Information of the Deck at Southern-Most Intermediate Support

From the figure, it is readily evident that the value of the maximum principal stress within a skewed deck is notably higher than that for a similar, non-skewed deck. This phenomenon becomes somewhat extreme when the skew angle is as severe as 60 degrees, as was the case for the actual US 331 bridge deck. The black lines in the figures are the symbols representing the maximum principal stresses in elements which have reached cracking level. (It is observed that there are cracked elements indicated for the 0° skew case, but no black lines are present. This is again due to the slight difference between integration point stress values and nodal point stress values.) Additionally, as was mentioned earlier, the direction of the black lines represents the normal to the axis of cracking.

From these figures, one can see that the black lines become longer and more densely populated as the skew angle increases. Their direction also varies as the skew angle varies. These results indicate that a more highly skewed deck not only results in higher tensile stresses and more cracking at the top surface, but also that the distribution and direction of cracking is affected. The larger the skewed angle is, the greater the number of cracks and presumably, the wider the cracks will be as many of the individual cracks will likely coalesce into wider cracks. It is also interesting to note that the cracking zone exhibited a similar skew angle as the deck in each model.

4.2 Effect of Settlement

Differential settlement of the supports was another possible influential factor affecting the cracking observed on the US 331 bridge deck. The effect of support settlement was examined numerically through the incorporation of changes in the boundary conditions for the US 331 bridge model (discussed in Chapter 3). As shown in Table 4.1 below, four

combinations of the settlement of supports A, B, C and D (see Figure 4.10 for their locations) were imposed on the model to study their effect. A unit settlement (1 inch) was used in each of the four cases. Figures 4.11 to 4.26 show results for the deformation, stress distribution, and cracking information at the top of the deck for all of these settlement combinations. These models possessed the same characteristics, and the same load, as the base model discussed in Chapter 3.

Table 4.1 Combinations of Support Settlement for Parametric Study

	Support A	Support B	Support C	Support D
Case 1	0	0	0	↓
Case 2	0	0	↓	0
Case 3	↓	0	0	↓
Case 4	0	↓	↓	0

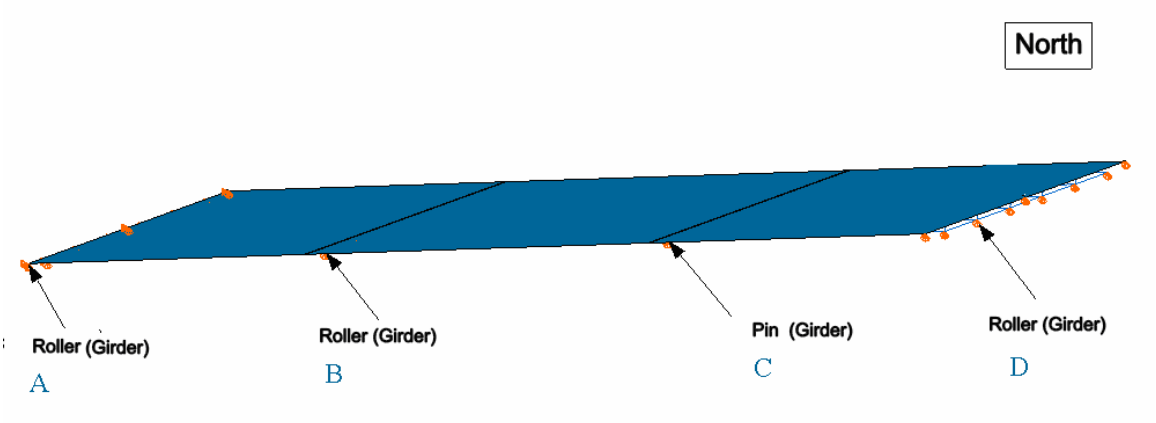

Figure 4.10 Locations of Supports A, B, C and D

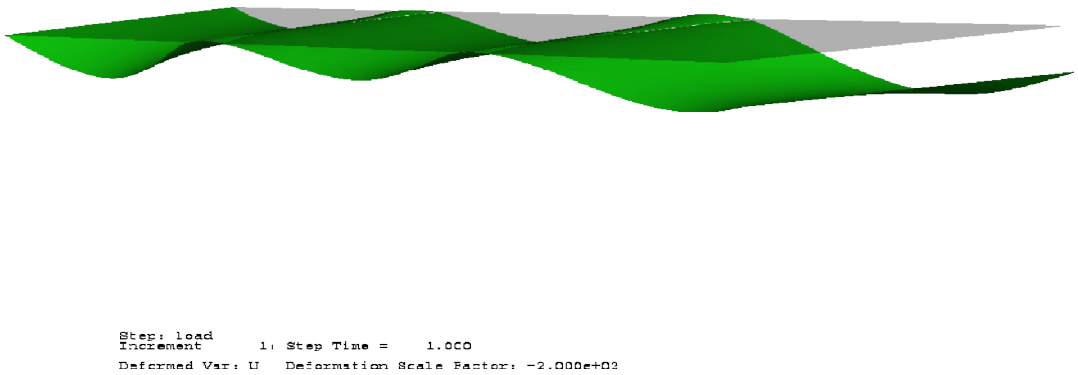

Figure 4.11 Deformed Shape for Case 1
(Green: Deformed Shape, Gray: Undeformed Shape)

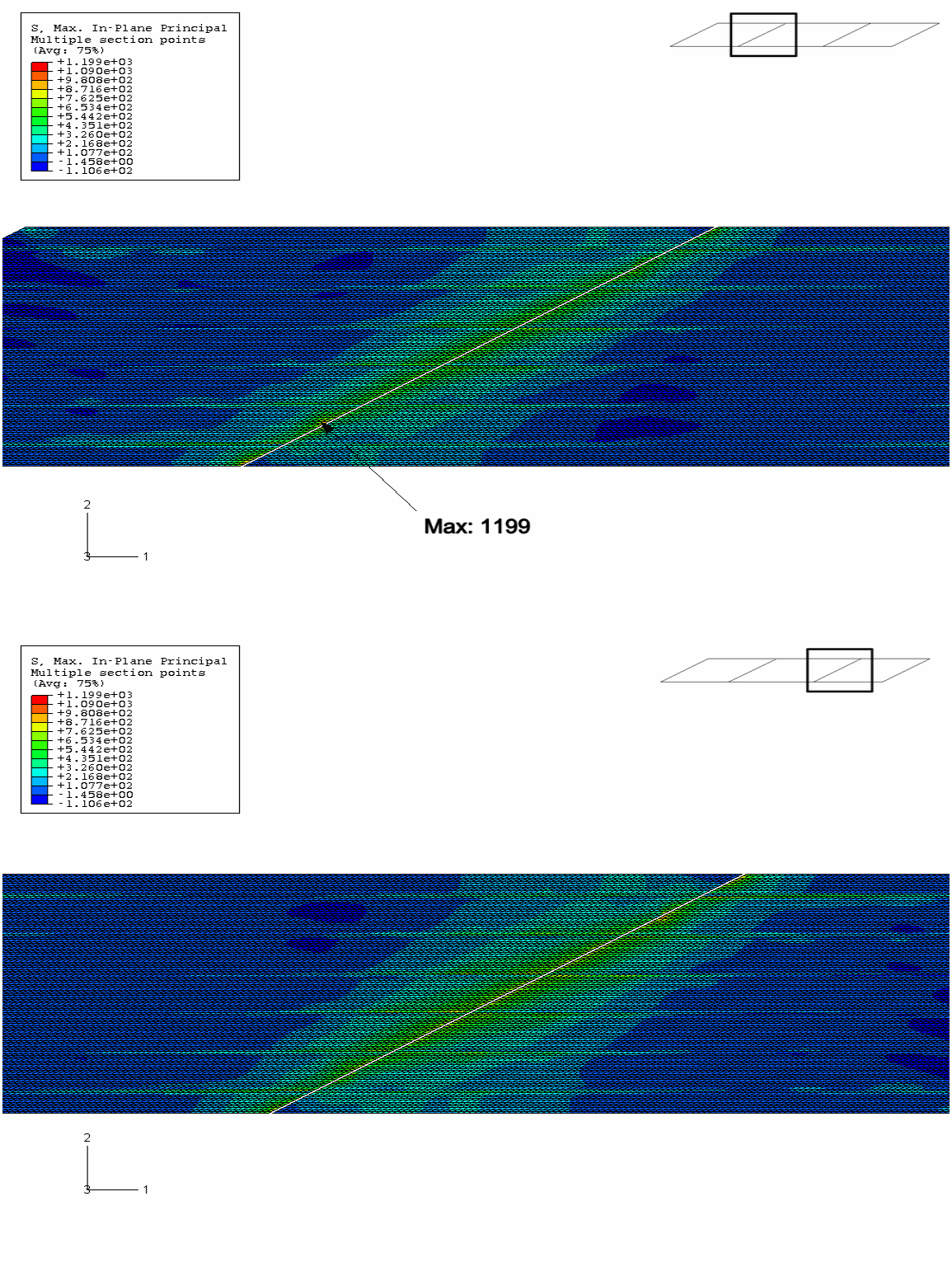

Figure 4.12 Maximum Principal Stress Distribution at Top of Deck for Case 1 (psi), $\alpha = 61°$

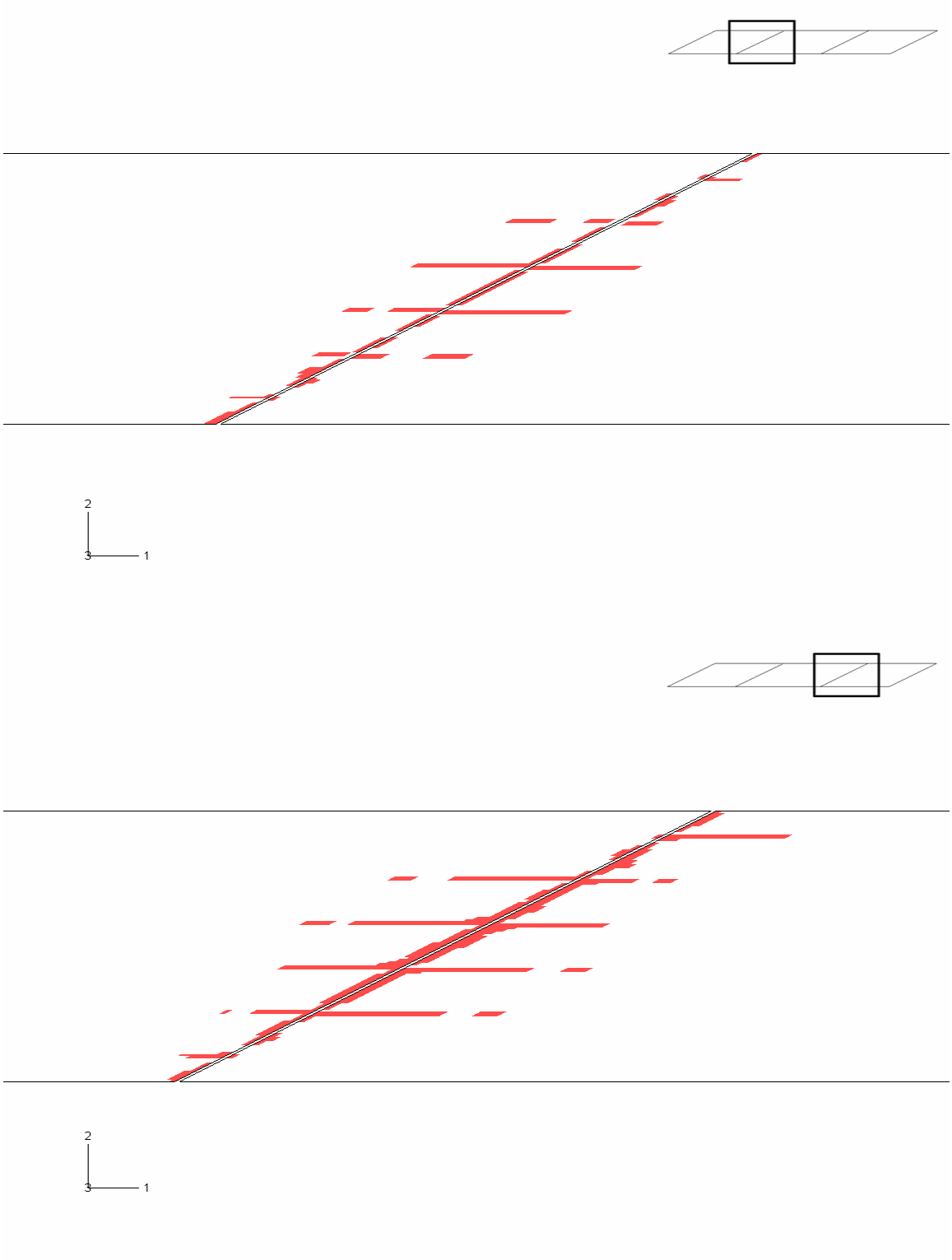

Figure 4.13 Cracking Zone at Top of Deck for Case 1, α = 61°

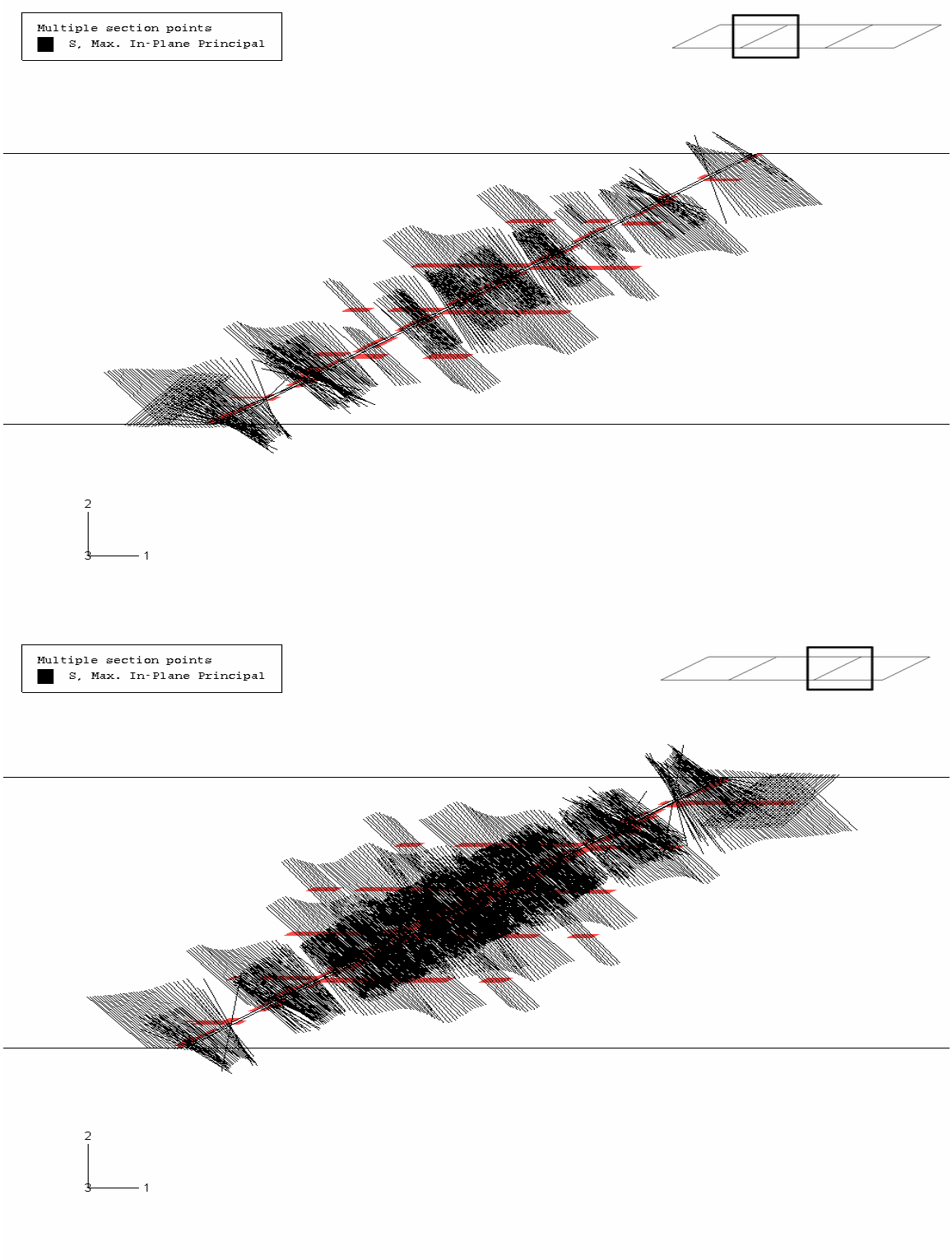

Figure 4.14 Normal Direction of Cracking (Black Lines) at Top of Deck for Case 1, $\alpha = 61°$

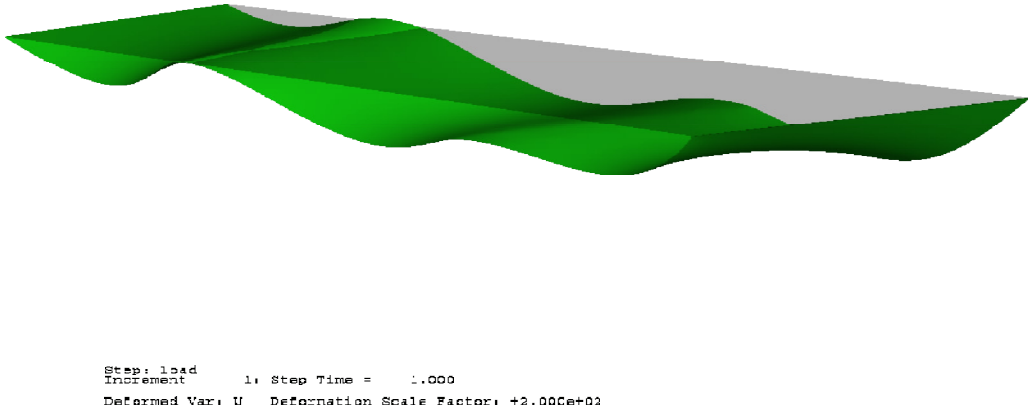

Figure 4.15 Deformed Shape for Case 2
(Green: Deformed Shape, Gray: Undeformed Shape)

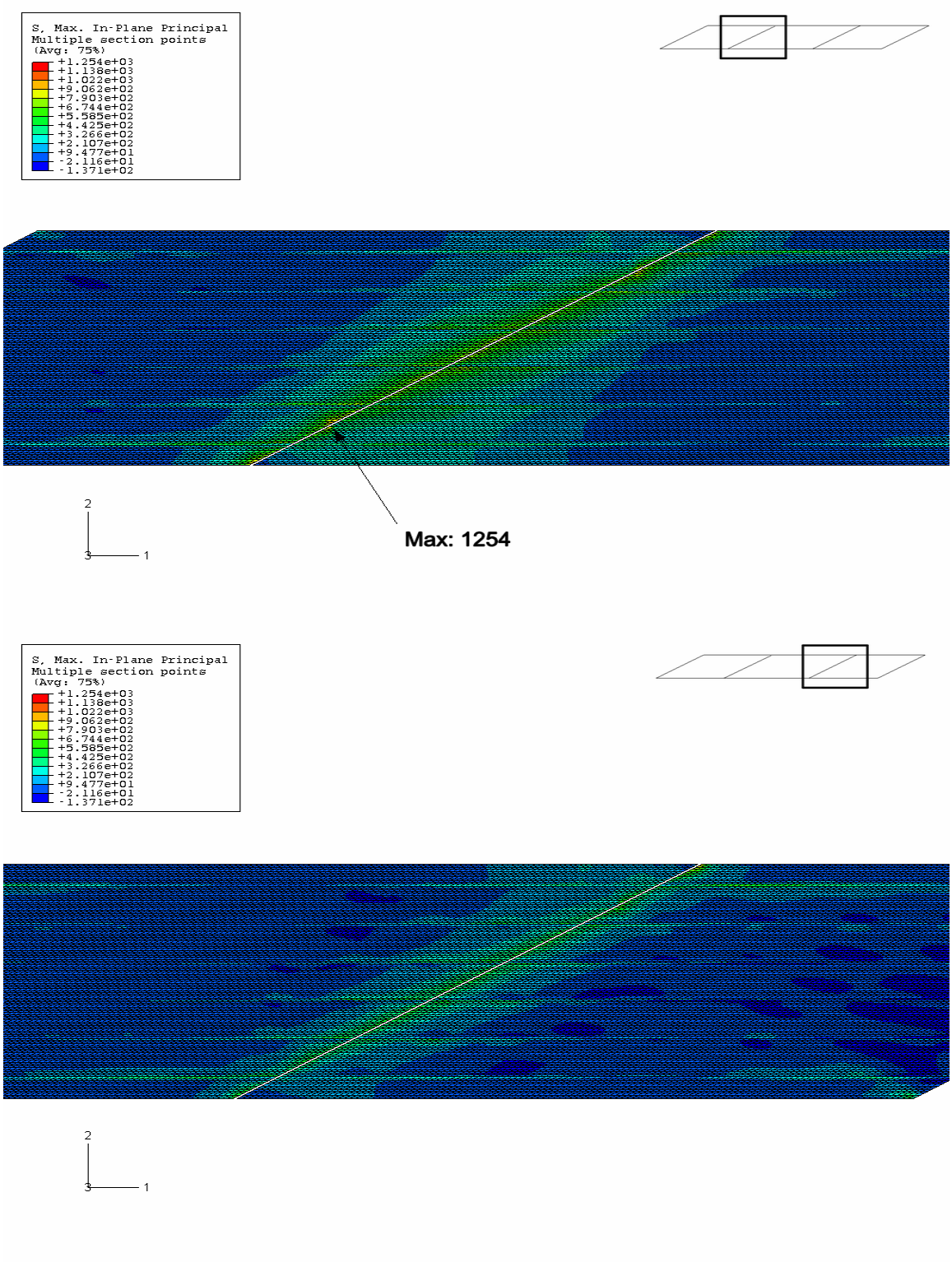

Figure 4.16 Maximum Principal Stress Distribution at Top of Deck for Case 2 (psi), $\alpha = 61°$

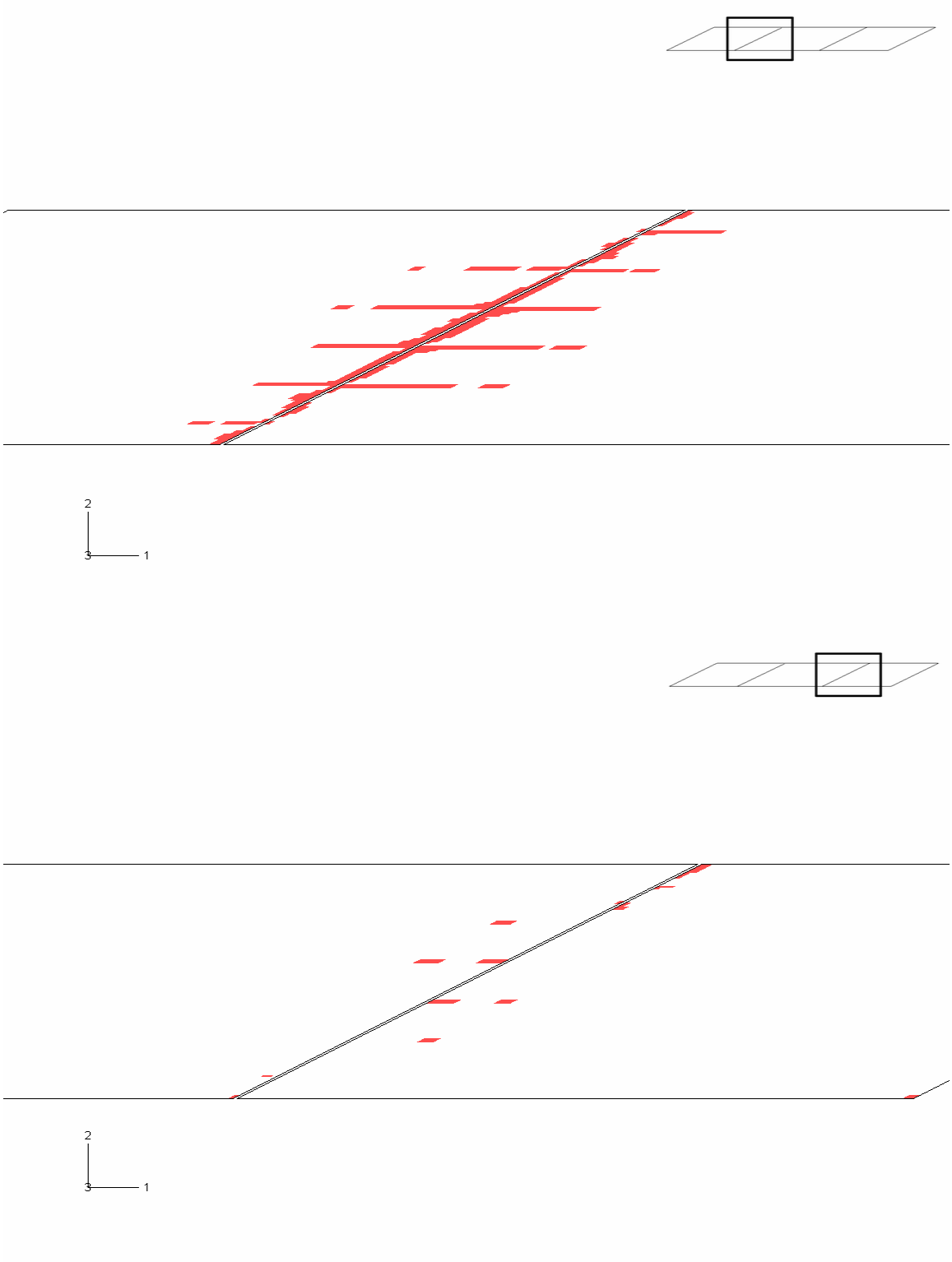

Figure 4.17 Cracking Zone at Top of Deck for Case 2, α = 61°

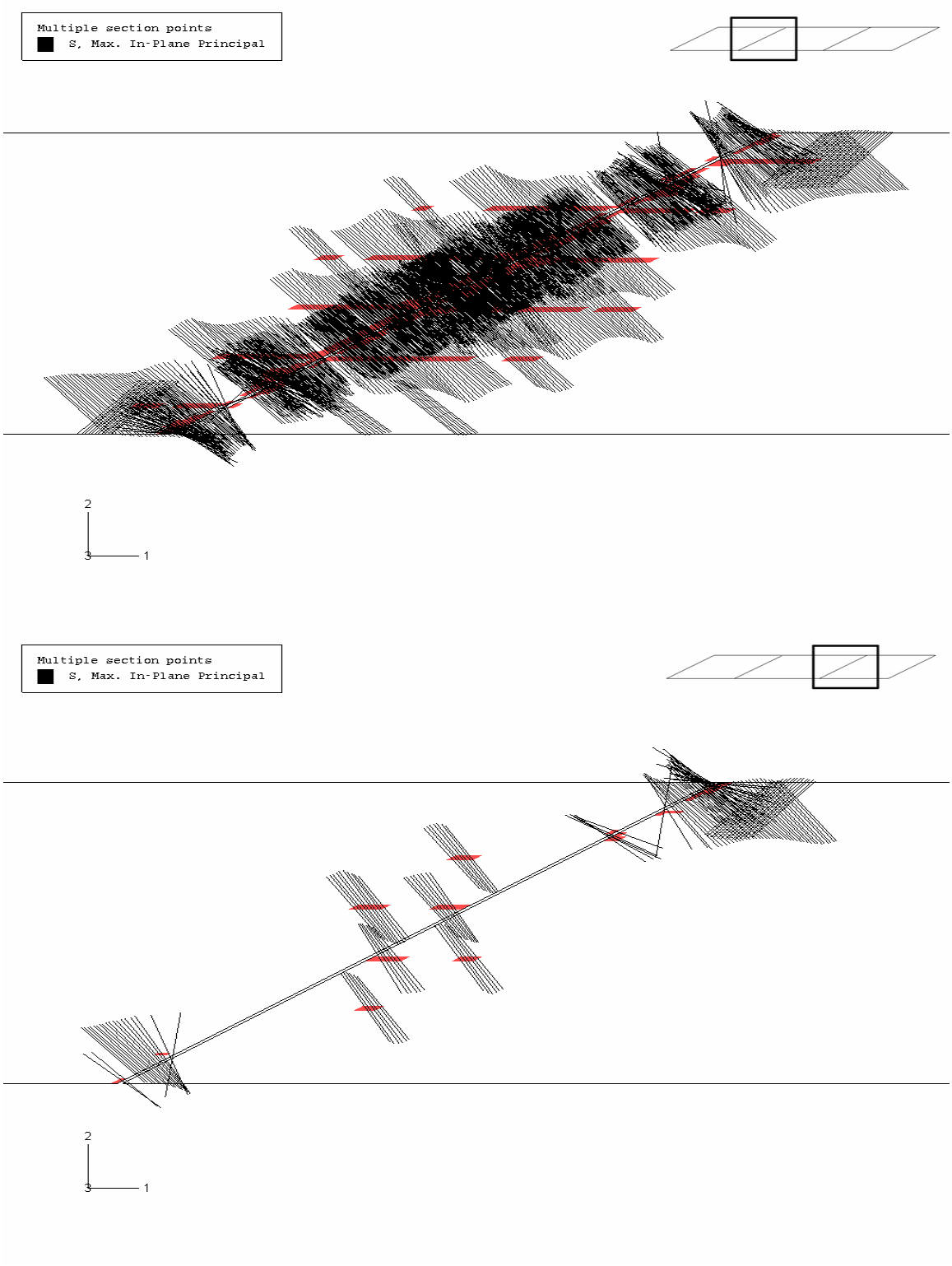

Figure 4.18 Normal Direction of Cracking (Black Lines) at Top Deck for Case 2, α = 61°

Figure 4.19 Deformed Shape for Case3
(Green: Deformed Shape, Gray: Undeformed Shape)

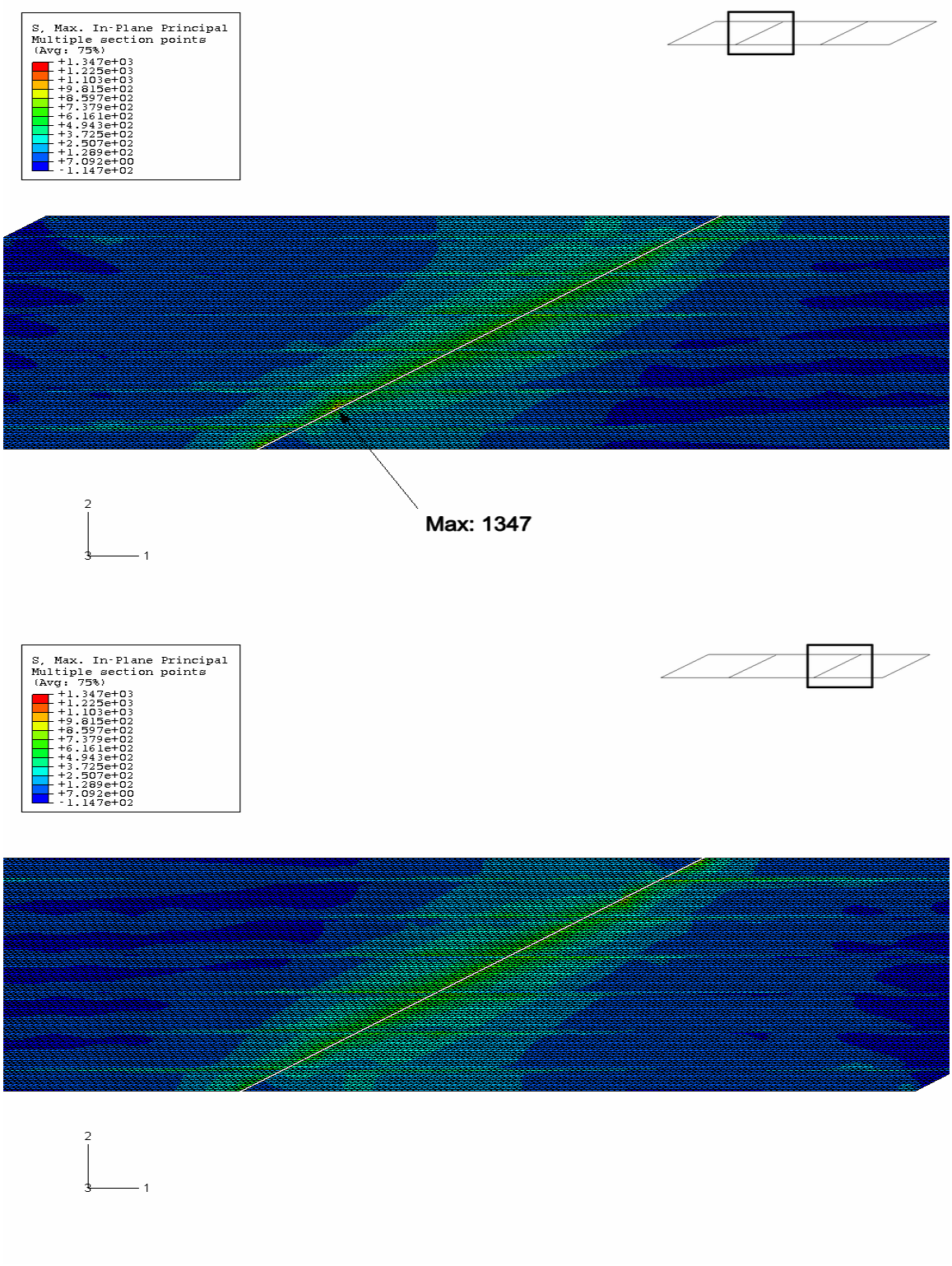

Figure 4.20 Maximum Principal Stress Distribution at Top of Deck for Case 3 (psi), $\alpha = 61°$

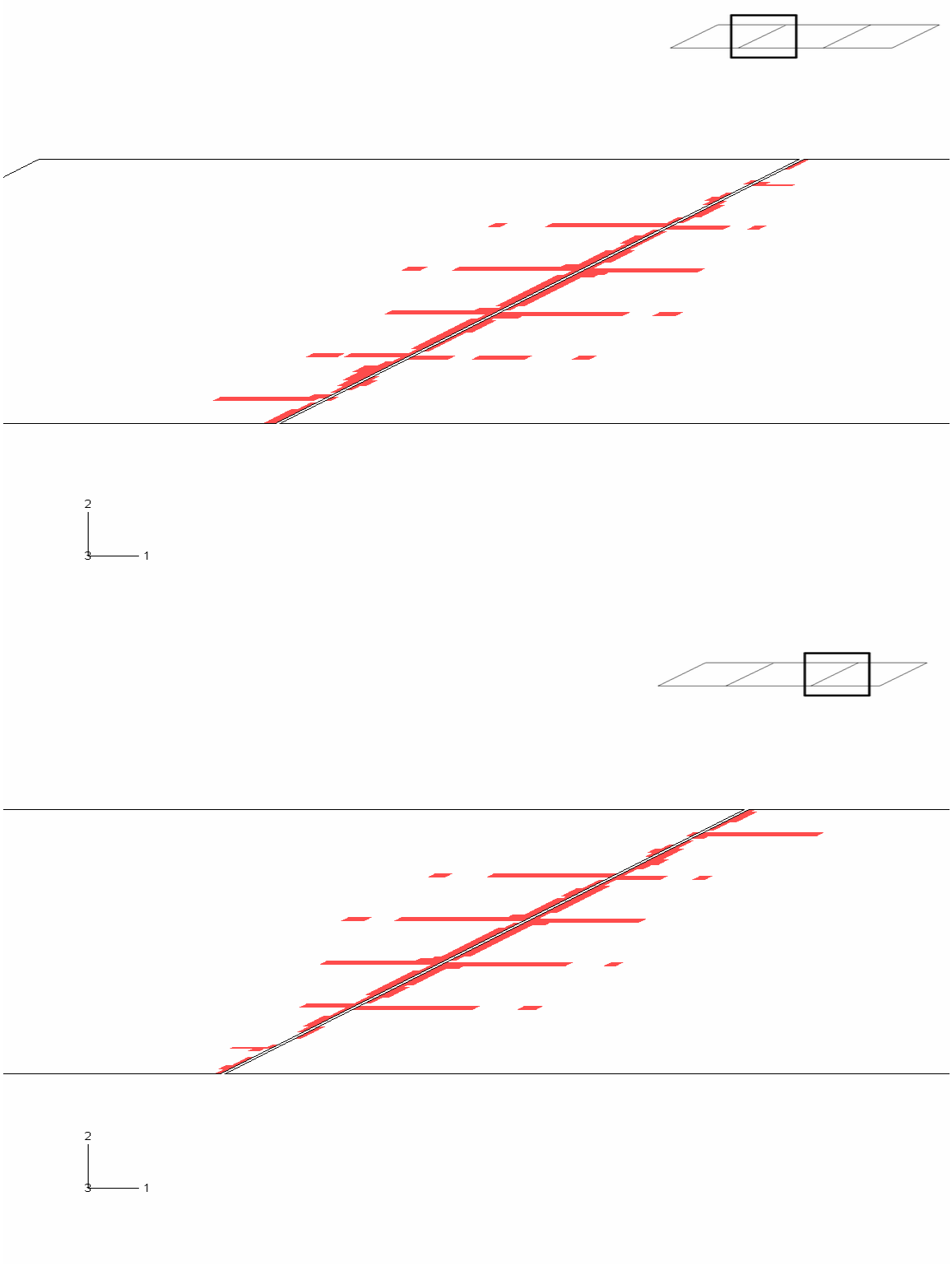

Figure 4.21 Cracking Zone at Top of Deck for Case 3, α = 61°

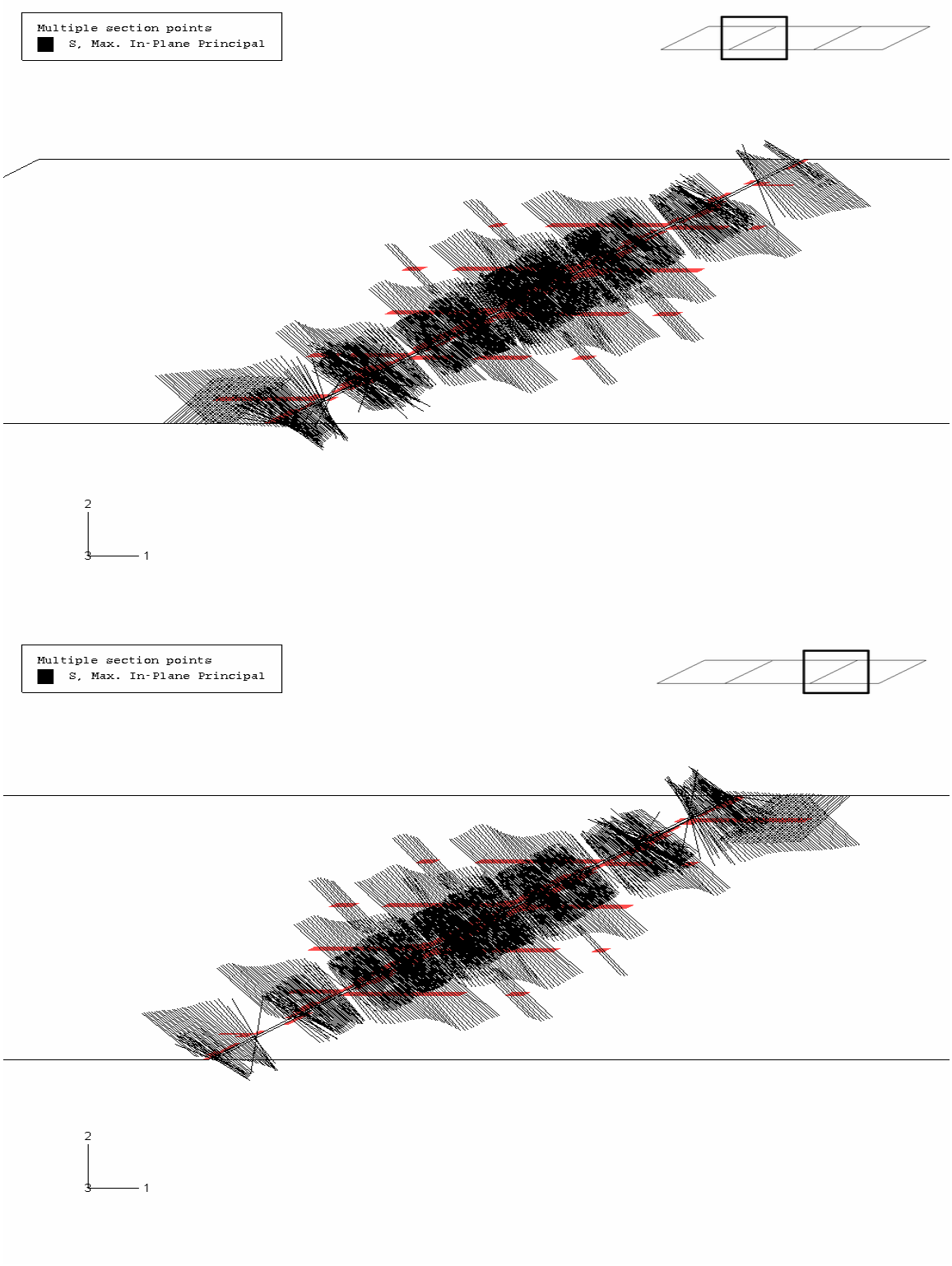

Figure 4.22 Normal Direction of Cracking (Black Lines) at Top Deck for Case 3, α = 61°

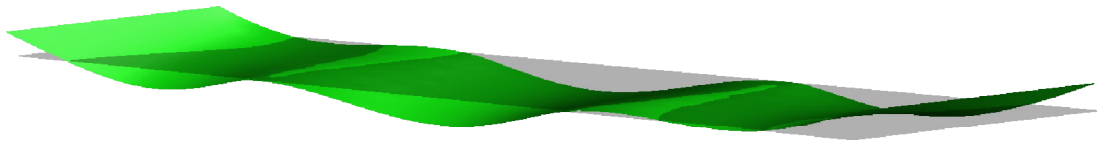

Figure 4.23 Deformed Shape for Case 4
(Green: Deformed Shape, Gray: Undeformed Shape)

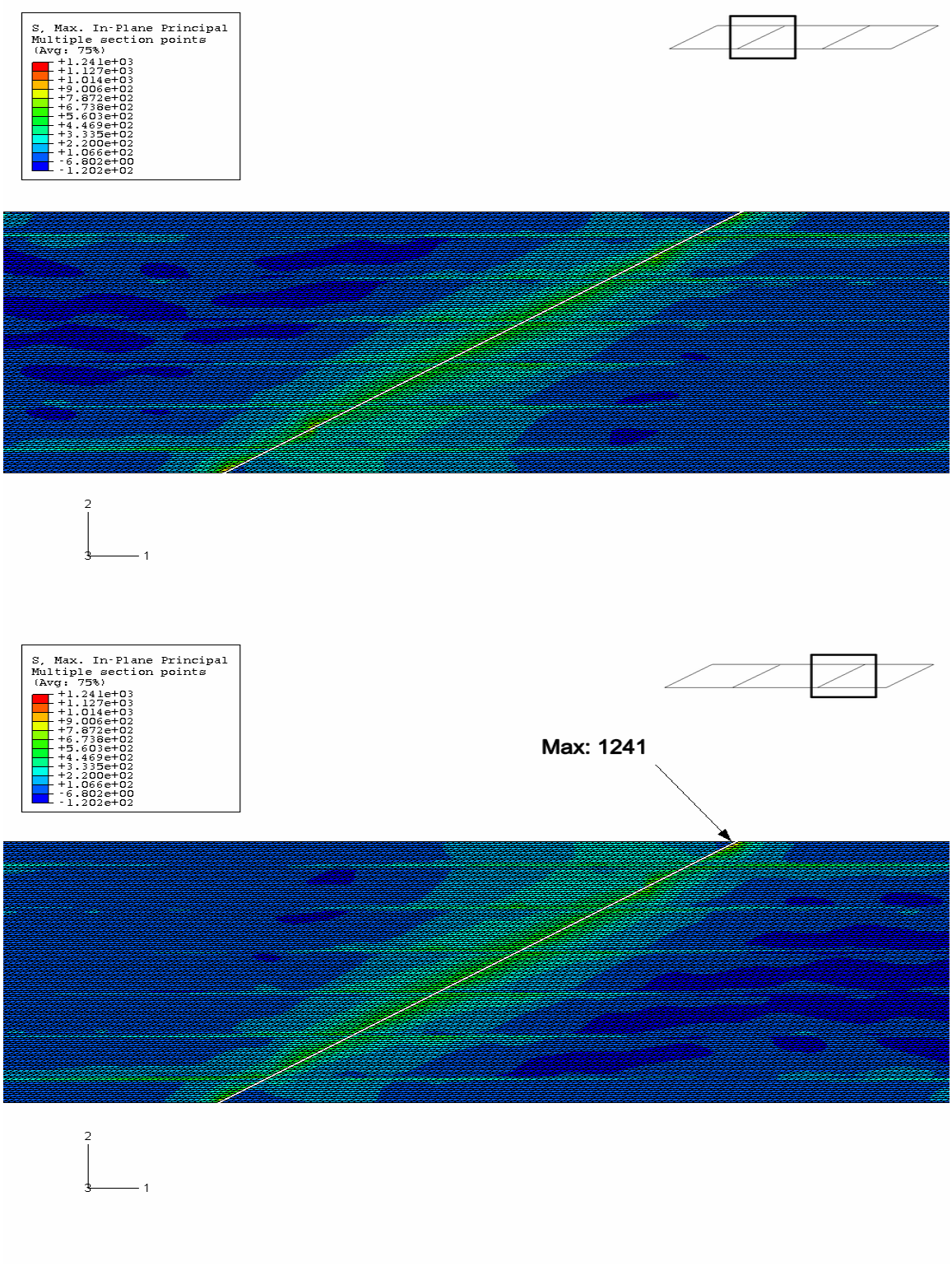

Figure 4.24 Maximum Principal Stress Distribution at Top of Deck for Case 4 (psi), $\alpha = 61°$

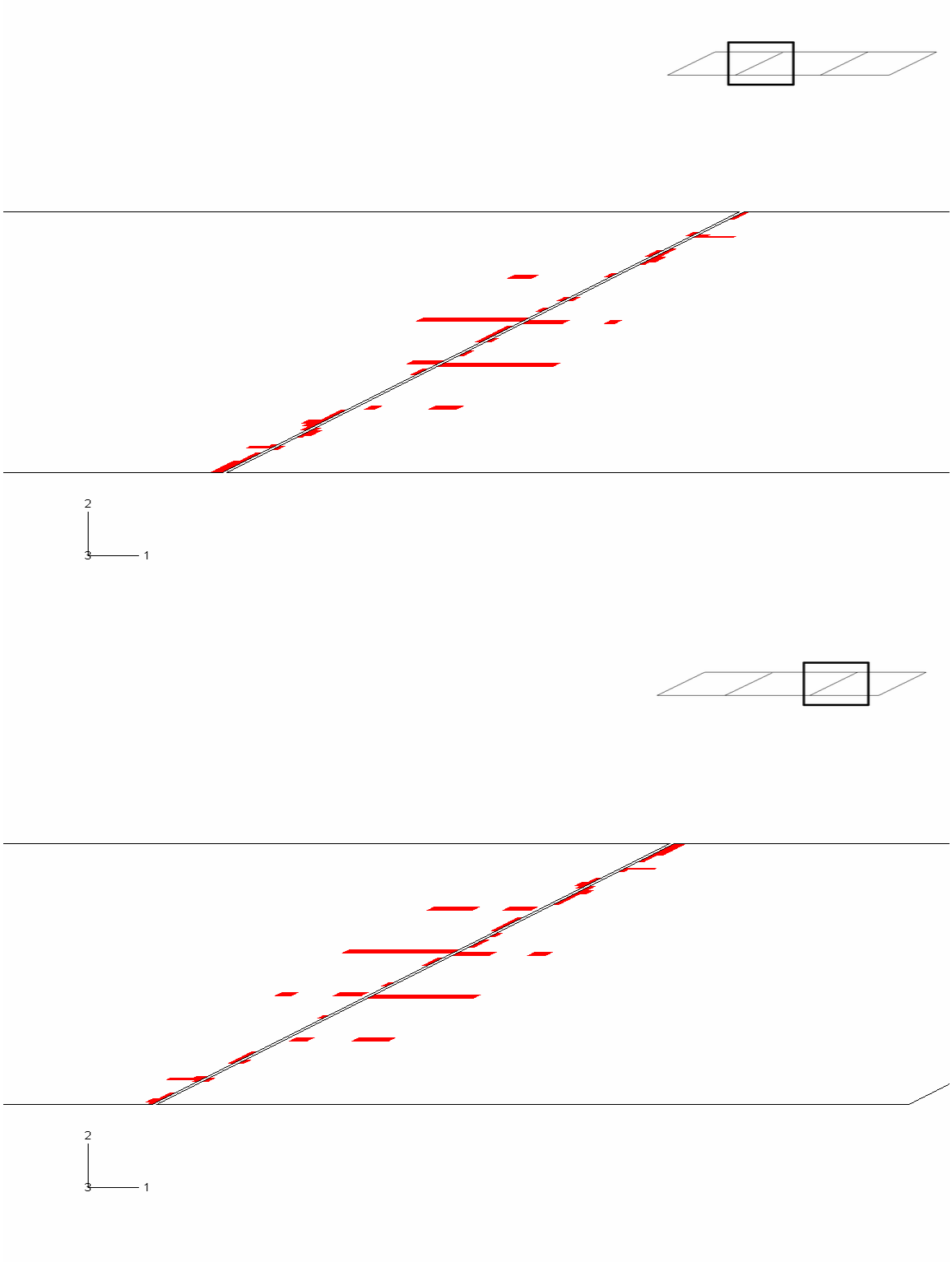

Figure 4.25 Cracking Zone at Top of Deck for Case 4, α = 61°

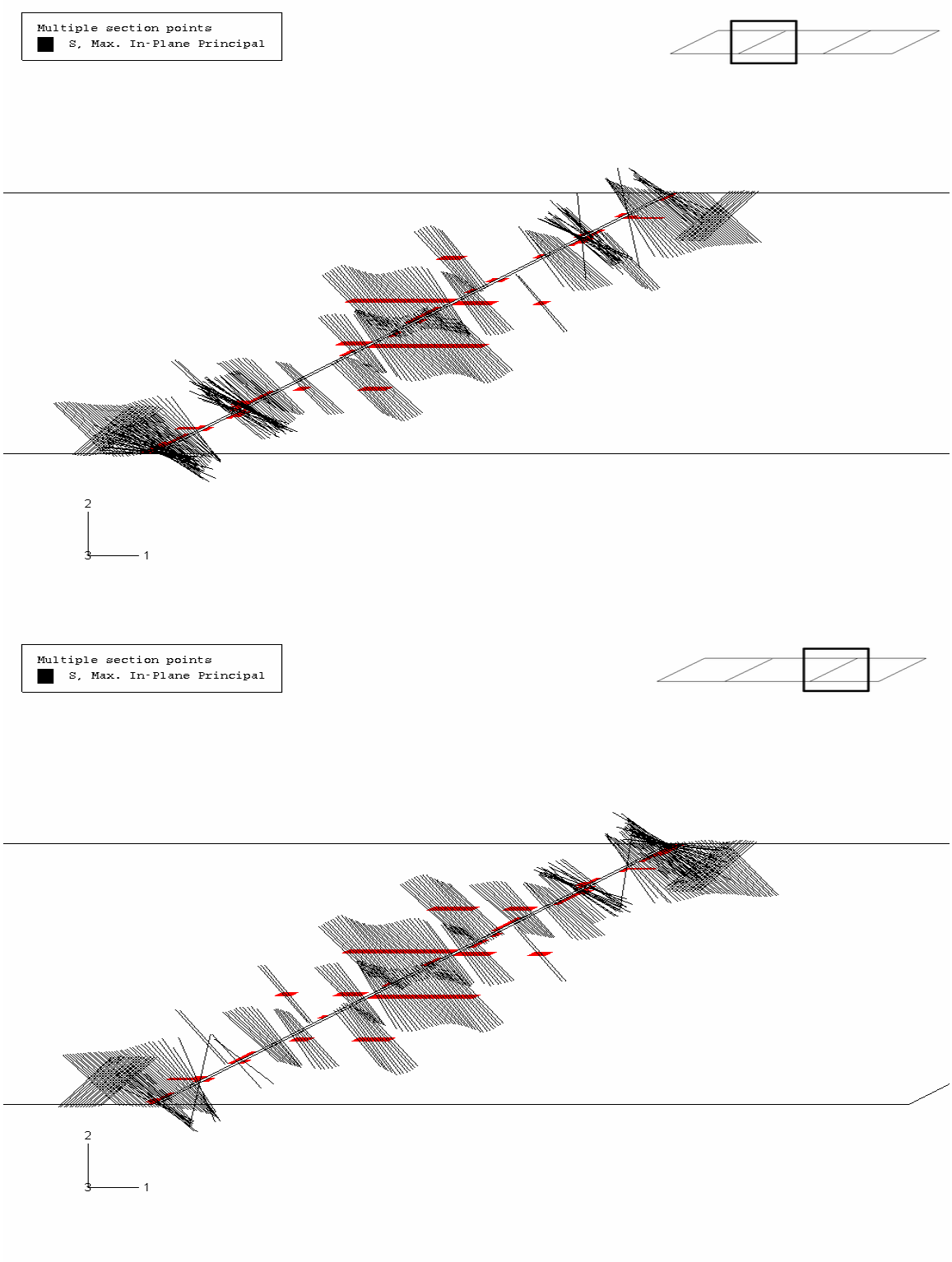

Figure 4.26 Normal Direction of Cracking (Black Lines) at Top Deck for Case 4, α = 61°

Analysis of the figures above shows that the unit support settlement combinations did have some effect on the level of stress and cracking behavior of the deck, but did not seem to produce a very considerable variation in the magnitude of tensile stress. Increasing the settlement's magnitude would certainly increase the magnitudes of the stress levels on the deck.

One can also observe that the stress contours and the cracking distribution did not change very much with the different settlements imposed in Cases 1 and 3. However, in Cases 2 and 4, the crack distribution was more noticeably different than the other cases. This is due to the fact that, in Case 2, the deck didn't undergo equal deformations at two intermediate supports, producing the "uneven" nature of the settlement (shown graphically in Figure 4.15). As a result, the deck portion experiencing less deformation carried less tensile stress, and exhibited less cracking.

As for Case 4, it is noticed that the number of cracks produced was much less than that for Cases 1 and 3. That is because, for Case 4, both intermediate supports experienced less deformation than in Cases 1 and 3, and consequently carried less tensile stress under this settlement combination, as shown in Figure 4.24.

These phenomena seem to indicate that if differential settlement occurred at critical areas of the deck, such as at the intermediate support locations, where the deck is in tension under gravity loading, the tensile stress distribution on the deck would be altered (from the results for the case with no differential settlement) and would result in a modified cracking behavior. For this particular type of multi-span, continuous deck bridge, the settlement at the intermediate supports appears to actually be helpful in reducing the cracking of the deck. Furthermore, the results indicate that single

intermediate support settlement (Case 2) is good, and double support settlement (Case 4) is better. However, it is not suggested to use different intermediate supports settlement to avoid cracking because it may cause other unsafe structural behavior in the bridge and affect the service quality of the bridge.

CHAPTER 5 SMEARED CRACK CONCRETE MODEL

A further advancement was made to the baseline US331 bridge model detailed in Chapter 3. The concrete material properties were modified, to specify that the smeared crack concrete model of ABAQUS be utilized. Use of this material model includes the capability not only of incorporating nonlinear material properties for a nonlinear numerical analysis, but also of predicting the crack distribution and crack directions automatically.

5.1 Smeared Crack Concrete Model Description

The following is the description of the smeared crack concrete model provided in the ABAQUS Manual:

> "The smeared crack concrete model in ABAQUS provides a general capability for modeling concrete in all types of structures. As a ‘smeared’ model, it does not track individual 'macro' cracks. Constitutive calculations are performed independently at each integration point of the finite element model. The presence of cracks enters into these calculations by the way in which the cracks affect the stress and material stiffness associated with the integration point. Cracking is assumed to occur when the stress of the element reaches the 'crack detection surface' which is a linear relationship between the equivalent pressure stress and the Mises equivalent deviatoric stress. As soon as the crack detection surface has

been activated, the crack direction is taken to be the direction of that part of the maximum principal plastic strain. Following the crack detection, the crack affects the response of the model because a damage elasticity model is used (ABAQUS 2006)."

5.2 Concrete Material Modeling

As stated above, nonlinear concrete material properties were considered for the bridge model in this portion of the study. Figure 5.1 shows the tensile stress-strain relationship used for the bridge deck concrete. The tensile behavior is defined as a linear elastic material until the stress reaches f_{tu}, the cracking stress of the concrete. Then, a linear softening model is used to represent post-cracking behavior using the "tension stiffening" option of ABAQUS. This option allows the user to define the strain-softening behavior for cracked concrete, and also allows for the effects of the reinforcement's interaction with concrete (bond behavior) to be simulated.

Figure 5.1 Tensile Stress-Strain Relationship for Concrete in ABAQUS (adapted from ABAQUS, 2006)

Details of the parameters that were specified for concrete material properties as input for ABAQUS are given in Table 5.1 below.

Table 5.1 Concrete Material Properties

Young's modulus	4.42×10^6 psi
Density	0.086 lb/in^3
Poisson's ratio	0.15
Yield stress (compression)	3000 lb/in^2
Failure stress (compression)	6000 lb/in^2
Plastic strain at failure (compression)	1.5×10^{-3}

ABAQUS uses a Rankine criterion to detect crack initiation, and to define a crack detection surface, then computes the value of f_{tu} in Figure 5.1 above from that crack detection surface. Based on that value of f_{tu}, and the modulus of elasticity, the value for ε_u is determined. A value is also supplied to ABAQUS to specify the amount of strain between ε_u and ε_0; for the model herein, this "span" of strain for the descending portion of the curve was defined to be 0.002. Finally, a user-defined value of the ratio of remaining stress to current cracking stress is provided to ABAQUS as input for the point at the apex of the triangle in Figure 5.1, and at the point where the descending branch of the curve meets the horizontal axis. For the present model, that ratio was defined as 1 for the apex, and 0 for the rightmost point of the triangle.

5.3 Results and Analysis of Results for Smeared Crack Bridge Model

As stated above, the smeared crack material model was used to replace the previous linear elastic concrete material utilized for the bridge model detailed in Chapter 3, for the same loading. The resulting maximum principal stress distribution is presented in Figure 5.2, and the maximum principal strain contour is presented in Figure 5.3. The maximum principal strain contour was plotted for this model because for the smeared crack model,

a certain value of stress could occur either in the pre-cracking or post-cracking stage, and there is no way to distinguish which is reported in the stress contour at each location. Therefore, strain was deemed to be more indicative of the deck behavior for this model. (However, maximum principal stress values are provided for "completeness," so that the same information is provided for this model as was provided for the previous models.)

A relatively coarse mesh was used for this model to avoid the mesh sensitivity mentioned in the ABAQUS manual associated with smeared cracking concrete models that utilize very fine meshes. The manual states that the finite element predictions have difficulty converging to a unique solution because increasing mesh refinement leads to narrower crack bands, which presents a problem since "specification of strain softening behavior in reinforced concrete generally means specifying the post-failure stress as a function of strain across the crack" (ABAQUS 2006).

For this smeared cracking model, the length of the deck was divided into 100 transverse strips, giving a length of approximately 42 inches for each element in the longitudinal direction. Each transverse strip of the deck, then, was divided into 16 elements, giving a width of approximately 30 inches in the transverse direction for each element. Incidentally, the much finer mesh of the previous models was tried first, but was too costly in running time to be practical, and was questionable as to whether it would ever finally converge. Subsequently, the coarser mesh was defined and used for this study.

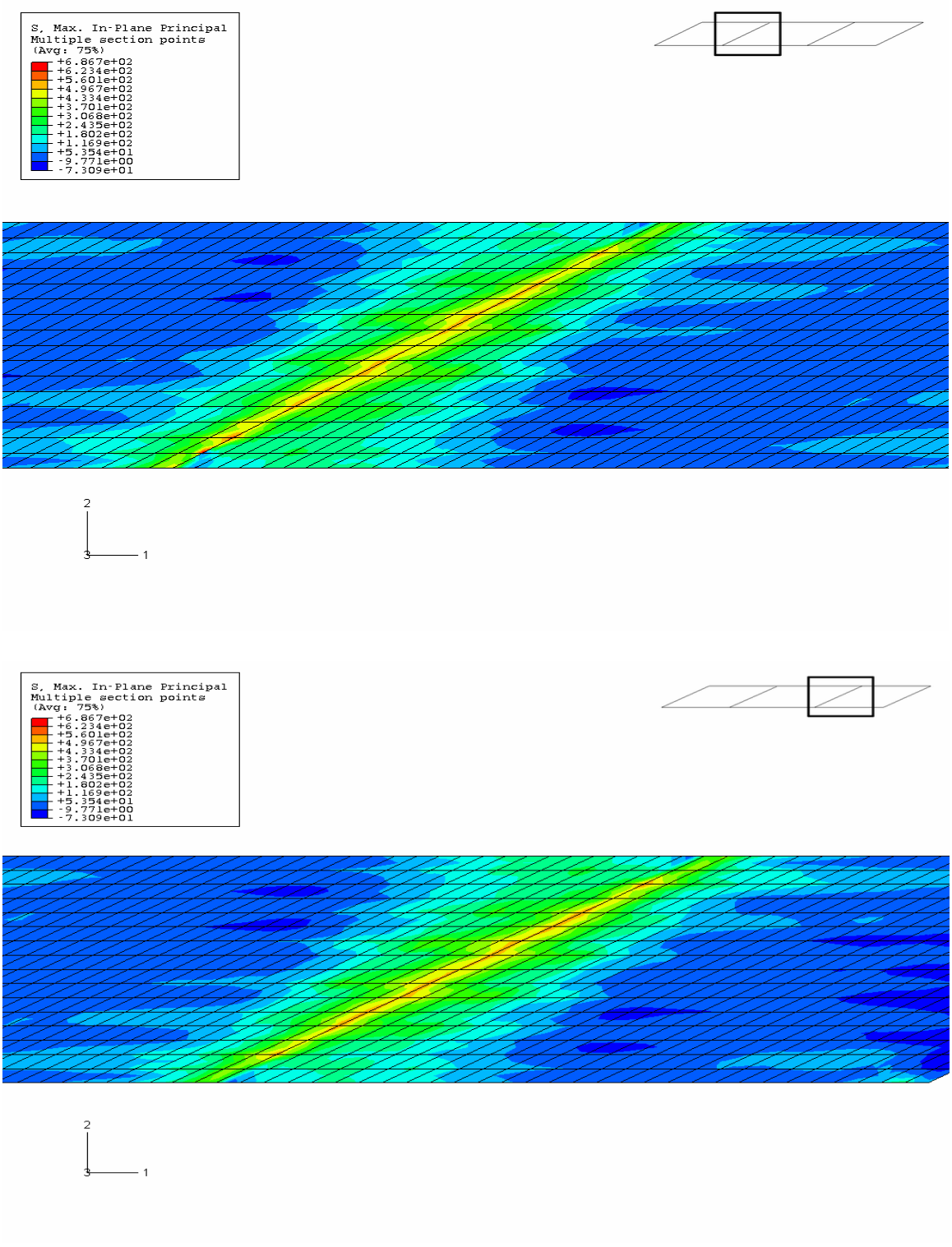

Figure 5.2 Maximum Principal Stress Distribution at Top of Deck for Smeared Crack Concrete Model of US 331 Bridge, $\alpha = 61°$

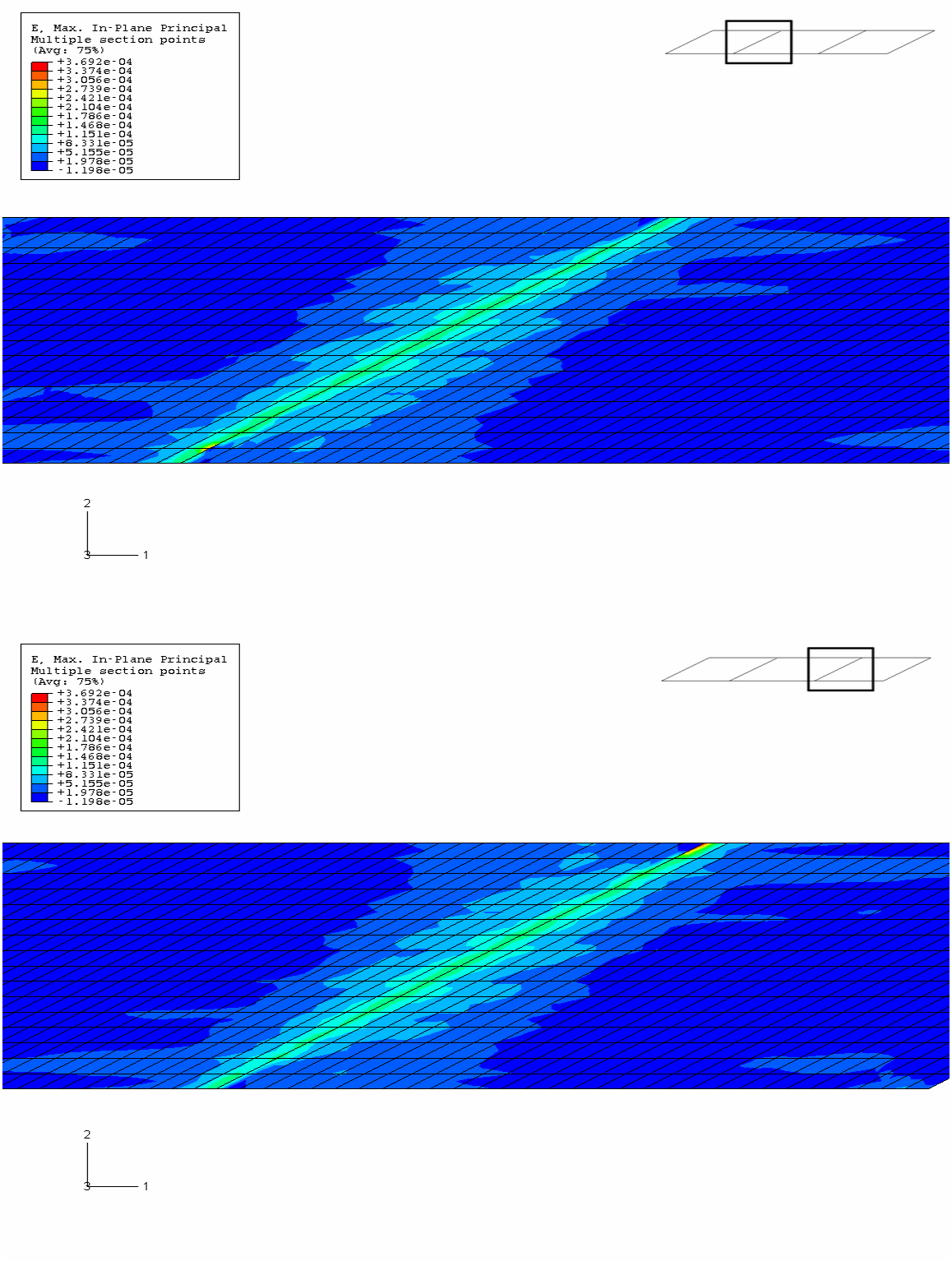

Figure 5.3 Maximum Principal Strain Distribution at Top of Deck for Smeared Crack Concrete Model of US 331 Bridge, $\alpha = 61°$

As can be seen in the figure, the general shape of the strain and stress contours is very similar to the stress contour results shown in Chapter 3 for the model with the linear elastic concrete material. The shape of the strain contour again follows the bridge's angle of skew, and the largest tensile strains are noted to lie exclusively in the areas surrounding the interior bents. The maximum stress achieved was approximately 687 psi, much lower than the maximum stress of 1216 psi for the corresponding linear elastic model. It is believed that the reason for this reduced stress level is that for the smeared crack model, the stress of the concrete elements was relieved after a crack was detected (i.e., after reaching the cracking surface), and began to follow the degraded portion of the curve in Figure 5.1. However, for the linear elastic concrete model used for the analysis described in the last two chapters, the tensile stress was allowed to increase, even after the cracking stress had been reached (since there was no descending portion of the tensile stress-strain curve defined for that model). It seems that the stress values obtained from this smeared crack concrete model may be more realistic, since it is known that cracking does relieve stress in concrete materials.

When the smeared crack model is incorporated, ABAQUS also generates a large amount of information related to cracking in its output data file (named a ".dat" file); this information for the US331 bridge model is presented in Appendix A. Among other information, the identity of each of the cracked elements is provided in this data file, as well as the Cartesian coordinates of the normal direction of the cracks, given at each integration point. In Appendix A, the fact that all cracking is identified for "section point 5" (depicted in Figure 5.4) indicates that all the cracks for this model occurred at the top of the deck.

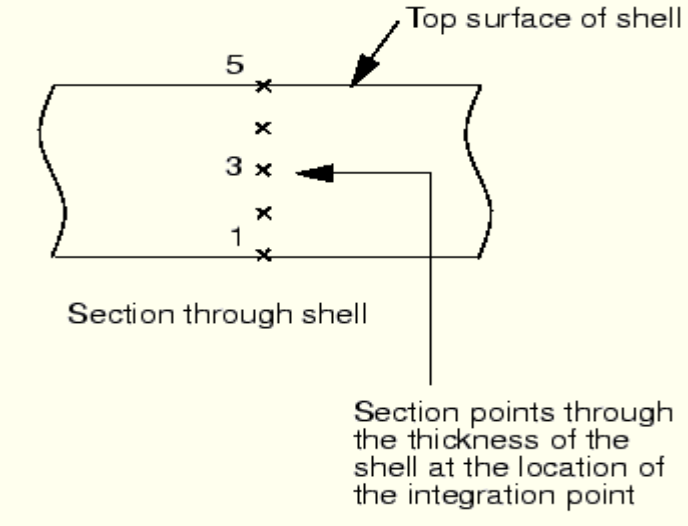

Figure 5.4 Configuration of Section Points

Based on the cracking information given in the output data file, the cracked zone on the top of the deck was identified, and is highlighted in Figure 5.5. From the figure one can discern that this distribution is fairly similar to the crack distribution shown in Figure 3.14, generated as a result of using an elastic material (linear) analysis, though the effects of the girder's influence are not as prominent for the smeared crack model. This general good agreement serves to indicate that the modeling techniques employed for the complex interaction between the deck and the girders, even when using a linear elastic concrete model, were at least qualitatively valid for simulating the cracking behavior for the nonlinear concrete deck material.

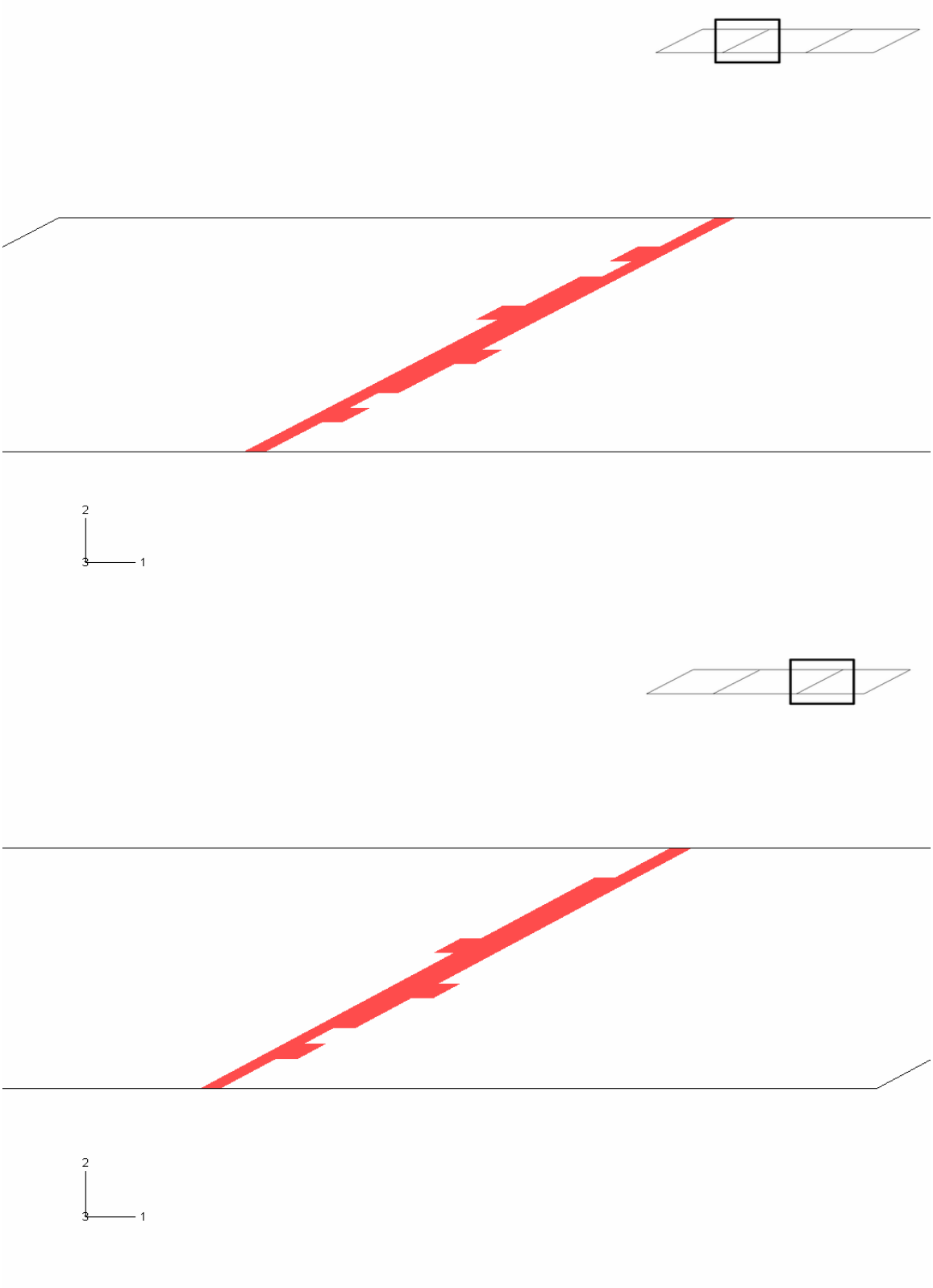

Figure 5.5 Cracking Zone at Top of Deck for Smeared Crack Concrete Model of US 331 Bridge, α = 61° (psi)

Use of the smeared cracking concrete model provides an alternative method for analyzing the cracking behavior of concrete structures. It is a more realistic representation, compared to use of a linear elastic model, since post-cracking behavior is considered. The capability of detecting cracks automatically (through the list provided in the output data file) is another plus. However, this modeling technique also brings the potential for large numerical difficulties in convergence, due to its complex material properties. As evidence of this phenomenon, Barth and Wu, and Baskar and Shanmugam, in their investigations (described in Chapter 2), were unable to achieve convergence with a smeared cracking model.

CHAPTER 6 SUMMARY AND CONCLUSIONS

6.1 Summary

The bridge deck on US 331 near Montgomery, AL developed transverse and longitudinal cracking just after construction was completed. A refined finite element model of this continuous, skewed, composite bridge was developed in detail to predict the stress distribution and cracking behavior of the deck. The commercially available finite element software ABAQUS was employed for the analysis. The maximum principal stress contours, the cracking zone, and the direction of cracking were obtained from the finite element analysis. The suggested modeling technique has been shown to accurately capture the composite bridge's behavior.

To investigate the possible causes of the cracking, a parametric study which incorporated a skew angle effect and a differential support settlement effect was conducted using this FE bridge model. In addition, an advanced smeared cracking concrete model was introduced to provide an alternative FE method for simulating RC structures.

6.2 Conclusions

Conclusions that were drawn from the results of the modeling study are as follows:

1. ABAQUS has the capacity of modeling the behavior of a concrete-steel bridge with shell elements, beam elements and its TIE connection.

2. A finite element model of an entire bridge is able to realistically predict the stress distribution on the deck. The magnitude and direction of the maximum principal tensile stresses are an important indicator of the crack distribution and direction of cracking.
3. For a continuous, skewed bridge, most cracking occurs at the top of the deck near the location of the intermediate supports.
4. The skew angle of the deck has a large effect on the stress levels exhibited, and the cracking behavior of the deck. Increasing the skew angle of the deck increases the tensile stresses experienced by the deck. As a result, the deck is more prone to cracking if the skew angle is severe. The cracking distribution for a skewed deck possesses a similar skew angle as that of the deck itself.
5. Differential settlement at the supports is of importance to the cracking distribution of the deck when it occurs at the intermediate supports of a continuous deck.
6. The smeared cracking concrete model of ABAQUS considers post-cracking concrete behavior, and is able to detect the cracking automatically (i.e., without making inferences based solely on a "cutoff" cracking stress). It is believed to be very efficient in RC structure modeling, if a well-configured model can be constructed that will allow for numerical convergence.

6.3 Recommendations

1. When new bridge construction is considered, an attempt should be made to minimize the skewed angle of the bridge, if possible. As has been shown, a bridge possessing a severe skew angle will have a higher tendency for cracking of the deck compared with a similar, non-skewed, or slightly-skewed bridge.

2. The potential for differential support settlement should be considered during the design and construction of a bridge, since it affects the cracking response of the bridge deck in a specific manner, depending on the location of the settlement, as described in Chapter 5.
3. No attempt was made to predict crack widths in the present study. The maximum principal tensile stress can indicate the distribution and direction of the cracks, but this information is not enough to provide an exact magnitude of the width of a crack. Future study should be considered to investigate the correlation of crack distribution and direction, along with maximum principal stress level, with width of cracking.
4. Despite the fact that the overclosure problem was solved by a complex interaction model at the interior support locations, this complex modeling technique also produced some unreasonable results for a very narrow zone of the model. Further investigation should be focused on developing an improved method that would still accurately represent the interaction behavior, but that would not produce such unrealistic results for the narrow zone just above the interior supports. It is not certain whether such a technique can be developed with the present capability of the available elements in ABAQUS (as was somewhat exhaustively attempted by the investigator), but further advancement of ABAQUS connection elements may offer a better chance that this could be achieved.
5. ABAQUS's smeared cracking concrete model is a very efficient tool for simulating the behavior of cracking RC structures if a well-configured model can be constructed that will allow for numerical convergence. Further investigation of its application

would be helpful in conquering its difficulties associated with numerical convergence.

6. No dedicated field tests were available for this study, since the bridge deck was destroyed prior to commencement of the study. For future modeling investigations of cracking behavior, a comparison between FE results and experimental data should certainly be conducted if at all possible.
7. Temperature effects may also a play a very important role in influencing the cracking behavior of a bridge deck, especially as related to shrinkage cracking. Temperature parameters should therefore be incorporated into the FE model in future studies, and their effects should be considered when attempting to predict the cracking behavior.

PART II: MODELING OF BOND-SLIP RELATIONSHIP BETWEEN CONCRETE AND REINFORCEMENT

CHAPTER 7 INTRODUCTION

7.1 Background

The behavior of the bond between the concrete and reinforcing steel in an RC structure is a many-faceted phenomenon which allows longitudinal forces to be transferred from the reinforcement to the surrounding concrete. When studying cracked reinforced concrete, characterization of the bond behavior is one of the most important issues. Once a crack develops, the concrete stress near the crack is relieved, but the tension in the steel can increase considerably. The high level of steel stress at the crack is transferred to the surrounding concrete through the interfacial bond (Won 1991). Therefore, it is helpful to understand the bond behavior and to model it appropriately before simulating the more advanced post-cracking behavior of the RC deck of interest in this study. This report describes an attempt to accurately model the bond-slip relationship between concrete and rebar using the FE software package ABAQUS.

ABAQUS, a commercial finite element analysis code developed by HKS, was used as the basic platform in this study. ABAQUS is a suite of powerful engineering simulation programs, based on the finite element method that can solve problems ranging from relatively simple linear analyses to the most challenging nonlinear simulations (ABAQUS, 2006). In the Interaction module of ABAQUS, users can define many types of constraints, interaction behaviors and connections between two parts. Those which are

suitable for simulating the bond between concrete and steel will be discussed in later chapters of this report.

7.2 Objective

The primary objective of this study was to develop a finite element model which could correctly simulate the bond-slip relationship in a RC member, and to accurately predict the level of stress transferred by the bond. Other objectives were to develop a better understanding of bond behavior, to compare previous RC models that included bond behavior, and to select the best modeling techniques available to accurately reflect the bond behavior.

7.3 Organization

Part II of the thesis is organized into six chapters. Following this chapter covering the background and research objectives, a literature review describing previous studies in which the FE method was used to model bond behavior and RC members is presented in Chapter 8. Chapter 9 introduces methods which are available in the FE software ABAQUS to simulate the bond behavior. Chapter 10 describes the development of the particular FE model used in this study to characterize the bond behavior, including descriptions of the model geometry, boundary conditions and data gathered from available literature to use as input for the model. Results of different types of bond simulation techniques are presented in Chapter 11. Finally, Chapter 12 includes a discussion of the conclusions that were drawn, and recommendations for future studies of this topic.

CHAPTER 8 LITERATURE REVIEW

8.1 Introduction

The action of the steel/concrete bond is a complex force transfer phenomenon occurring between the reinforcing steel and the surrounding concrete in RC members. The existence of the bond is the basic condition for these two materials to work together as a kind of composite material. Without bond, the rebar would not be able to resist any external load, and the RC beam would behave exactly like a plain concrete member does. For instance, this type of beam would fracture quickly under a small tensile load.

The connection between the reinforcing bars and the concrete is also responsible for controlling of the crack opening behavior in an RC member (Filho et al. 2004). Between significant cracks, the concrete still "works" and will absorb part of the tensile load from the rebar because the bond allows the load transfer between these two materials. Consequently, the average and total strains resulting in the rebar are smaller than those that would be experienced under the same load in a plain rebar. This mechanism, attributed to the bond, reduces the width of the cracks that develop and increases the stiffness of the structure.

Because of its importance, the bond-slip relationship is considered in most of the design and analysis efforts involving RC. Researchers have conducted numerous studies to characterize the constitutive bond-slip relationship. In the finite element analysis field, many different methods were also employed to represent the nature of the interaction

between the concrete and reinforcement. This chapter consists of a review of bond-related literature.

8.2 Bond-slip Relationship

The pull-out experiment is perhaps the earliest and easiest method used to test the bond-slip relationship. In the state-of-the-art report "Bond of reinforcement in concrete" from CEB-FIP (The International Federation for Structural Concrete), the authors agree that the interaction between the concrete and the rebar subjected to a pull out force is characterized by four different stages, as represented in Fig 8.1, and described below (CEB-FIP 2000).

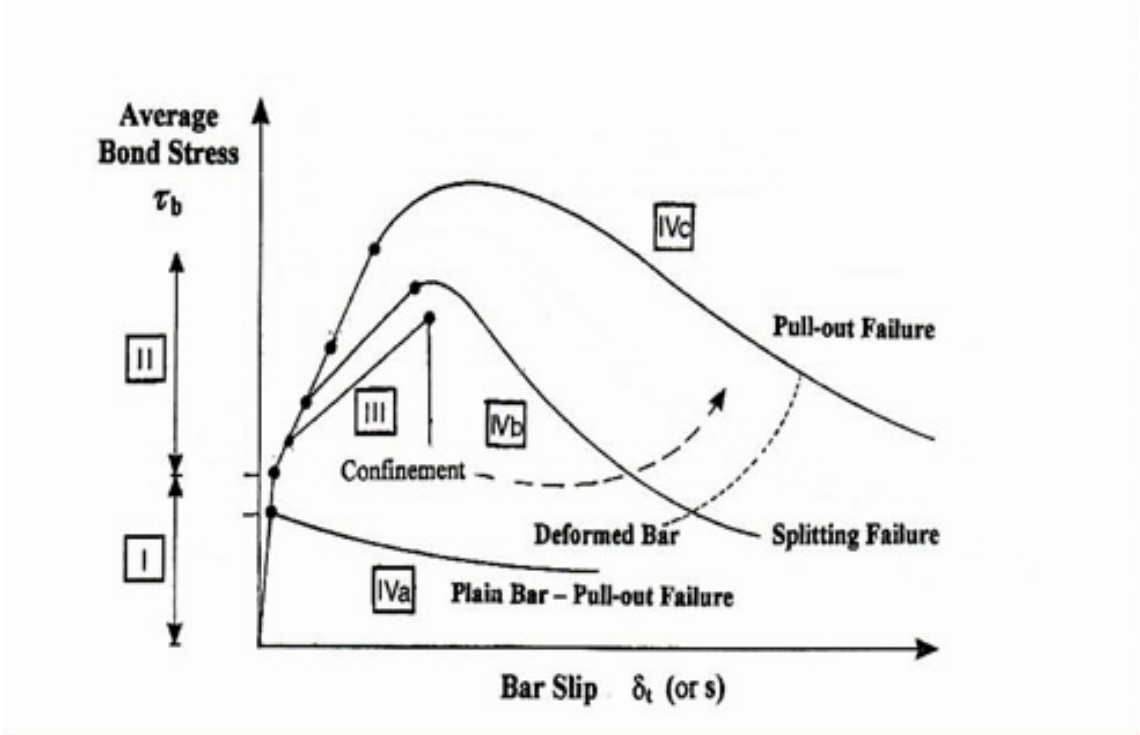

Figure 8.1 Local Bond Stress-Slip Laws (adapted from CEB-FIP 2000)

In Stage I the concrete is uncracked. For the low bond stress levels present in Stage I, bond efficiency is assured mostly by chemical adhesion, and there is little rebar slip, but highly localized stresses arise close to lug tips (CEB-FIP 2000).

Stage II is the stage in which first cracking occurs. For the higher bond stresses present in Stage II, the chemical adhesion breaks down; in deformed bars, the lugs induce large bearing stresses and transverse microcracks originate at the tips of the lugs, allowing the bar to slip (CEB-FIP 2000).

The progression through the relationship for regular reinforced concrete (i.e., including deformed bars) will be from Stage I to Stage II, then either to Stage III, or Stage IVb, or Stage IVc, depending on the confinement level and amount of transverse reinforcement present. Stage IVa, as indicated in the figure, is a special case for plain bars (i.e., without deformations).

Stage IVc is the stage in which deformed bar pull-out failure occurs. In the case of deformed bars confined by sufficient transverse reinforcement, splitting failure does not occur and bond failure is caused by bar pull out, as indicated in Fig. 8.1 (CEB-FIP, 2000).

Stage IVb is characterized as the deformed bar-splitting failure stage; in the case of deformed bars confined by light transverse reinforcement, the splitting cracks break out through the whole cover and between bars, and the bond tends to fail abruptly. On the other hand, a sufficient amount of transverse reinforcement can assure bond efficiency in spite of concrete splitting. In this situation, the bond strength reaches a peak and then starts decreasing as slipping value increases, but still the bond strength remains significant at very large slip values, as shown in Fig. 8.1. (CEB-FIP 2000) .

In Stage III, a more sudden failure occurs in concrete with lighter transverse and confinement. This stage ends as soon as concrete splitting reaches the outer surface of the member (CEB-FIP 2000).

Stage IVa is called the plain bar-pull out failure stage: in plain bars, this stage immediately follows the breakage of the adhesive bond. The sliding interface reduces the friction and the bond stress decreases (CEB-FIP 2000).

For better use of the bond mechanism in practical design and analysis, the bond slip relationship above has been simplified to a linear or bilinear curve by many researchers. There are several popular bilinear models, such as the three segments model (Nilson 1972), the five segments model (Guo and Shi 2003), and the six segments model (Tassios 1982); these three models are illustrated in Fig. 8.2. In Figure 8.2, τ represents bond stress, while S represents the magnitude of bond slip. In CEB-FIP MC90, a four segment model is suggested, as shown in Figure 8.3; Table 8.1 shows the characteristic values for the different parameters specified in this model.

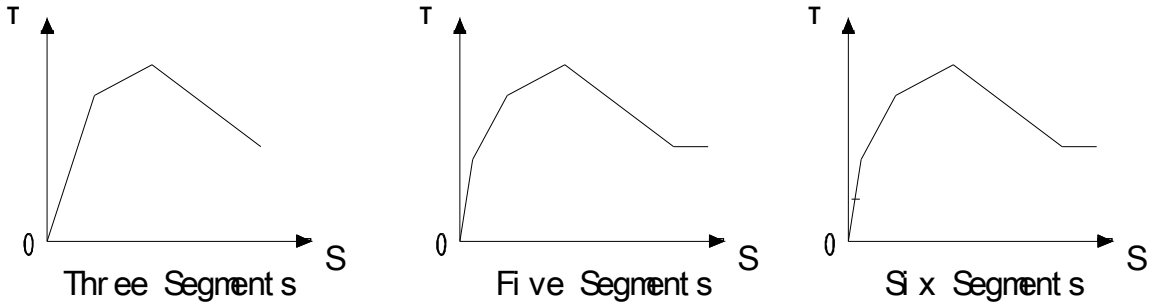

Figure 8.2 Bilinear Bond Slip Relationships

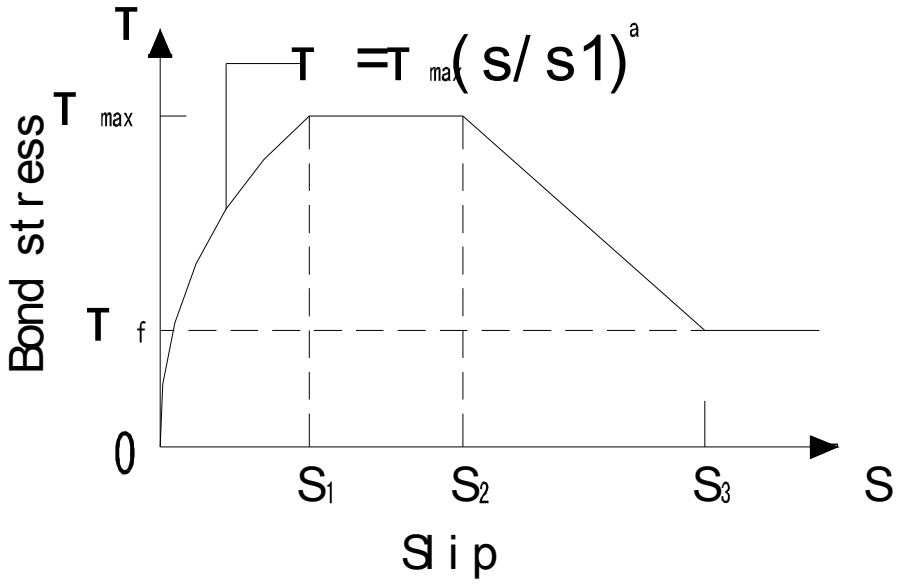

Figure 8.3 CEB-FIP MC90 Model (CEB-FIP, 1993) for Bond-Slip

Table 8.1 Values of Parameters for CEB-FIP MC90 Model

	Unconfined concrete		Confined concrete	
	Good bond conditions	All other bond conditions	Good bond conditions	All other bond conditions
S1	0.6 mm	0.6 mm	1.0 mm	1.0 mm
S2	0.6 mm	0.6 mm	3.0 mm	3.0 mm
S3	1.0 mm	2.5 mm	Clear rib spacing	Clear rib spacing
a	0.4	0.4	0.4	0.4
τ_{max} (MPa)	$2.0\sqrt{f_{ck}}$	$1.0\sqrt{f_{ck}}$	$2.5\sqrt{f_{ck}}$	$1.25\sqrt{f_{ck}}$
τ_f	0.15 τ_{max}	0.15 τ_{max}	0.40 τ_{max}	0.40 τ_{max}

* f_{ck} = characteristic concrete compressive strength, MPa

Engstrom modified the degrading part of the CEB model recently in order to consider the effect of yielding of the rebar (CEB-FIP 2000). He found that the bond stress decreases more when the steel strain exceeds the yield strain than when the steel bar is still elastic. Fig 8.4 and Table 8.2 illustrate the different bond slip relationships under these two situations.

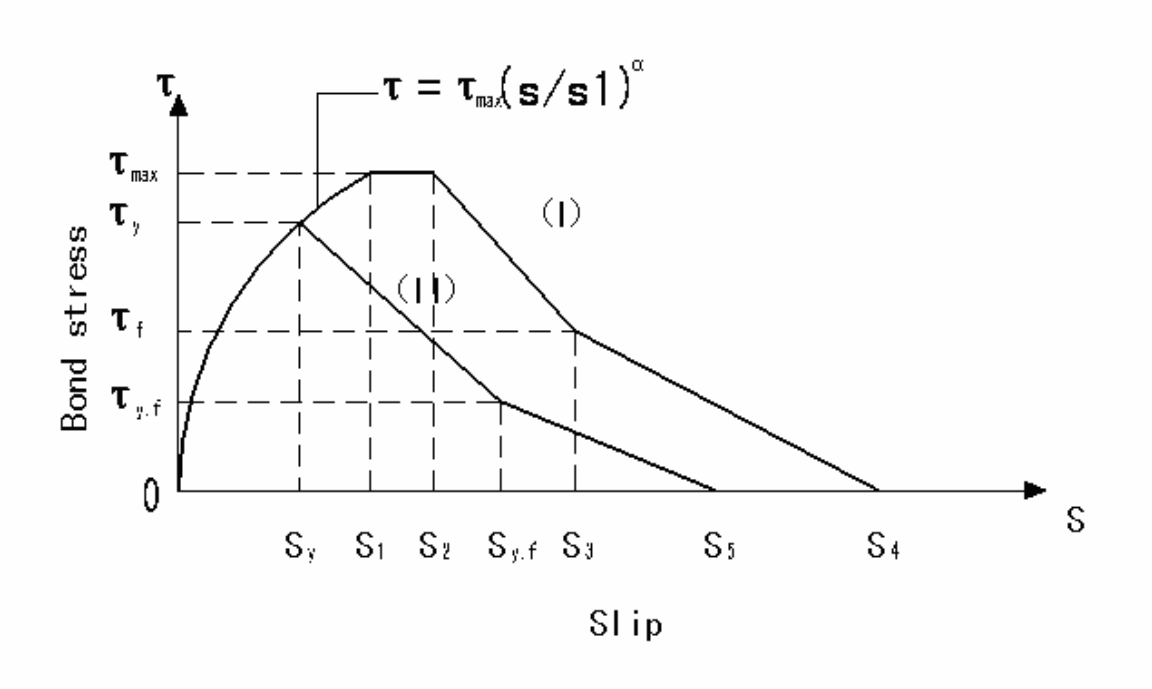

Figure 8.4 Engstrom's Model (CEB-FIP 2000)
(I) Steel Bar in Elastic Stage (II) Steel Bar in The Plastic Stage

Table 8.2 Values of Parameters in Engstrom's Model (CEB-FIP 2000) for Bond-Slip

	S1	S2	S3	S4	τ_{max}	τ_f	α
Normal strength concrete	1.0mm	3.0mm	Clear rib spacing	3*S3	0.45fcm	$0.4\tau_{max}$	0.4
High strength concrete	0.5mm	1.5mm	Clear rib spacing	3*S3	0.45fcm	$0.4\tau_{max}$	0.3

* f_{cm} =mean value of concrete compressive strength, MPa

In the past, researchers have also attempted to establish an equation to mathematically describe the bond-slip relationship. It is very convenient to use these equations to simulate bond behavior in finite element analysis. For example, Nilson (1968) proposed the following equation:

$$u = 3.606\times10^{6} d - 5.356\times10^{9} d^{2} + 1.986\times10^{12} d^{3}$$

where

u = nominal bond stress, psi, and

d = local slip, in.

Mirza and Houde (1979) also proposed an equation of similar form to describe the bond-slip relationship, as shown here:

$$u = 1.95\times10^{6} d - 2.35\times10^{9} d^{2} + 1.39\times10^{12} d^{3} - 0.33\times10^{15} d^{4}$$

where

u = nominal bond stress, psi, and

d = local slip, in.

Again, it is sometimes convenient to utilize equations of this type to mathematically prescribe the bond-slip relationship to investigate the behavior exhibited by a reinforced concrete specimen when simulating the response of the specimen to external stimuli.

8.3 Current Study and Existing Models

8.3.1 FE Model of Reinforced Concrete

Unlike steel and aluminum, which have uniform constitutive properties, reinforced concrete consists of two totally different materials working together to resist various types of loadings. Therefore, it is somewhat complex to predict reinforced concrete behavior that includes the bond-slip relationship using the FE method. Currently there are three different FE models which are widely used to simulate reinforced concrete behavior. They are discrete, distributed and embedded models.

For the discrete modeling technique, separate, distinct elements are used to represent the concrete and the reinforcement. For instance, it is sometimes convenient to use a solid finite element to represent the concrete and to use a beam element to simulate the reinforcing bars. In the discrete model, concrete and steel are two totally independent

parts. For this modeling technique, special elements must be placed at the interface between the concrete and steel to represent the bond mechanism.

When using the embedded modeling technique, the rebar is considered as an axial member that is built into the concrete element. Because the rebar is embedded, the rebar has the same displacement as the concrete element. Perfect bond is assumed in this modeling technique, so that the two materials are assumed to work together completely as one unit (ASCE 1982).

When using the distributed modeling technique, the reinforcement is assumed to be smeared into every element of the concrete (as is the case for the smeared cracking concrete model described in Chapter 5). Compared to the embedded model, in which the contribution of the concrete and steel is calculated independently, for the distributed modeling technique, the rebar is transferred to an equivalent amount of concrete and the RC is considered as a homogeneous material in this model. Perfect bond is again assumed for this technique.

Each of these three models has its own strong points. The distributed model is frequently used in practical structural design and analysis, based on its simplicity of implementation. However, the internal force of the reinforcement is not available to be quantified in this model since the steel has been smeared. The discrete model is the only model of the three which can consider the bond slip mechanism directly, so it is very useful in more accurate RC simulations, despite the fact that the modeling process for this technique is the most complex. Moreover, it is more convenient to simulate irregular reinforcement in the discrete model, because the concrete and steel are separate entities. The embedded modeling technique falls between the distributed and discrete model in

terms of complexity and ease of implementation. It is, in general then, not used as often because it has few distinct advantages over the other techniques.

With the development and advancement of computer technology, most finite element software packages such as ABAQUS, ADINA, ANSYS, and MSC/NASTRAN have their own concrete constitutive models, and corresponding concrete and rebar elements. Through the combination of these elements, the users can develop the three basic RC models above, and can then add advanced properties into the model such as the representation of bond, fracture and cracking behaviors.

8.3.2 FE Model of Bond

Based on the different FE models of concrete, there are various corresponding methods to represent the bond behavior. In a discrete concrete model, the bond may be considered as a contact problem between two different materials. Some dedicated elements have been developed to simulate this contact in earlier research and presently they are widely used in the commercial FE software. Some of these research efforts and the elements involved are described below.

In 1968, Bresler and Bertero developed a layered model to represent the bond. Because bond only occurs in concrete closest to the steel bar, they divided the concrete into two regions: an inner "boundary layer" and an outer layer of undamaged concrete, as shown in Figure 8.5. The thickness of the boundary layer was assumed to be 0.4 times the rebar diameter. The boundary layer was assumed to consist of a special homogenized material which included the bond slip relationship, instead of just normal concrete material. This layer was able to transfer the stress and displacement from the reinforcement to the concrete. (Bresler and Bertero 1968).

A connecting element was first used by Nilson in 1968. He introduced a double spring element to model the bond slip phenomena, as shown schematically in Figure 8.6. This double spring element consisted of two springs, one acting parallel to the bar axis and one acting perpendicular to it (Nilson 1968). These two springs were used to transmit normal and shear forces between the nodes of concrete and reinforcement. The springs were not considered to have dimension, and their stiffness were necessarily based on the characteristics of the bond slip relationship. In 1991, in the FE code ANSYS, the double spring element was modified into various possible unidirectional spring element configurations, as illustrated in Figure 8.7.

The study described in this report will focus on the spring-element model shown in Figure 8.7(a) using ABAQUS software. The detailed information and the calculation of equivalent spring stiffness will be discussed in a later chapter.

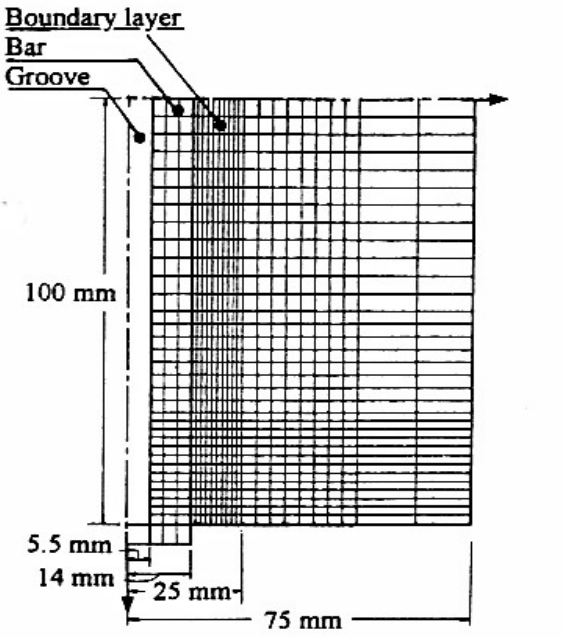

Figure 8.5 FE Model according to Bresler and Bertero (CEB-FIP 2000)

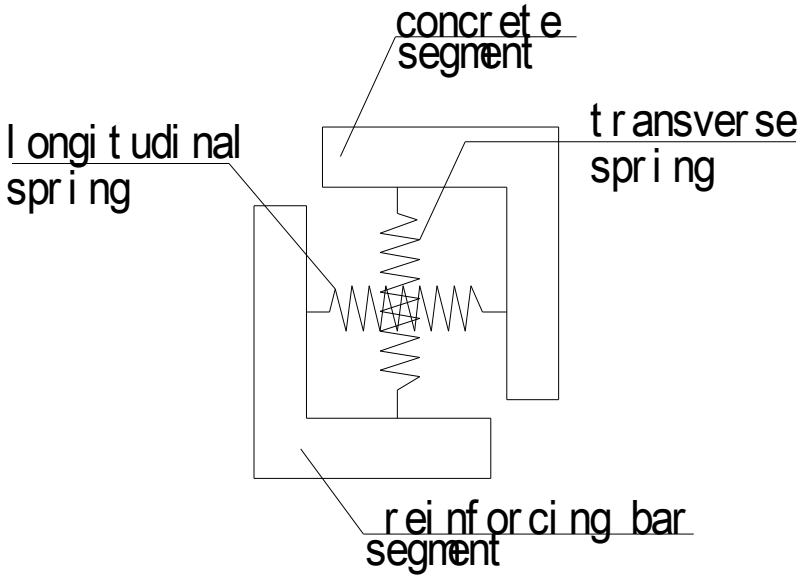

Figure 8.6 FE Model according to Nilson (Nilson 1968)

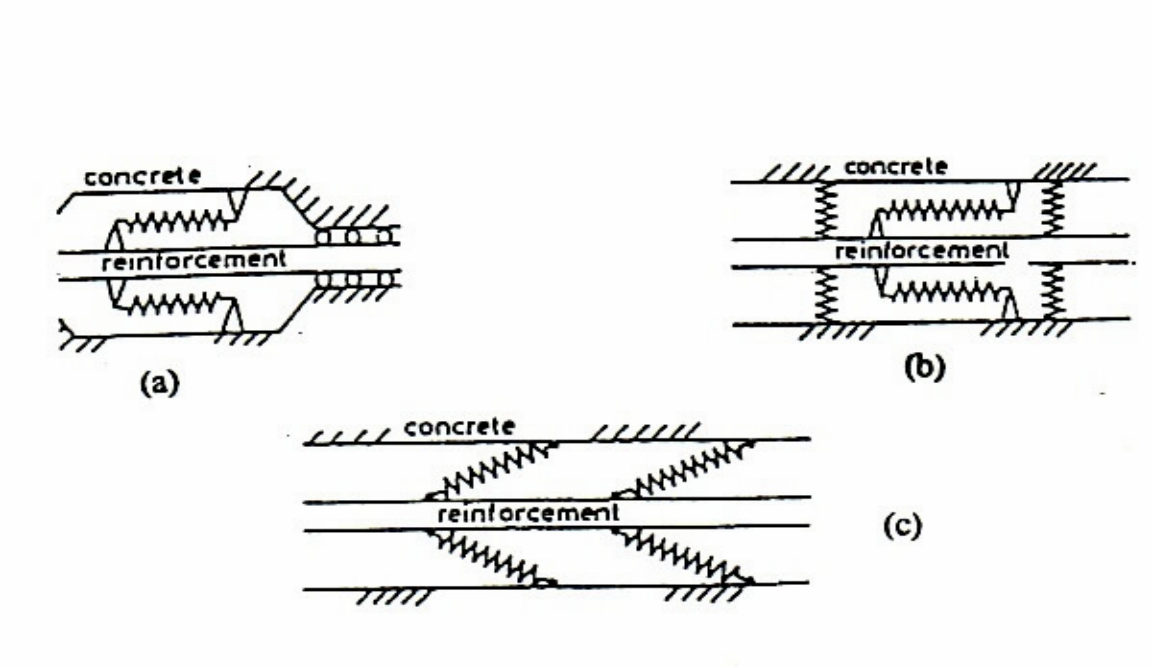

Figure 8.7 Various Possible Spring Model Configurations (CEB-FIP 2000)

In the distributed concrete model, bond phenomena can be represented by a special property of the material, rather than by a connection, since the reinforcement is smeared into the concrete in the distributed model. In ABAQUS code, bond-slip is

implicitly approximated by introducing some “tension stiffening” into the concrete model to simulate load transfer through the rebar (ABAQUS 2006). Tension stiffening is a bond-related behavior which decreases the tension in the steel due to bond, and increases the stiffness of the reinforcement, compared to that for a naked bar, after the RC cracks. Figure 8.8 shows the nature of this post-crack behavior for reinforced concrete in ABAQUS. The user can define the curve in Figure 8.8 by inputting different tension stiffening parameters. The tensile behavior is defined as having elastic behavior until the stress reaches f_{tu} , the failure point of the material. Then, a linear or nonlinear softening model is used to represent post-cracking behavior including bond effect using the "tension stiffening" option of ABAQUS.

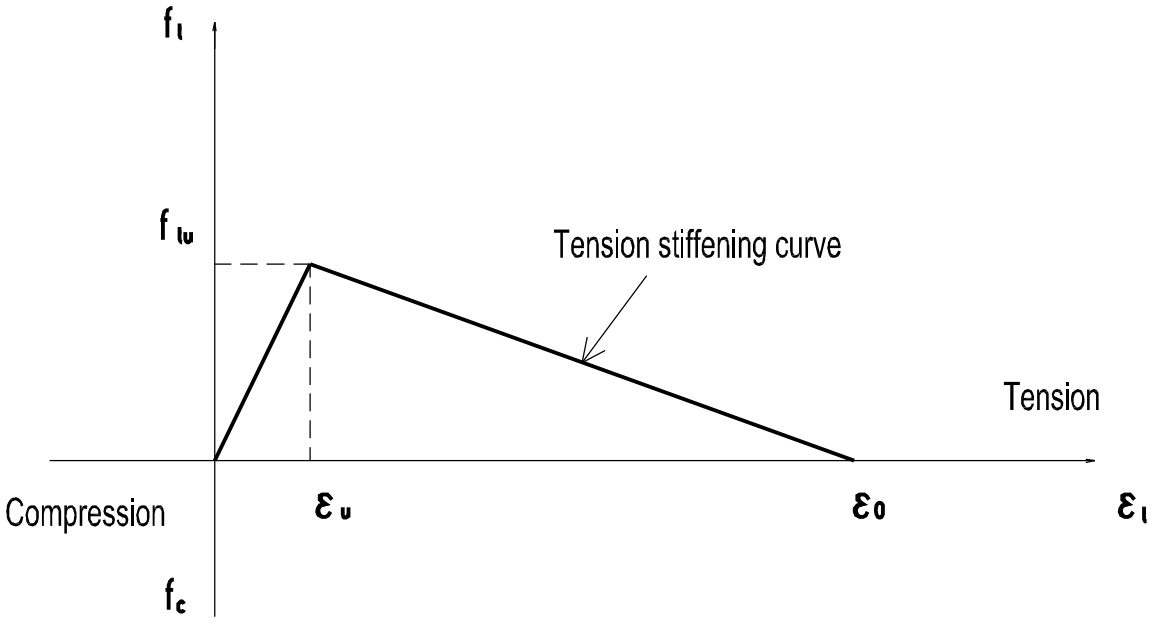

Figure 8.8 Tension Stiffening Behavior in ABAQUS (adapted from ABAQUS 2006)

Characteristics of twenty-four finite element model studies of reinforced concrete, performed between 1985 and 1991, were summarized by Darwin (1993), as shown in

Table 8.3, to illustrate the diversity in available options when developing a FE model of RC.

Table 8.3 Research on Reinforced-Concrete Finite Element Modeling (Darwin 1993)

Subject	Options	% of References
Type of model	2-dimensional	88
	3-dimensional	12
Concrete compression	Linear elastic	8
	Nonlinear elastic	80
	Elastoplastic	12
Tension stiffening	Incorporated	67
	Not used	33
FE model	Distributed	58
	Discrete	37
	Embedded	5
Crack representation	Fixed orthogonal	29
	Fixed non-orthogonal	37
	Rotating	34
Bond representation	Perfect	63
	Bond slip	37

As can be seen, because of the limitation of the computer technology at the time of these studies, it was very popular to assume that bond slip performance between concrete and steel was a perfect bond. Even if the bond effect was considered, researchers were still inclined to use a relatively simpler FE model, usually a two-dimensional distributed model. Today, with advanced FE software like ABAQUS available, one can afford to build a better three-dimensional discrete model of concrete which can not only predict concrete behavior more accurately, but can also simulate a more complex bond slip effect.

For the present study, a discrete reinforced concrete model was developed, and a complete bond-slip relationship like the one shown in Figure 8.4 was employed, which included the nonlinear portion and the degradation for the bond simulation.

CHAPTER 9 NUMERICAL SIMULATION METHOD

9.1 Interaction Module of ABAQUS

As mentioned earlier, a discrete reinforced concrete model, in which complex bond behavior can be simulated directly, was developed for the present study. As such, the first step in producing a model was to select a method for building a contact between concrete and steel. ABAQUS, in its interaction modules, provides various methods for simulating this contact, such as constraints, contact elements, and connector elements. Since bond slip is a force (stress) versus displacement (slip) relationship, the interaction types in ABAQUS which can couple a force with a relative displacement were first considered.

9.2 Spring Element

A spring element, whose stiffness is based on a force displacement relationship, is a special element available in ABAQUS. This element behaves like an actual spring, and it is obviously the best choice for implementation of the double spring bond model described in Chapter 8. The spring behavior can be defined in a linear manner by inputting a stiffness value, or it can be defined in a nonlinear fashion by supplying pairs of force-relative displacement values (see Figure 9.1). The deficiency related to using a spring element is that the degradation portion of the bond-slip relationship can not be simulated using this method. Moreover, the definition of the nonlinear spring behavior is not supported in ABAQUS/CAE, which is an interactive environment for creating ABAQUS models (ABAQUS 2006).

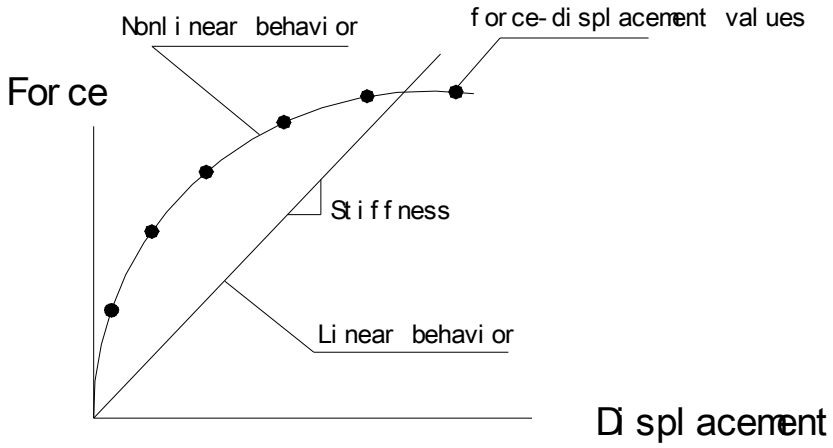

Figure 9.1 Linear and Nonlinear Spring Element Behavior

9.3 Friction

Friction is another modeling tool available in ABAQUS that is commonly used to describe the behavior of the contacting surfaces. The basic equation for the friction model is $\tau_{crit} = \mu p$, where τ_{crit} is critical shear stress at which sliding of the surfaces starts, μ is the coefficient of friction and p is the contact pressure between the two surfaces. Figure 9.2 summarizes the behavior of the friction model in ABAQUS. There is only a very small amount of slip allowed between the two contact faces before the shear stress across the interface equals the limiting frictional stress, μp (ABAQUS 2006).

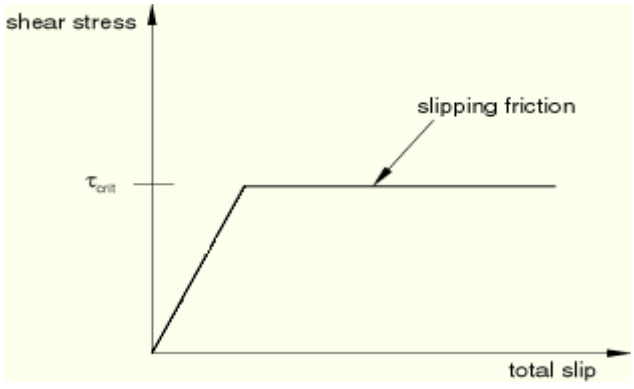

Figure 9.2 Frictional Behavior in ABAQUS (ABAQUS, 2006)

The transmission of the shear forces caused by friction is very similar to the bond behavior exhibited between concrete and steel. Comparing the curve in Figure 9.2 with the bond-slip relationships in Chapter 8, it seemed obvious that the friction model would be a good choice for simulating a linear bond phenomenon. The advantage of using a friction model is that it is defined through a face-to-face contact, unlike the spring element, which can only connect two nodes (rather than surfaces). A friction model's shortcoming, though, is also very obvious. Friction can simulate neither the nonlinear bond behavior, nor the degradation portion of the bond behavior.

9.4 Embedded Element

An embedded element in ABAQUS is used to specify that an element or group of elements is embedded in another "host" element or group of elements (ABAQUS, 2006). Despite the fact that, in the ABAQUS manual, it is claimed that an embedded element can be used to model rebar reinforcement, in actuality, it can only simulate a perfect bond condition, because the degree of freedom of the slave (reinforcement) nodes are all eliminated and forced to be the same as the master (concrete) nodes.

9.5 Translator

A translator is a type of connector in ABAQUS which provides a slot constraint between two nodes and aligns their local directions. The translator connection is best interpreted when node *b* is located at the center of the device enforcing the constraint (ABAQUS, 2006). Figure 9.3 shows its basic behavior.

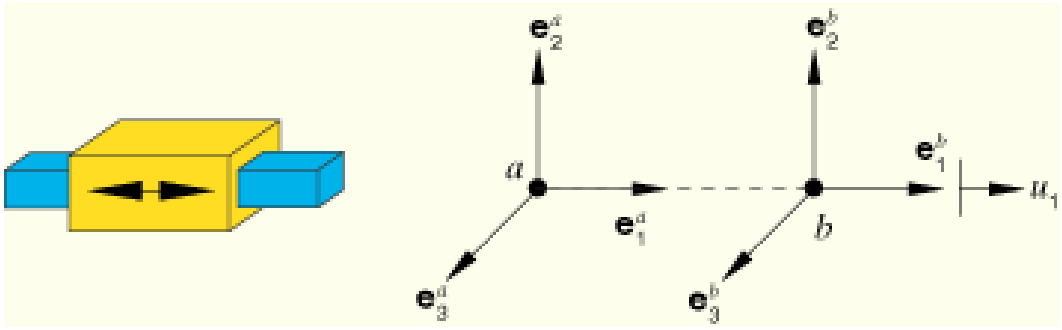

Figure 9.3 Translator Type of Connector (ABAQUS 2006)

As can be seen in Figure 9.3, the relationship between the blue and yellow parts is very similar to the relationship between reinforcement and concrete in an RC member. The only available component of relative motion in the translator is u1, which is translation in the direction parallel to the blue bar axis. Two parts can have a relative displacement in this direction. The interaction between parts in other directions (other than the u1 direction) in a translator is considered as a hard contact, or master-slave relationship (i.e., the degrees of freedom of node b are all constrained to be the same as those for node a).

In addition to the connecting capabilities described above, various specific connector behaviors can be defined in a connecting element in ABAQUS. For example, in a translator, the user can define a spring-like elastic behavior, plastic behavior, damage behavior, and other diverse behaviors associated with the available component of relative motion. Two of these translator behaviors are very critical in the development of bond model. The first is elasticity, which defines spring-like connector behavior in a translator, allowing the translator to have the same function as a spring element. The second is the ability to model damage by defining damage initiation and evolution behavior in the

translator; this capability allows simulation of the degradation portion of the bond slip relationship (ABAQUS 2006).

For the present study, a translator element was selected to simulate the bond behavior, since its connection type simulates behavior that agrees well with the contact between concrete and steel, and because of its capability for including multiple facets of connector behavior pertinent to that contact. After adding the spring like elasticity and damage behaviors, the translator was able to model the whole bond-slip relationship discussed in Chapter 8.

CHAPTER 10 FINITE ELEMENT MODEL DEVELOPMENT

10.1 Assumptions and Scope

The finite element software package ABAQUS was used to develop the numerical example model described in this chapter. Several assumptions were made to simplify the development of the model without sacrificing the integrity of the representation. First, there is no variability in material properties within each of the two materials. Secondly, the bond slip relationship is assumed to be constant between the concrete and the steel. Finally, splitting failure, which is caused by the circumferential tensile stresses in the concrete around the rebar, is not considered in this model.

This model was used to simulate the static behavior of an axially loaded tensile specimen (commonly known as a pull out test). This test has been used frequently in the past to study bond behavior, and consequently, there is data available in the literature that could be used for modeling. Dynamic, fatigue, and thermal analyses of bond behavior, although certainly worth investigating in a future project, were not included in this study.

10.2 Definition of the FE model

When it is claimed that this FE model can simulate observed bond behavior, a fundamental question still hangs overhead: "What is the definition of a FE model?" In the state-of-the-art report "Bond of reinforcement in concrete" (Perry and Thompson 1966), the authors supplied two alternative definitions of an FE model. The first stated that “The model is intended as a system of mathematical and physical laws, rules, assumptions and

numerical procedures aimed at the description of a phenomenon". The second definition was stated as follows: "The model is intended as a self-contained set of rational relations aimed at giving a closed –form response on the basis of a set of input data" (Fib, 2000). The authors also believed that the second expression was slightly preferred for bond modeling since there is no universally-accepted definition in the world. The FE model in this report was also considered as a model described by the second definition.

10.3 Model Characteristics

A 3D finite element model is discussed in this chapter. The geometry of this model was simplified from the specimen of the pull-out experiment detailed in E. Perry and J. Thompson's article "Bond stress distribution on reinforcing steel in beams and pullout specimens" (Perry and Thompson 1966). Figure 10.1 shows the simplification employed. As can be seen, a standard No.7 steel bar was embedded into a 5"×5.75"×9" concrete prism. Figure 10.2 shows the 3D profile of the model in the CAE environment of ABAQUS. Both the concrete and reinforcement were modeled by quadratic, reduced-integration solid elements of ABAQUS.

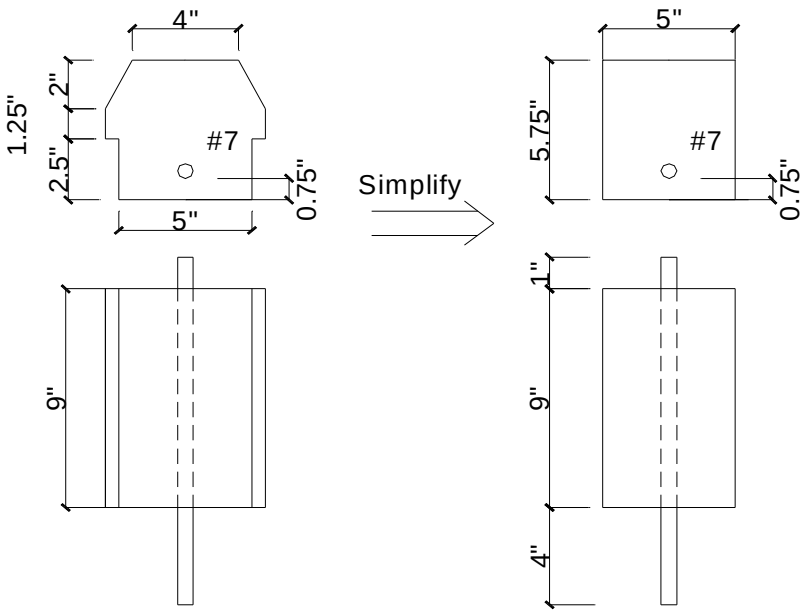

Figure 10.1 Simplification of the Specimen

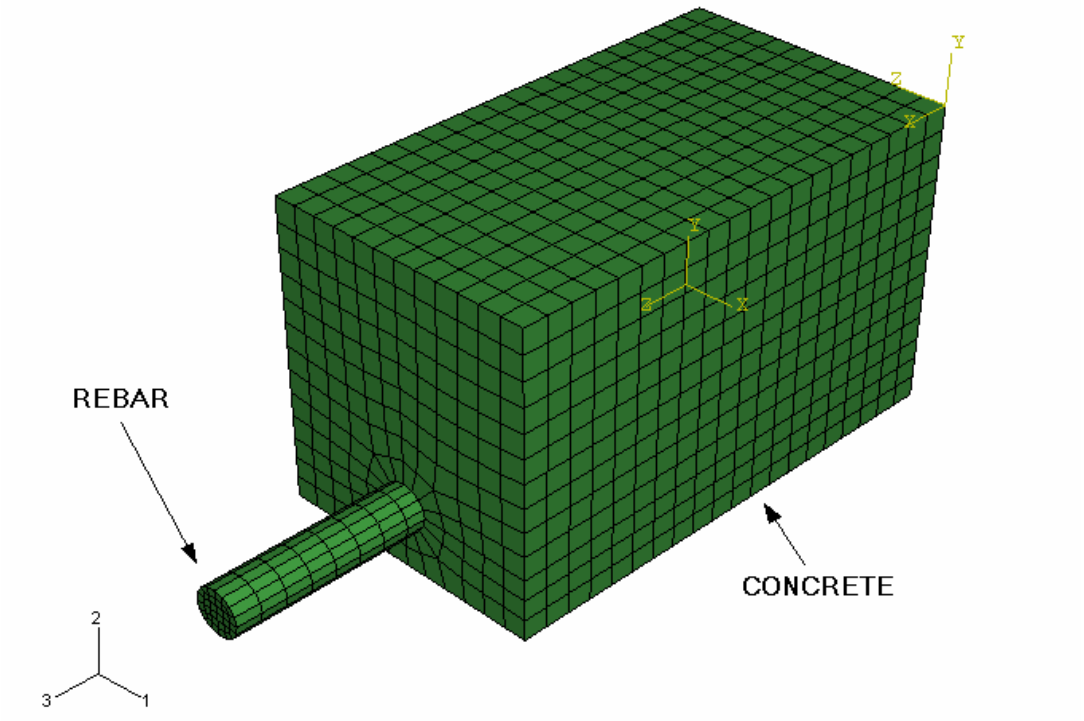

Figure 10.2 Geometry of the Model in ABAQUS

Elastic material properties were used for both concrete and reinforcement in this model since the focus of the model was to investigate the bond between these two materials, rather than the response of the materials themselves. (In Chapter 5, a nonlinear reinforced concrete model including bond behavior (tension stiffening) and cracking was discussed.) Table 10.1 shows the material properties used in the model.

Table 10.1 Material Properties of the Model

	Modulus of Elasticity, E (psi)	Poisson's Ratio, ν	Density, ρ (lb/in^3)
Concrete	4.42×10^6	0.15	0.086
Steel	29×10^6	0.32	0.286

10.4 Load and Boundary Conditions

The applied loading consisted of an axial displacement imposed at the exposed end of the rebar, applied in the pull out direction, which generated a force used to pull the rebar for a certain distance. The load was applied in small increments to overcome numerical instability difficulties that could have occurred had a large load been applied suddenly. The end of the rebar opposite the loaded end could have been modeled using either a free or fixed boundary condition. A fixed boundary condition could produce larger variations in stress along the length of the rebar, making it easier to study the effects of bond behavior at various locations along the rebar length. To accurately simulate the effect of bearing on the block in the pull out test, a fixed boundary condition was also assigned at the surface of the concrete specimen to fix the concrete, as illustrated in Figure 10.3 below.

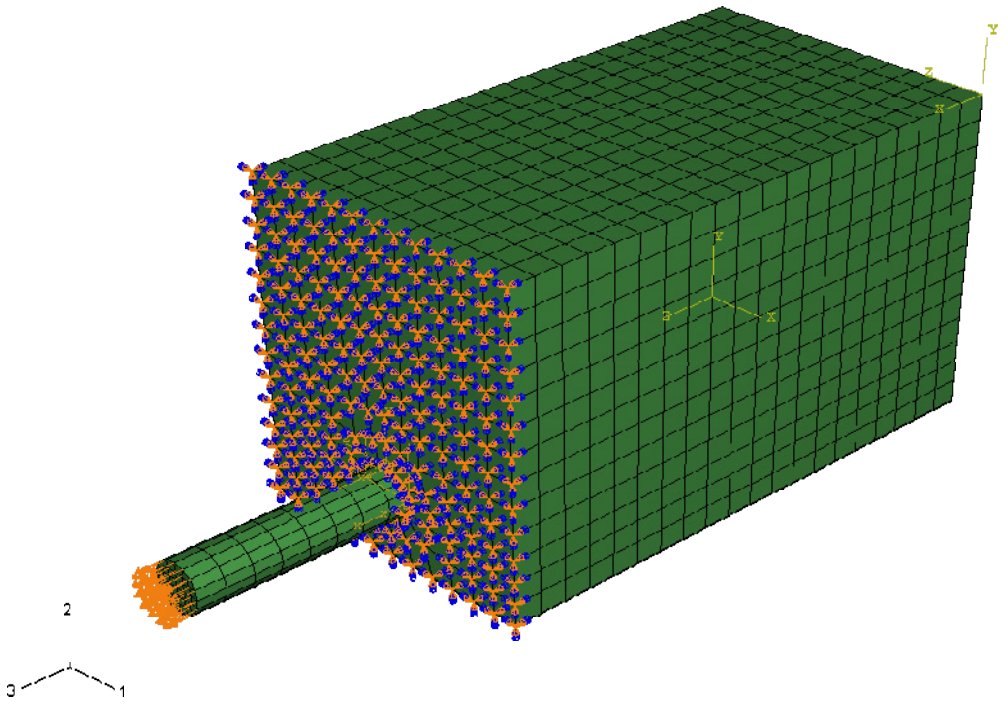

Figure 10.3 Boundary Conditions and Loading of the Model in ABAQUS

10.5 Translator Data Transfer

As a special element available in ABAQUS, spring-like translators were selected to simulate the bond phenomena between concrete and steel in this model as shown in Figure 10.4. These special elements were used to connect the nodes at the interface between the concrete and steel (along the length of the rebar) with a spring-like behavior in the longitudinal (pull out) direction. A hard contact (an interface involving a master-slave relationship) was employed in the other directions. The mathematical bond-slip relationship from the study described in the CEB-FIP report mentioned in Chapter 8 (CEB-FIP, 2000) was used, and was transferred to the translator by defining its stiffness as that mathematical relationship (i.e., incorporating that force displacement

relationship). Referring to Figure 8.4 and Table 8.2 (CEB-FIP 2000), the values that were used in the model are:

f_{cm} = 41.37 MPa

$\tau_{max} = 0.45 f_{cm}$ = 18.62 MPa

$\tau_f = 0.4\,\tau_{max}$ = 7.45 MPa

S3 =10 mm

S4 = *3***S3* = 30mm

$$\tau = \tau_{max}(\frac{S}{S_1})^{\alpha} = 18.62(\frac{S}{1})^{0.4} = 18.62S^{0.4} \text{ (MPa)}$$

The resulting bond slip relationship is shown in Figure 10.5, and is transferred into U.S. units in Figure 10.6.

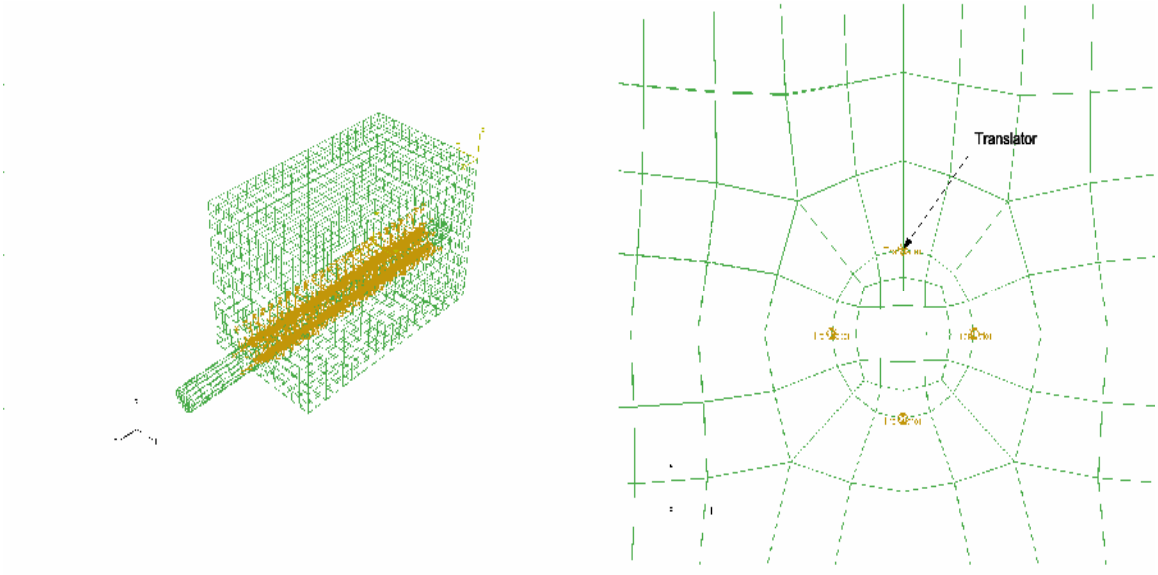

Figure 10.4 Translators in the Model

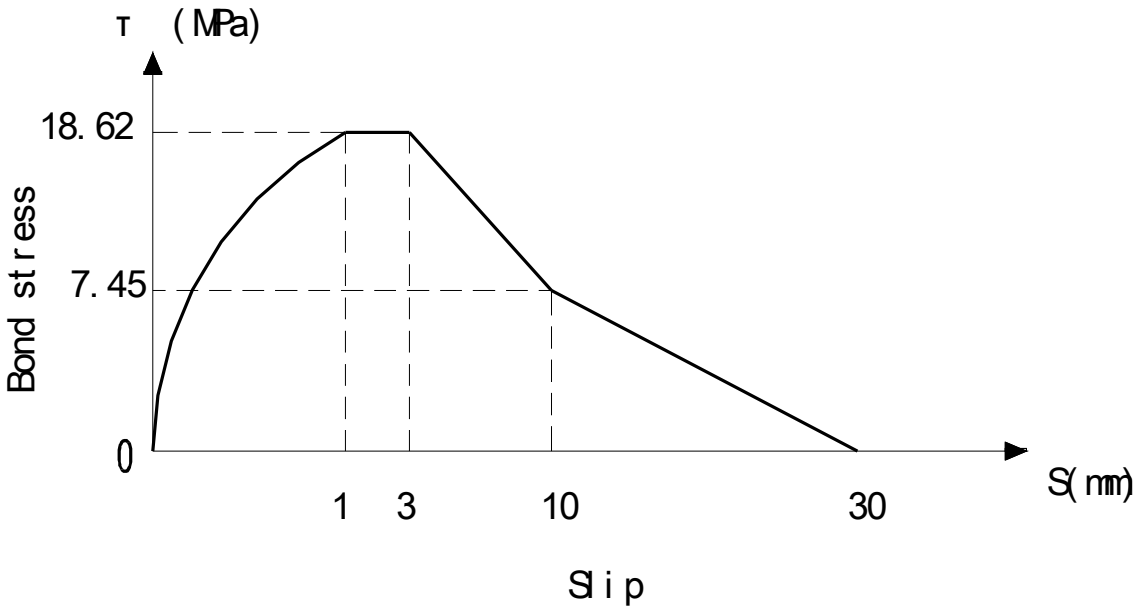

Figure 10.5 Bond-Slip Relationship

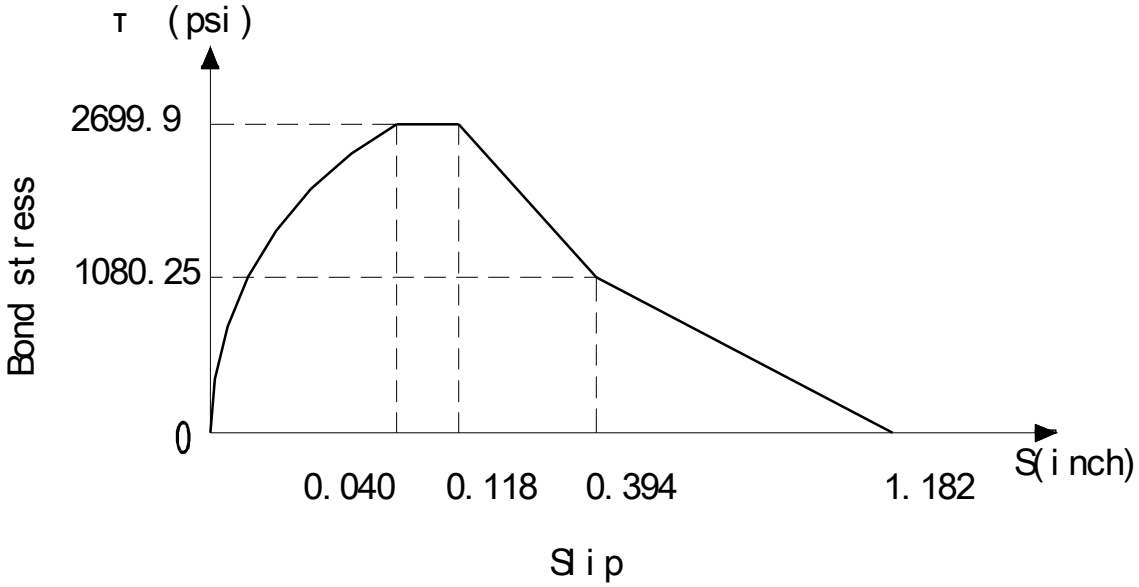

Figure 10.6 Bond-Slip Relationship (U.S. Units)

The stiffness (force-displacement relationship) of the spring like translator was obtained using the relationships below:

$$F = \tau \times A_{contact}\text{, and}$$

$$D \approx slip$$

where F represents the force in each translator, τ is the bond stress, $A_{contact}$ is the surface contact area between the concrete and steel, per translator, and D is the relative distance between the two nodes connected by a single translator. Using the (bond stress, slip) coordinate pairs shown in Figure 10.6, and the equations shown, the corresponding (force, displacement) coordinate pairs were calculated, and then were used to define the stiffness relationship for the ABAQUS spring-like translators. The $A_{contact}$ value was calculated as

$$A_{contact} = \frac{\pi dL}{n}$$

where d is the diameter of the rebar, L is the length of the finite element, and n is the number of translators around the circumference of the rebar for each element (four in this study). A list of input parameters generated using this method is presented below:

Table 10.2 Force-displacement Coordinate Pairs for Each Translator

Force (lb)	Displacement (in)
0	0.000
438.6	0.008
578.7	0.016
680.6	0.024
763.6	0.032
834.9	0.040
834.9	0.118
334.1	0.394
0	1.182

10.6 Output

Total force, moment, relative displacement and relative rotation were requested as output from the ABAQUS computer model of the pull-out test for each translator because these variables could reflect the bond force and slip behavior. Element stresses and strains were also requested as field outputs. Results from the computer simulations will be reported and discussed in the following chapter.

CHAPTER 11 RESULTS

11.1 Nonlinear Bond-Slip Behavior

The ABAQUS variables CU (relative displacement in the spring-like translator connector element, measured between its endpoints) and CTF (total force in the spring-like translator connector element) can be reviewed using the visualization modulus of ABAQUS. The "X-Y data" function of ABAQUS can combine the results for these two variables into a single CU-CTF curve. This curve can then be used to describe the variation of force as related to displacement in the translators as the pull out test progresses, and the specific components reported for the pull out direction (CU1 and CTF1) can reflect the bond slip behavior between the concrete and steel. One of the translators closest to the loaded end of the rebar, shown in Figure 11.1, was monitored and studied in this investigation.

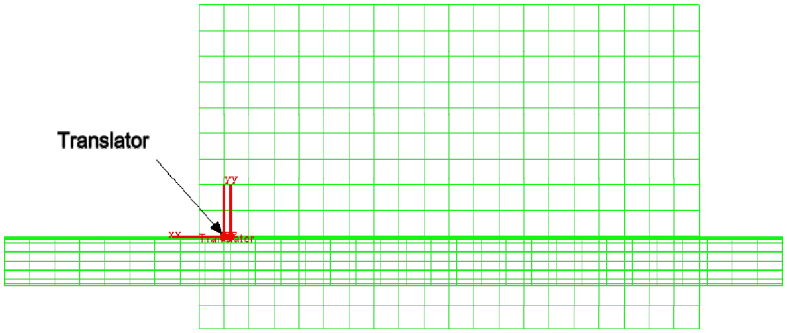

Figure 11.1 Location of the Monitored Translator

At the beginning of this investigation, only an elasticity bond behavior (formulated using the increasing part of the bond slip curve in Figure 10.6) was used as input into the model. A 0.05 in displacement boundary condition was imposed at one end of the rebar to "force" the rebar to undergo a displacement (in essence causing the rebar to pull out of the concrete block), while the other end of the rebar had a fixed boundary condition. The results of this model for a single translator were reviewed; these results are shown in Figure 11.2. From the figure, it can be seen that under the pull-out load, this translator had a relative displacement of approximately 0.025 in, corresponding to an internal force of about 700 lb.

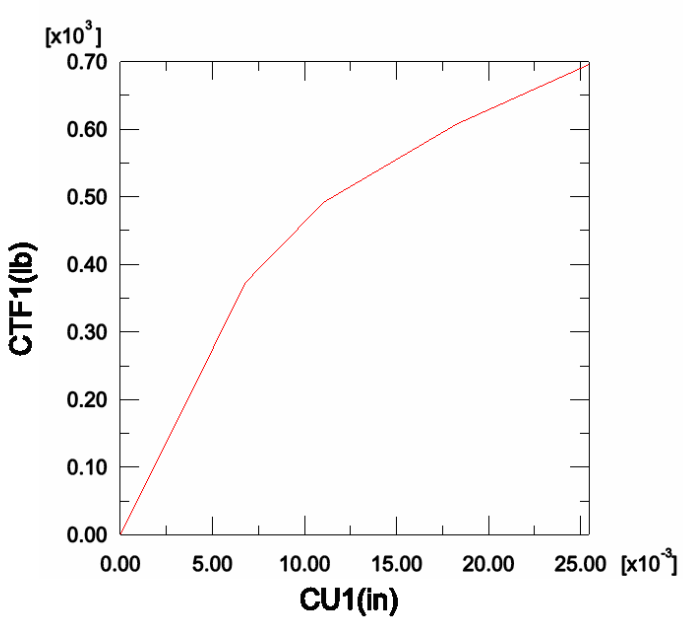

Figure 11.2 Nonlinear Force-Displacement Relationship in a Single Translator

In Chapter 10, the method for transferring a local bond-slip relationship into a force-displacement relationship for a translator was described. Using this method, in a reverse manner, one can easily deduce the resulting bond slip relationship at the location of this translator using the CU1-CTF1 curve. The result of this procedure is shown in Figure 11.3. As can been seen, the relationship reported for the bond-slip relation is exactly the same as what was input for the increasing portion of the bond-slip curve (shown in Figure 10.6). This agreement indicates that the translators successfully responded to the bond-slip behavior that was input. Therefore, the formulation of the spring-like translator elements was deemed satisfactory.

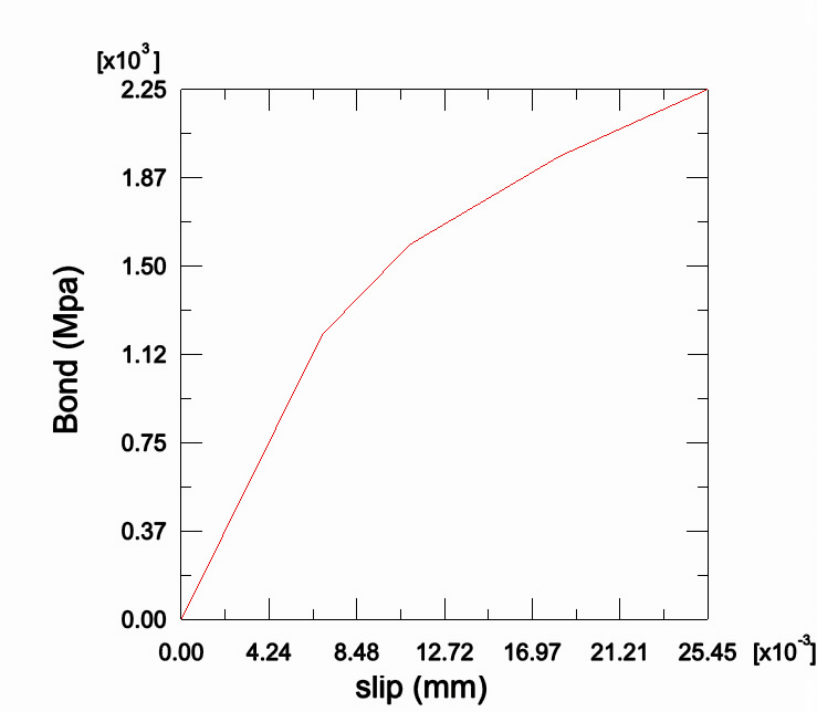

Figure 11.3 Resulting Nonlinear Bond Slip Relationship in a Single Translator

11.2 Bond-Slip Behavior with Damage

The decreasing part of the bond slip relationship, capable of representing the degraded behavior occurring after damage has been incurred, was then added to the translator properties for the model. This type of model capability is only available in the dynamic, explicit analysis routine in ABAQUS, so the time of loading was forced to be very short. Figure 11.4 shows the results of a single translator under a pull out displacement "load" of 1.2 in. This increase of displacement load was used to make the results more dramatic, and to make certain that damage would, in fact, occur.

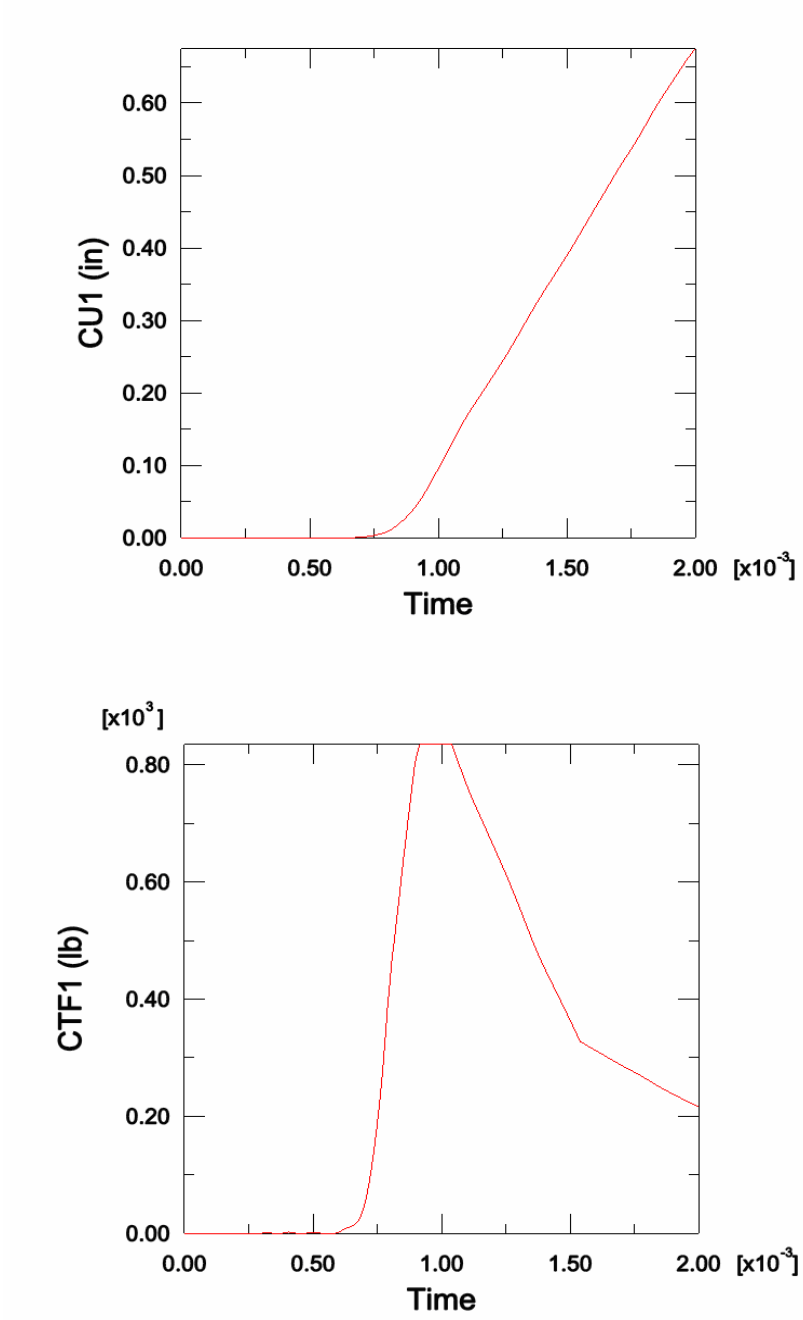

Figure 11.4 CU1 and CTF1 Results of a Single Translator

As can be seen, before the time of approximately 0.7 x 10^{-3} seconds, both the force and relative displacement of the translator increased very slowly, but after that time both of them exhibited a sudden increase. This is an indication that damage was modeled by the translator at this time (representing a degradation of the bond between the concrete and steel). Combining the CU1 curve with CTF1 curve, to produce the relationship shown below, the bond-slip behavior at the location of this translator was then obtained from this figure, through the reverse data transfer process described earlier.

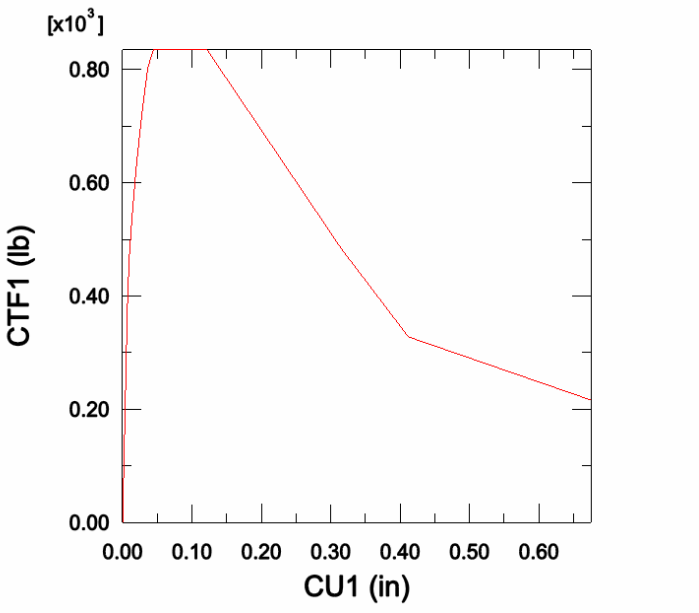

Figure 11.5 Force-displacement Relationship in a Single Translator

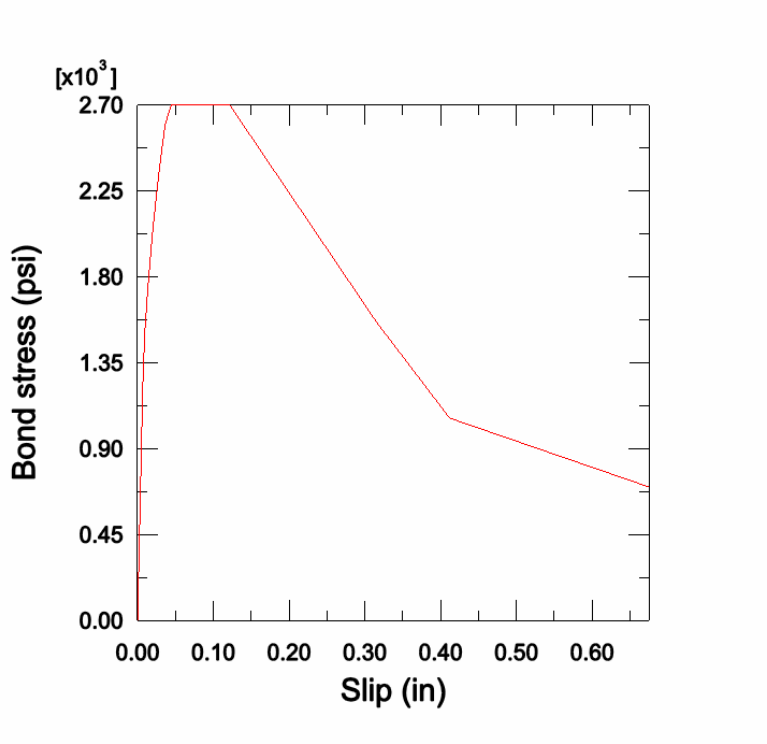

Figure 11.6 Bond-slip Relationship including Damage Behavior for a Single Translator

As shown in Figure 11.6, the bond-slip relationship in the model again was same as the bond-slip curve that was used as input to the model (Figure 10.6). Again, the translator formulation successfully simulated the entire bond phenomena, including damaged behavior.

11.3 Bond-Slip Behavior in Different Locations

As shown in Figure 11.7, three translators (c1, c2 and c3), chosen at varying locations along the length of the rebar were monitored in this study. Figures 11.8 to Figure 11.11 give the bond-slip relationships which were deduced from the CU1-CTF1 curves produced for these three translators when the rebar was pulled out 0.23 in. This displacement load was chosen strategically to produce a particular response at each of these three monitored translators.

Figure 11.8 shows the behavior of the translator nearest the loaded end (c1). Since this translator has the largest displacement of the three, its results indicate that the bond at this location has begun to experience damage. This is indicated by the presence of the negatively sloping line at the right of this figure. Figure 11.9 shows the behavior of the connector nearest the fixed end of the rebar (c3), which has smallest displacement. One can see by its response that the bond at that location remained undamaged, since the curve is still increasing and has not reached the limiting plateau. Figure 11.10 shows the behavior of the connector at the middle of rebar (c2). As can be seen, the bond at this location has reached the limit of its elastic behavior (shown by the plateau in the middle of the curve), but it hasn't started to damage, since no decreasing portion of the curve is present. Figure 11.11 is the superposition of these three figures, given so that the behaviors can be easily compared.

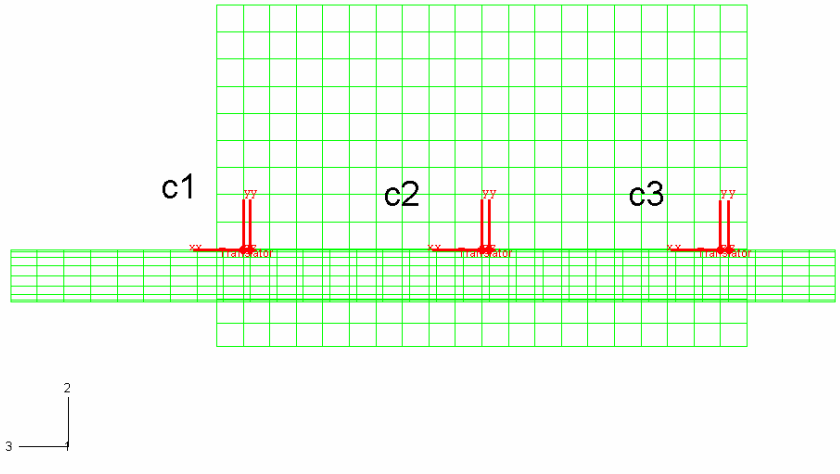

Figure 11.7 Three Translators (c1, c2 and c3) Who's Results Were Monitored

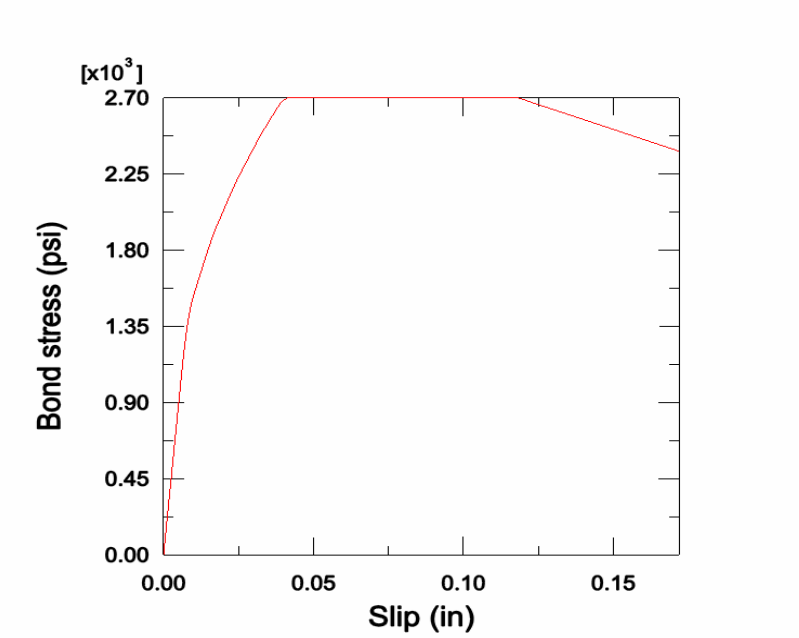

Figure 11.8 Bond Slip Relationship of Translator c1

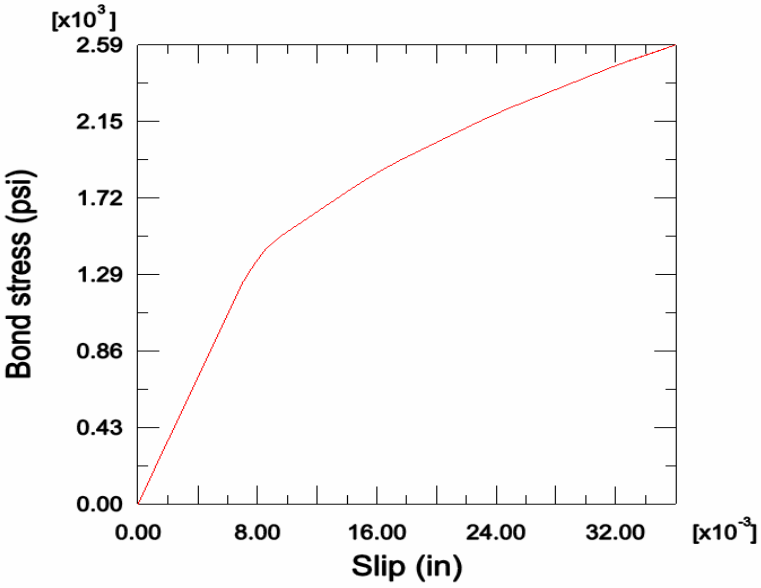

Figure 11.9 Bond Slip Relationship of Translator c3

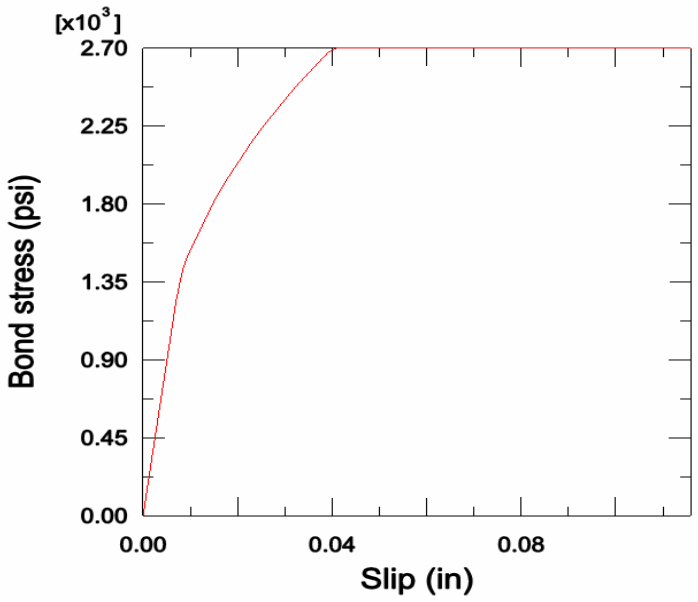

Figure 11.10 Bond Slip Relationship of Translator c2

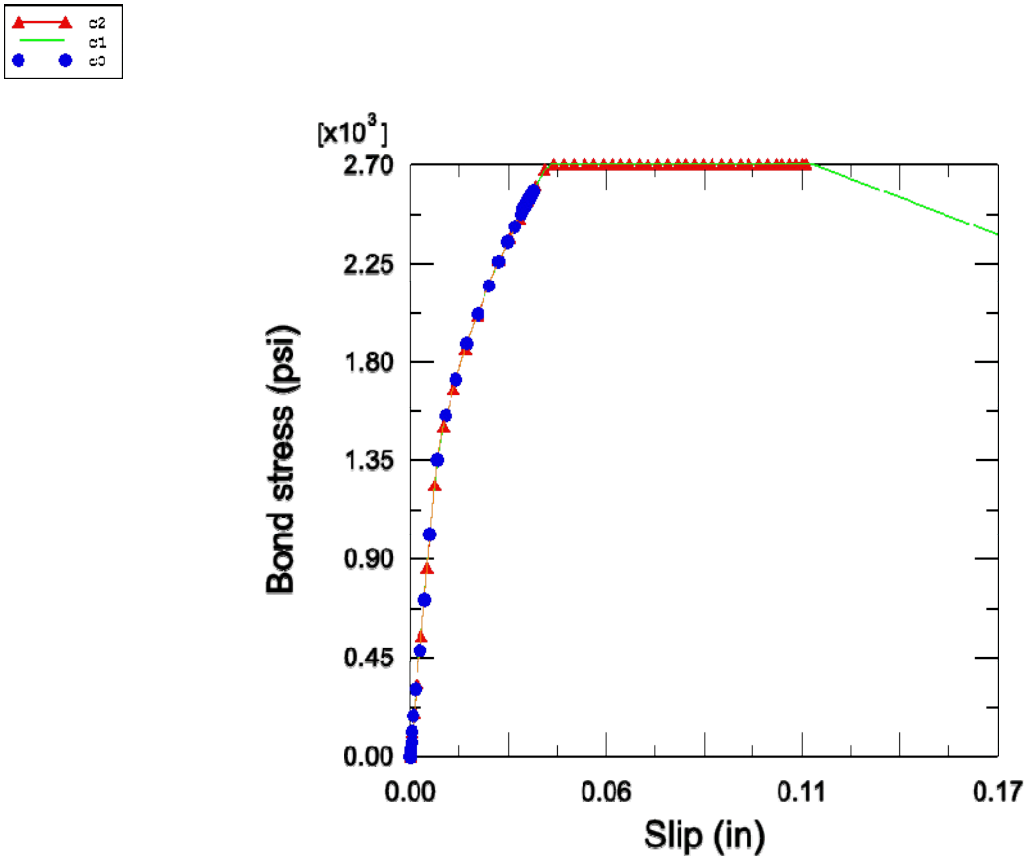

Figure 11.11 Bond Slip Relationships of Translator c1, c2 & c3

As can be seen, using the same input stiffness for each of the hundreds of translators located along the length of the rebar, and around the circumference, the different locations along the length of the rebar experienced different bond behaviors corresponding to the different relative amounts of slip that they experienced in response to the loading condition. This phenomenon again proved the feasibility of bond simulation using spring-like translators.

11.4 Rebar and Concrete Stress Distribution

The longitudinal stress distribution in the steel bar for the pull-out test can be predicted by the ABAQUS model (again using an imposed displacement in the axial direction). The longitudinal stress contour for the rebar is shown in Figure 11.15.

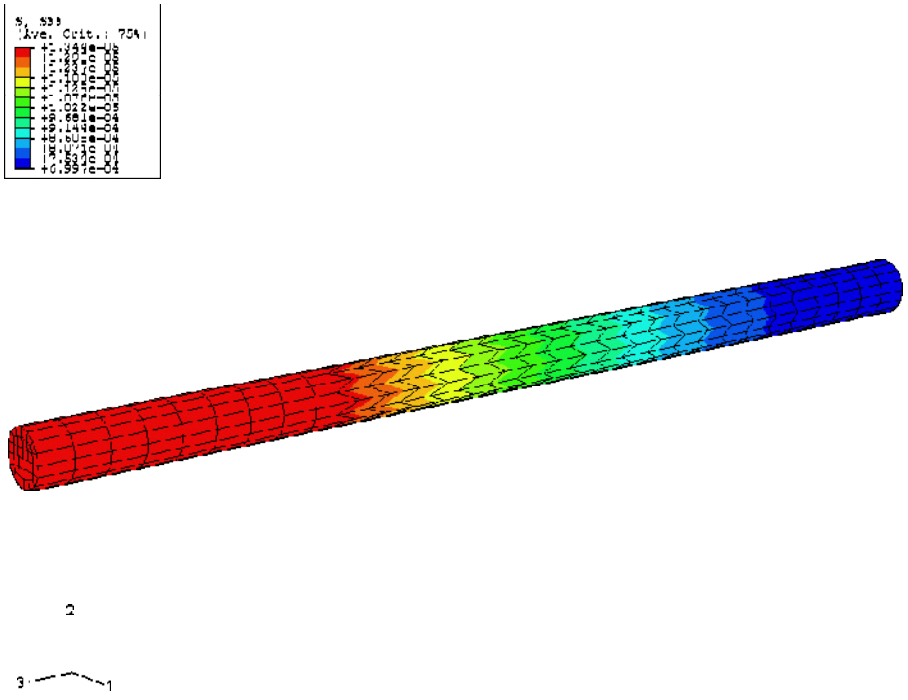

Figure 11.12 Longitudinal Stress Distribution for the Rebar

As can be seen, the rebar exhibits its largest tensile stress at the end nearest the applied load, and the stress level decreases toward the fixed end. This distribution of stress shows that the translators, representing the bond behavior, are affecting the rebar response; if there were no bond effect, the bar would exhibit a constant tensile stress. The stress distribution result for the bar agrees well qualitatively with the result shown by MacGregor in his textbook *Reinforced Concrete: Mechanics and Design,* as he describes

the stress distribution for a similar pull-out test. Figure 11.16 shows MacGregor's representation of the pull-out test method and the resulting rebar stress distribution. There is clearly some difference in the results of the present model and MacGregor's results; these are due to the difference in the pull-out test parameters (i.e., for the present study, the rebar was fixed at the end opposite the loaded end, while for MacGregor's study, the rebar end opposite the loaded end was not fixed, but was embedded in the concrete).

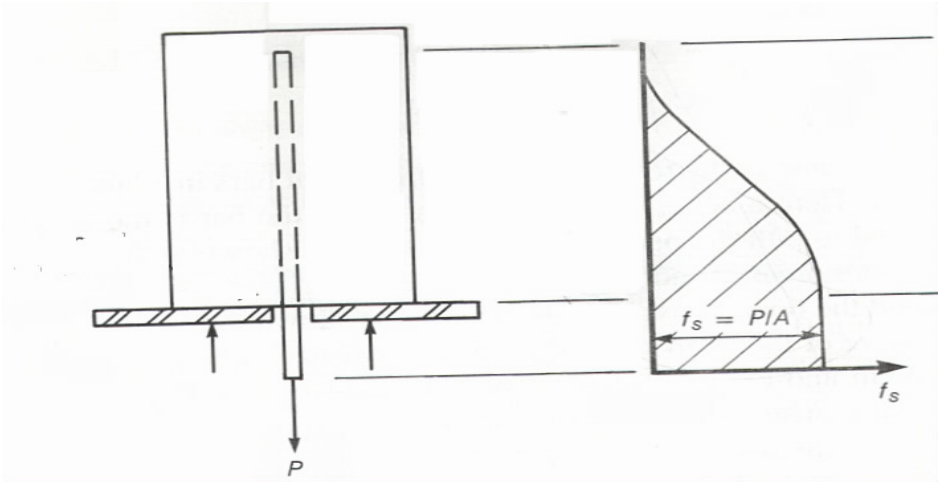

Figure 11.13 Rebar Stress Distribution of a Pull-out Test (MacGregor 1997)

The stress in the concrete specimen was also computed for the pull-out test; the results are shown in Figure 11.14. Due to the transfer of stress between the rebar and steel via the bond (translators), and due to the fixed condition of the concrete at the end nearest the loaded end of the rebar, the concrete is primarily in compression, as can be seen in the contour plot. However, the distortion of the stress contours surrounding the rebar location reflects the influence of the bond in modifying the concrete stress.

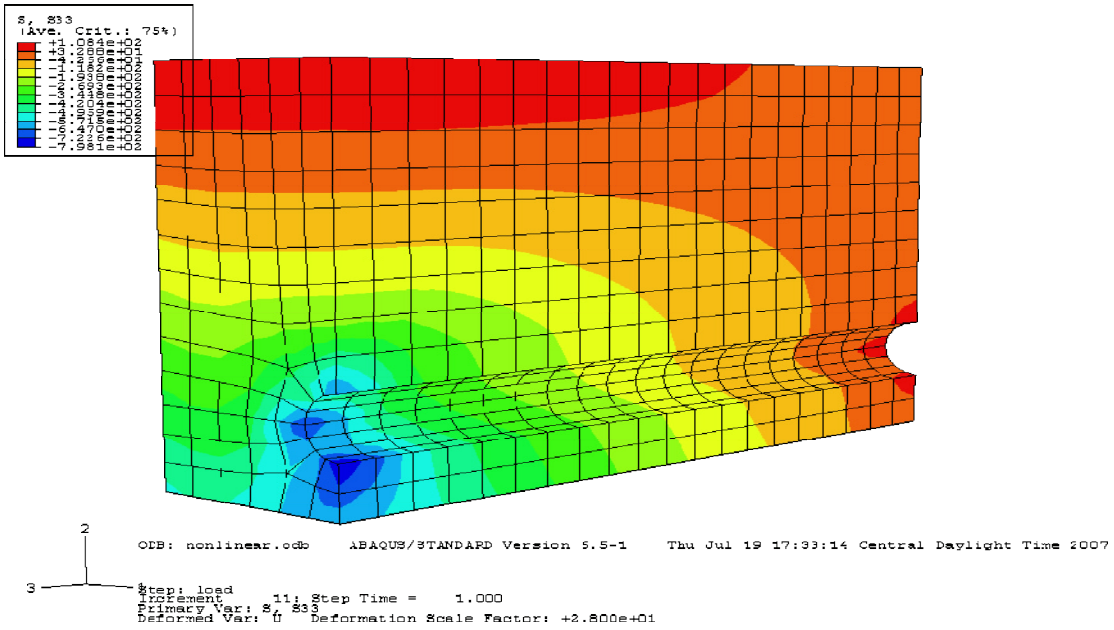

Figure 11.14 Longitudinal Stress Distribution for the Concrete

CHAPTER 12 SUMMARY, CONCLUSIONS AND RECOMMENDATIONS

12.1 Summary

A 3D finite element model was developed to simulate the bond behavior that exists between concrete and steel in reinforced concrete material using ABAQUS software. The spring-like translator, a connector element available in ABAQUS, was used to simulate the bond phenomena between concrete and steel in a pull-out test specimen model. The analysis results show that the translators did a very good job in simulating both the elastic range of response, and the behavior in the damaged range of the bond slip relationship. It was also shown that this element can be used to simulate the bond behavior under the influence of a load that produces a bending moment, and that a realistic bond stress distribution can be predicted along the length of the rebar. This study also led to a deeper understanding of the bond phenomena through the review of available literature describing other possible methods for representing bond behavior in numerical studies.

12.2 Conclusions

Conclusions that were drawn from the results of the modeling study are as follows:

1. The finite element software ABAQUS was capable of modeling reinforced concrete response, including the bond-slip behavior experienced between concrete and steel.

2. In a discrete reinforced concrete model (i.e., a model in which the concrete and rebar are both explicitly defined as unique components), the spring-like translator, a connector element available in ABAQUS, was very effective in not only connecting the concrete

and steel at the interface, but also accurately representing the bond-slip relationship and behavior existing between them.

3. Compared with other available methods in ABAQUS, the translator connector element has an advantage over other available connector elements in simulating bond behavior because it is capable of including various characteristics of the bond-slip relationship, i.e., one can define either a linear, bilinear, and nonlinear relationship. It can also represent the complex damage behavior of the bond.

12.3 Recommendations for Future Study

Based on the experience gained in performing this investigation of modeling strategies for simulating the bond behavior in reinforced concrete material, the following recommendations are made for future studies of this type:

1. Although the spring-like translator has been shown to be capable of simulating the complex bond behavior successfully, it does require a node-to-node connection. When the model has a large size and has hundreds of nodes at the interface, it will be very inefficient to connect them one-by-one using a very large number of translators. Therefore, in future studies of this type, the researcher should consider investigating the use of a surface-to-surface connecting element, rather than a node-to-node connecting element, to facilitate an efficient simulation, without losing the strong points of the spring-like translators.

2. The load condition employed in this study (axial load) was very simple. The feasibility of using spring-like translators to simulate bond behavior under more complex load cases still needs to be verified.

3. Bond is a very important factor related to the secondary cracking of reinforced concrete members. The successful prediction of bond stress distributions in this study can be used in the further study of crack behavior influenced by the effects of bond behavior.

4. Thermal effects were not considered in this study due to the lack sufficient time to fully investigate their influence on bond behavior. In fact, temperature effects can be defined as a variable of the spring-like translator properties. In addition, the user can create a thermal environment in the load modulus of ABAQUS. With these two basic functions, a bond slip model with thermal effects could be considered in future studies of this subject.

REFERENCES

AASHTO. 2004. *AASHTO LRFD Bridge Design Specifications*. 3rd ed. Washington, D.C. American Association of State Highway and Transportation Officials (AASHTO).

ABAQUS. 2004. *User's manual: version 6.5-1*. ABAQUS, Inc., Providence, RI.

ABAQUS. 2006. *User's manual: version 6.6-1*. ABAQUS, Inc., Providence, RI.

ABAQUS 2006 *Benchmark Manual: Version 6.6-1*. ABAQUS, Inc., Providence, RI.

Ala Saadeghvaziri, M., and R. Hadidi. 2005. Transverse Cracking of Concrete Bridge Decks: Effects of Design Factors. *Journal of Bridge Engineering.* 10 (5): 511-519.

ASCE. 1982. *State-of-the-Art Report on Finite Element Analysis of Reinforced Concrete.* Chapter 3: Modeling of Reinforcement and Representation of Bond. Task Committee - FE Analysis of Reinforced Concrete Structures of the Structural Division Committee on Concrete and Masonry Structures. Chairman: Arthur H. Nilson.

Barth, Karl E. and Wu, H. 2006. Efficient Nonlinear Finite Element Modeling of Slab on Steel Stringer Bridges. *Finite Elements in Analysis and Design* 42: 1304 – 1313.

Basker, K., N.E. Shanmugam, and V. Thevendran. 2002. Finite-element Analysis of Steel-concrete Composite Plate Girder. *J. Struct. Eng*. 128 (9): 1158–1168.

Biggs, R. M., F. W. Barton, J. P. Gomez, P. J. Massarelli, and W. T. McKeel. 2000. *Final Report: Finite Element Modeling and Analysis of Reinforced-Concrete Bridge Decks.* VTRC 01-R4, Virginia Transportation Research Council, Charlottesville, VA.

Bresler, B., and V. Bertero. 1968. Behaviour of Reinforced Concrete Under Repeated Load. *ASCE Journal of Structural Division* 94 (6): 1567-1590.

CEB-FIP. 1993. *CEB-FIP Model Code 1990: Design Code*. London. T. Telford.

CEB-FIP. 2000. *State-of-the-Art Report on Bond of Reinforcement in Concrete.* State-of-Art Report Prepared by Task Group *Bond Models* (former CEB Task Group 2.5) FIB - Féd. Int. du Béton: 1-97.

Choo, Tze-Wei., D. G. Linzell, J. Lee, and J. A Swanson. 2005. Response of a Continuous, Skewed, Steel Bridge during Deck Placement. *Journal of Constructional Steel Research.* 61: 567-586.

Ciampi, V., Eligehausen, R., Bertero, V.V., Popov, E.P. 1981. Analytical Model for Deformed Bar Bond under Generalized Excitations. *Reports of Working Commissions.* 34: 53-67.

Darwin, D. 1993. Reinforced Concrete. *Finite Element Analysis of Reinforced-Concrete Structures II: Proceedings of the International Workshop.* New York: American Society of Civil Engineers: 203-232.

Dicleli, Murat. 2000. Simplified Model for Computer-aided Analysis of Integral Bridges. *Journal of Bridge Engineering*. 5 (8): 240-248.

Filho, Josafá de Oliveira, and Ana Lúcia H. de C. El Debs. 2004. Stiffness Loss on RC Elements with Simulation of Contact on Steel-concrete Interface. *2004 ABAQUS Users' Conference:* 267-280.

Hadidi, Rambod and M. Ala Saadeghvaziri. 2005. Transverse Cracking of Concrete Bridge Decks: State-of-the-Art. *Journal of Bridge Engineering.* 10 (5): 503-509.

Gan, Y. 2000. *Bond Stress and Slip Modeling in Nonlinear Finite Element Analysis of Reinforced Concrete Structures*. Thesis, University of Toronto.

Guo, Zhenhai, and Xudong Shi. 2003. *Reinforced Concrete Theory and Analysis.* Super Star Digital Library. Qing Hua Da Xue Chu Ban She: Beijing, China.

Jiang, Jianjing, X. Lu, and L. Ye. 2004. *Finite Element Analysis of Concrete Structures.* Tsinghua University Press. Beijing, China.

Kim, Seong-Min, and Moon C. Won. 2004. Horizontal Cracking in Continuously Reinforced Concrete Pavements. *ACI Structural Journal* 101 (6): 784-791.

Kim, Seong-Min, Moon C. Won, and B. Frank McCullough. 2000. Three Dimensional Analysis of Continuously Reinforced Concrete Pavements. *Transportation Research Record* No. 1730: 43-52.

Kim, Seong-Min, Moon C. Won, and B. Frank McCullough. 2001. CRCP-9: Improved Computer Program for Mechanistic Analysis of Continuously Reinforced Concrete Pavements. *Research Report 1831-2.* Center for Transportation Research, University of Texas at Austin.

Kim, Seong-Min, Moon C. Won, and B. Frank McCullough. 2003. Mechanistic Modeling of Continuously Reinforced Concrete Pavement. *ACI Structural Journal* 100 (5): 674-681.

Lin, J. J., M. Fafard, D. Beaulieu, and B. Massicotte. 1991. Nonlinear Analysis of Composite Bridges by the Finite Element Method. *Computers & Structures*. 40 (5): 1151–1167.

MacGregor, J. G. 1997. *Reinforced Concrete: Mechanics and Design, Third Edition*. Pearson Education, Upper Saddle River, NJ.

Maleki, S. 2002. Deck modeling for seismic analysis of skewed slab-girder bridges. *Engineering Structures*, 24 (10): 1315-1326.

Mirza, Saeed M, and Jules Houde. 1979. Study of Bond Stress-Slip Relationships in Reinforced Concrete. *ACI Journal.* 76 (2): 19-47.

Nilson, A H. 1968. Nonlinear Analysis of Reinforced Concrete by the Finite Element Method. *ACI Journal, Proceedings.* 65 (9): 757-766.

Nilson, A H. 1972. Internal Measurement of Bond-Slip. *ACI Journal Proceedings.* 69 (7): 439-441.

Perry, Ervin S., and J. Neils Thompson. 1966. Bond Stress Distribution on Reinforcing Steel in Beams and Pullout Specimens. *Journal of the American Concrete Institute* 63-64: 865-874.

Schindler, A. 2005. *Causes of Cracking of Bridge Deck on US331*, Presentation, ALDOT.

Shapiro, K. 2006. *Finite-Element Modeling of a Damaged Prestressed Concrete Bridge.* M.S. Thesis, Auburn University: 67-98.

Tassios, T P. 1982. Properties of Bond between Concrete and Steel under Load Cycles Idealizing Seismic Action. *National Technical University Athens*. Greece.

Thevendran, V., S. Chen, N.E. Shanmugam, and J.Y.R. Liew. 1999. Nonlinear Analysis of Steel-concrete Composite Beams Curved in Plan. *Finite Elements in Analysis and Design* 32: 125-139.

Weathersby, J H. 2003. *Investigation of Bond Slip between Concrete and Steel Reinforcement under Dynamic Loading Conditions.* Dissertation, Louisiana State University: 131-162.

Won, M., K. Hankins, B. F. McCullough. 1991. *Mechanistic Analysis of Continuously Reinforced Concrete Pavements Considering Material Characteristics, Variability, and Fatigue*. Research Report 1169-2. Center for Transportation Research, The University of Texas at Austin.

APPENDIX: Cracking Data from ABAQUS Data File

CK: Crack occurs in the concrete model

CRACK1X and CRACK1X: Vector coordinates of the normal direction of the crack

ELEMENT	INTEGRATION POINT	SECTION POINT	FOOT-NOTE	CRACK1X	CRACK1Y
1	1	5	CK	0.9152	-0.403
1	2	5	CK	0.7255	-0.6882
2	1	5	CK	0.7108	-0.7034
2	2	5	CK	0.7305	-0.683
3	1	5	CK	-0.6254	0.7803
3	2	5	CK	-0.5055	0.8628
4	1	5	CK	-0.6707	0.7417
4	2	5	CK	0.7288	-0.6848
4	3	5	CK	0.877	-0.4804
5	1	5	CK	0.7187	-0.6954
5	2	5	CK	0.7119	-0.7023
6	2	5	CK	-0.6259	0.7799
7	1	5	CK	-0.6791	0.7341
7	2	5	CK	-0.6718	0.7407
8	1	5	CK	-0.6444	0.7647
8	2	5	CK	-0.6661	0.7458
9	1	5	CK	-0.6632	0.7485
9	2	5	CK	-0.6728	0.7398
10	1	5	CK	-0.6754	0.7375
10	2	5	CK	-0.6587	0.7524
10	4	5	CK	-0.6594	0.7518
11	1	5	CK	-0.6368	0.771
11	2	5	CK	-0.6994	0.7147
12	1	5	CK	-0.6299	0.7767
14	2	5	CK	-0.6857	0.7278
26	2	5	CK	-0.6367	0.7711
481	1	5	CK	-0.7007	0.7135
481	2	5	CK	-0.6523	0.758
482	1	5	CK	-0.687	0.7267
482	2	5	CK	-0.6681	0.744

483	1	5	CK	-0.5803	0.8144
483	2	5	CK	-0.4218	0.9067
484	1	5	CK	0.7152	-0.699
484	2	5	CK	0.7388	-0.674
485	1	5	CK	0.7163	-0.6978
485	2	5	CK	0.7085	-0.7057
486	2	5	CK	-0.6265	0.7794
487	1	5	CK	-0.676	0.7369
487	2	5	CK	-0.6662	0.7458
488	1	5	CK	-0.6397	0.7686
488	2	5	CK	-0.6617	0.7498
489	1	5	CK	-0.6795	0.7337
489	2	5	CK	-0.6512	0.7589
490	1	5	CK	-0.6715	0.741
490	2	5	CK	-0.6542	0.7563
490	4	5	CK	-0.6454	0.7639
491	1	5	CK	-0.6355	0.7721
491	2	5	CK	-0.6941	0.7199
492	1	5	CK	-0.6391	0.7692
494	2	5	CK	0.7162	-0.6979
506	2	5	CK	-0.6222	0.7829
961	1	5	CK	0.7132	-0.701
961	2	5	CK	-0.6601	0.7512
962	1	5	CK	-0.7036	0.7106
962	2	5	CK	-0.676	0.7369
963	1	5	CK	-0.5749	0.8182
963	2	5	CK	-0.4128	0.9108
964	1	5	CK	0.7075	-0.7067
964	2	5	CK	0.7253	-0.6884
965	1	5	CK	-0.705	0.7092
965	2	5	CK	-0.691	0.7229
966	1	5	CK	0.7075	-0.7067
966	2	5	CK	-0.6253	0.7804
967	1	5	CK	-0.6741	0.7386
967	2	5	CK	-0.6605	0.7508
968	1	5	CK	-0.6312	0.7756
968	2	5	CK	-0.6619	0.7496
969	1	5	CK	-0.6485	0.7612
969	2	5	CK	-0.6509	0.7592
970	1	5	CK	-0.6757	0.7372
970	2	5	CK	-0.6585	0.7526
970	4	5	CK	-0.6496	0.7602
971	1	5	CK	-0.6378	0.7702
971	2	5	CK	0.7106	-0.7035
972	1	5	CK	-0.6445	0.7646
972	2	5	CK	-0.6426	0.7662

973	1	5	CK	-0.6666	0.7454
974	2	5	CK	0.728	-0.6856
986	2	5	CK	-0.6357	0.772
1575	3	5	CK	-0.6415	0.7671
1587	3	5	CK	-0.7039	0.7103
1589	4	5	CK	-0.6284	0.7779
1590	4	5	CK	-0.6411	0.7675
1591	1	5	CK	-0.6518	0.7584
1591	3	5	CK	-0.6579	0.7531
1591	4	5	CK	-0.6765	0.7364
1592	3	5	CK	-0.6549	0.7557
1592	4	5	CK	-0.6744	0.7383
1593	3	5	CK	-0.6512	0.7589
1593	4	5	CK	-0.6306	0.7761
1594	3	5	CK	-0.6553	0.7554
1594	4	5	CK	-0.6761	0.7368
1595	3	5	CK	-0.6194	0.7851
1596	3	5	CK	-0.6959	0.7181
1596	4	5	CK	-0.7028	0.7114
1597	3	5	CK	0.7118	-0.7024
1597	4	5	CK	-0.6632	0.7485
1598	3	5	CK	-0.4747	0.8801
1598	4	5	CK	-0.5962	0.8029
1599	3	5	CK	-0.6973	0.7168
1599	4	5	CK	0.7161	-0.698
1600	3	5	CK	-0.6701	0.7423
1600	4	5	CK	0.7274	-0.6862